Development of an Electron Gun Design Optimisation Methodology

A thesis submitted in partial fulfilment of the requirements for the Degree of Doctor of Philosophy

by

Colin Nigel Ribton

Department of Electronic and Computer Engineering

College of Engineering, Design and Physical Sciences

Brunel University London

28th September 2017

Development of an Electron Gun Design Optimisation Methodology

Colin Nigel Ribton

Abstract

The design of high quality electron generators to meet specific requirements is important in the application of these devices to a variety of materials processing systems (including welding, cutting and additive manufacture), X-ray tubes for medical, scientific and industrial applications, microscopy and lithography. Designs can be analysed by field solvers, and electron trajectories plotted to provide an indication of the beam quality. Incremental improvement of designs has normally been executed by trial and error, and this can be a time consuming activity requiring expert intervention for each iteration of the design process. The unique contribution made to knowledge by this work is the application of optimisation techniques to the design of electron guns to produce beams with the required optical properties. This thesis presents a review of the design of electron guns, including a discussion of thermionic cathode material properties and their suitability for use in electron guns for processing materials, the influence of space-charge on gun design and the derivation of salient beam metrics to characterise the beam. Beam quality metrics have been developed that allow quantification of electron beam characteristics, allowing objectives to be set for the optimisation process. Additionally, a method is presented that enables real world measurements to be directly compared with modelled beams. Various optimisation methods are reviewed. A genetic algorithm was selected, which would use gun modelling and beam characterisation calculations as the objective function, as a suitable method for application to this problem. However, it was recognised that selections for the best evolutionary parameters, the population size, number of parents, the mutation rate and mutation scale, were not readily determined from published work. An investigation is presented where a range of evolutionary

parameters was tested for a set of geometrical problems, which had some similarity to electron gun design but could be computed sufficiently quickly to enable an extensive survey, and the most efficient combination of parameters was identified. Detail is given of the customisation of a genetic evolutionary optimisation method for the design of electron guns. Examples are presented of electron gun design optimisation processes to meet specified beam requirements within defined geometric and electrical constraints. The results of this work show that optimum evolutionary parameter settings for the geometric problem vary with the complexity of the problem and trends have been identified. Application of these parameters to an electron gun optimisation has been successful. The derived beam parameter metrics have been applied to electron guns as an objective function. Comparisons of modelled predictions of the beam characteristics with the measured real world values have been shown to be reasonable.

Contents

Table of Figures

Table of Tables

Abbreviations

CWAD	Current weighted average diameter
EB, EBW	Electron beam, electron beam welding
FEA	Finite element analysis
FWHM	Full width at half maximum
FWHP	Full width for half power
HV	High voltage
LHCD	Laser heated cathode diode
PSO	Particle swarm optimisation

Symbols used

Symbol	Meaning	Units
A	Richardson's constant, 1.202 x 10^6	$Am^{-2}K^{-2}$
Ang_{imean}	Current weighted average beam divergence angle	rad
Ang_{var}	Variance in the beam divergence angle	rad^2
B	Beam brightness	$Am^{-2}sr^{-1}$
B_{max}	Maximum beam brightness	$Am^{-2}sr^{-1}$
BPP	Beam parameter product	mmrad
d	Distance between the cathode and anode	m
d_f	Beam diameter at focus	m
D	Internal bore diameter of the lens shroud	mm
e, m	electron charge and mass	C and kg respectively
f	Focal length of the lens	mm
i	Beam current	A
i_n	Current assigned to the n^{th} beamlet	A
Int_{src}	Beam source intensity	Amm^{-2}
J	Emission current density	Am^{-2}
k	Boltzmann's constant, 8.6173 x 10^{-5}	eV K^{-1}
L	Constant combining lens characteristics with the accelerating potential	mmA^{-2}
M	Lens magnification	No units
N	Total number of beamlets	No units
NI	Lens coil current excitation	A-turns
P	Perveance	$AV^{-1.5}$
r	Parallel beam diameter	m
rad_{src_imean}	Current weighted average radius of the beam at the source	mm
$r_f,\ z_f$	Coordinates of the trajectory at the beam focal position	mm
r_{f_n}	Radial position of the n^{th} trajectory at the beam focal position	mm
$r_l,\ z_l$	Coordinates of the trajectory at the lens centre plane	mm
r_s	Radius of confusion at the focal plane	mm
S	Pole piece gap in the lens shroud	mm
T	Cathode temperature	K
T_m	Material melting point	K
u	Distance of the apparent source of the gun to the lens centre plane	mm
v	Distance from the lens centre plane to the beam focus position	mm
v_r	Radial velocity component of the beamlet	mms^{-1}

v_t	Transverse component of the electron velocity	ms^{-1}
v_v	Axial component of the electron velocity	ms^{-1}
v_z	Axial velocity component of the beamlet	mms^{-1}
V	Accelerating potential	V
V^*	Relativistically corrected beam acceleration voltage	V
z_{cross}	Position where the trajectory crosses or virtually crosses the Z axis near to the beam	mm
z_{pos}	Axial position of the beamlet captured from the model data at the sample plane	mm
z_{src_imean}	Current weighted average apparent electron source position	mm
z_{src_n}	Position where the n^{th} beamlet projected backwards crosses the Z axis	mm
z_{src_var}	Variance in the Z source position	mm^2
ε_0	Electric constant, 8.854×10^{-12}	Fm^{-1}
θ	Total included beam angle	rad
ρ	Number density of electrons in a beam	m^{-3}
ϕ	Work function	eV
$\Omega_{\min}$	Solid angle of the beam	sr

Declaration

I hereby declare that no part of this thesis has been previously submitted to this or any other university as part of the requirements for a higher degree. The work described herein was conducted solely by the undersigned except for those colleagues and others acknowledged in the text.

Colin Ribton

28th September 2017

Acknowledgements

Foremost, I thank my good friend and supervisor, Professor Wamadeva Balachandran, for his excellent guidance and encouragement in the research work I have carried out. I am very grateful to the support given to me by TWI that allowed me to pursue this research whilst employed by them. I have only been able to carry out this research in parallel with my normal work because of the patience and support of my family, Caroline, Jake and Ollie. I am indebted to my students, Aman Preet Kaur and Sofia del Pozo, who inspired me to be a better scientist and to become a student again. Thank you also to the researchers at Brunel University London, who were always ready to help with their expertise. In particular, David Ryan Smith, who reviewed my work and provided much advice.

This research work has been supported by TWI Ltd., The National Structural Integrity Research Foundation and Brunel University London.

Chapter 1: Introduction

This chapter provides background to the problems with the design process for electron guns, introduces the main and secondary research questions addressed by this work, outlines the aims and objectives of the work, and the methodology used to address it. The thesis structure is described, the unique contributions to knowledge generated within this work are presented and relevant publications from the research are listed.

1.1 Statement of problem

Design of electron guns is carried out with analysis tools to test whether tentative designs will meet the design requirements for the proposed application. As such, the design of guns is at best an informed trial-and-error process. Using present techniques, the final design settled upon may not be the best available, and may just be a local optimum for the feature and dimension changes attempted. Confidence that the best design has been found can be increased by carrying out further analysis of different designs, but this can be time consuming and ultimately not satisfactory.

Requirements for electron guns for material processing are generally specified by beam characteristics suitable for the application (ISO, 2008). Typically, this would be a required intensity at a certain working distance from the end of the gun column, or a range of required values – but the beam angle also may be important. For example, lower angles are specified for thick section welding applications so that the beam is intense through the thickness of the weld pool, whereas for thin section welding the beam angle can be higher, as a shallower depth of focus can be tolerated, and this facilitates higher intensities. Normally, an electron gun will be designed to be suitable for a range of applications, so the beam requirements may be stated as a list of intensities and powers at a working distance. The accelerating potential is influential on the beam characteristics but usually this parameter has a fixed maximum for a particular application, constrained by the specification of high voltage components and X-ray shielding.

The present state-of-the-art of electron gun design uses software analysis tools to test tentative geometries. There are several tools available that can derive the field and electron trajectories for a given electrode geometry, such as Opera, Trak, EGUN, CST and MICHELLE for example. For the types of electron gun being examined, it is necessary for the analysis to take into account the space charge distribution in the beam, as this will usually have a significant effect on the trajectories. Methods for deriving some simple forms of geometry have been developed, most notably by (Pierce, 1954). The design process usually involves starting with such a form of geometry, and then adapting that to optimise the beam characteristics. The software tools either do not produce beam characterisation data from the trajectories, or only provide rudimentary quantification of beam quality.

In design optimisation terminology, electron guns have many variables of geometry and electrical operation, and are likely to have multiple objectives in all but the simplest of cases. This research aims to address the problem of how to efficiently optimise electron gun designs.

1.2 Research questions

The primary research question addressed by this work is:

> Can automated optimisation methodologies be successfully applied to electron gun design for applications requiring intense, focused beams?

Secondary to this question are:

> How can proposed electron gun geometries, including those of cathodes, grid cups and anodes, be automatically generated?
>
> How can viable simulation models be generated from proposed gun geometries, where a viable model is one that will be accurately solved when beam characteristics extracted from the models are compared with real world measurements?

How can a simulated gun model be post-processed to derive the beam characteristics that then can be compared with beam requirements and/or measurements in real world equipment?

Can this approach produce gun designs in a reasonable time when using reasonable computing resource?

1.3 Aims and objectives

The focus of this research was upon the development of a method for optimisation of designs to enable automatic design of electron guns to meet specified requirements within defined geometric and electrical constraints. The aim was to develop a method whereby a designer could identify beam requirements and system constraints that were then used to find an optimum electron gun geometry.

The new design process was required to be efficient and more effective than current practice, where a designer reviews the analysis of tentative designs and then adjusts geometries to attempt to optimise the beam quality. The methodology to be developed aimed to provide a high confidence that the optimum design had been found.

It was expected that the methodology to be developed within this research work could be applied using any of the available programs for the design analysis, as the analysis program was to be used as a ‘black box’ providing the beam characteristics of a particular gun model.

The objectives of the research work were as follows:

- To produce a review of gun design methods and beam quality metrics, with the objective of establishing the best and most relevant development work in this area.
- To investigate the best way of assessing the beam quality from an electron gun design.
- To develop a means of quantifying the beam quality over the operational range of the gun.

- To develop an optimisation methodology for design of electron guns. This will use the quantified beam characteristics as a quality factor.
- To carry out a case study where the methodology will be applied to at least one electron gun design with the aim of demonstrating the viability of the design process. The gun will be manufactured and tested. Real world measurements will be compared with the model outputs.

1.4 Summary of the methodology

The research work has been approached by reviewing activities on electron gun design that are especially relevant to the electrode design and thermionic emitters. Methods of characterising electron beams were investigated and a number of equations derived that could give quantified measurement of beam quality. This was pertinent to the use of optimisation algorithms, which require a means of scoring tentative solutions. These algorithms were reviewed and investigated. An evolutionary algorithm was selected for further investigation, following trials on an analogous problem involving geometric shape fitting. The algorithms used in this work were developed from scratch, so that their operation was fully understood and could be customised to the gun design optimisation problem. Special adaptations were made to this algorithm to make it particularly suitable for application to the design of electron guns. The algorithm provided the management of the evolution process, but relied upon an external commercial finite element modeller to simulate the field in the electron gun and plot trajectories to form the beam. In this work, Opera 2D was used with a space charge solver, although it is expected that the algorithm could be interfaced to any of the gun modelling and beam simulation tools available. The beam metrics developed earlier in the work were then derived from the modelled beam and used to provide the objective function i.e. scoring function for the evolutionary process. The algorithm has been applied to a number of design challenges and the design process for these was monitored. Finally, the beam characteristics predicted for a design were

compared with the measured beam properties for a system that was manufactured and operated.

1.5 Thesis structure

Background literature relevant to the research has been reviewed in the opening part of both Chapters 2 and 3. The work reported includes a review of the development of electron guns since their invention at the end of the 19th century and introduces beam quality metrics, which could be used as quantified measurements of electron beam quality in Chapter 2: Electron beam generation and characterisation. Beam quality could be expressed as brightness, emissivity, focused spot size – e.g. full width at half maximum, or other quality factors. This part of the work considers not only the assessment of beam quality by interrogation of the output from models but also how real world measurements could be carried out to verify the design.

Optimisation techniques were also reviewed and techniques suitable for developing a gun geometry were investigated in Chapter 3: Investigation of optimisation methods. Optimisation research, in design challenges closely related to electron beam generators, was reviewed to establish the state-of-the-art. This chapter also describes trials that were carried out on a simple evolutionary example from literature and a geometry optimisation problem. An optimisation technique was selected and developed to make use of electron gun analysis and beam characterisation for the objective function – this is described in Chapter 4: Application of optimisation method to electron gun design. Examples of electron gun design optimisation is reported in Chapter 5: Electron gun model examples, and the real world measurements were compared with modelled characteristics, reported in Chapter 6: Beam measurements and comparison.

The work carried out was critically assessed, conclusions drawn and future work discussed in Chapter 7: Conclusions and recommendations for future work.

1.6 Contribution to knowledge

The unique contribution made to knowledge by this work is the development of bespoke optimisation techniques for the design of electron guns. Techniques have been developed for assessing the electron optical properties of beams produced by analytical simulations of prospective gun designs. Methods have been developed to compare the characteristics from simulations to real world beam measurements enabling verification of modelling methods. A methodology has been developed to automatically generate electron gun models which give accurate prediction of electron trajectories. Methods for encoding the design have been developed and tested – allowing tuning of the adopted optimisation techniques.

The novel contributions arising for work are outlined below for each chapter:

Chapter 2: Electron beam generation and characterisation

A review is given of electron gun design. Data has been collated and is graphically presented to allow comparison of different cathode materials and their lifetime in use. Diode and triode emission are contrasted. Within this chapter the derivation is given of a range of beam characteristics from a set of trajectories. A means of predicting a beam probe signal from a model output is described with a method for determining the apparent electron source position from experimental measurements.

Chapter 3: Investigation of optimisation methods

After a review of the most relevant optimisation methods presently in use, a demonstration is presented of the effectiveness of cumulative selection. The influence of evolutionary parameter combinations on the efficiency of a solution algorithm has been investigated and is presented.

Chapter 4: Application of optimisation method to electron gun design

The implementation of a specialised genetic evolutionary algorithm for the design of electron guns, where parts of the design can be constrained either entirely or within dimensional limits, is described in detail.

Chapter 5: Electron gun model examples

Examples of gun design optimisations using the novel optimisation algorithm are given.

Chapter 6: Beam measurements and comparison

Experimental measurements of the beam have been processed to allow comparison with outputs from the gun simulations.

1.7 Publications

During the course of this research the work has been published and presented at conferences. A full list of these publications is given in Table 1-1:

Table 1-1 List of publications from this research work.

Publication
Ribton, C., 2017. Design of electron beam guns using evolutionary algorithms and finite element modelling. In *Opera EUGM 2017*. Cobham.
Ribton, C., del Pozo, S., Smith, D., Balachandran, W., 2017. Design of a plasma cathode electron gun using evolutionary optimisation. In *4th International Electron Beam Welding Conference*. Aachen.
Ribton, C. & Balachandran, W., 2016. Genetic algorithms for automatic optimisation of electron beam processing guns. In *NSIRC Annual Conference*. Cambridge.
Ribton, C., del Pozo, S., Balachandran, W., Smith, D., 2016. Design of electron guns using a bespoke genetic algorithm. *Elektrotechnica & Elektronica E+E*, 51(5-6).
Ribton, C., del Pozo, S., Smith, D., Balachandran, W., 2016. Applying evolutionary design to plasma cathode electron guns for material processing. In *Proceedings of the 10th International Conference Beam Technology*. Halle.
Ribton, C. & Balachandran, W., 2015. Development of an evolutionary algorithm for design of electron guns for material processing. In *Computational Intelligence (IJCCI), 2015 7th International Joint Conference on*. pp. 138–148.

Chapter 2: Electron beam generation and characterisation

This chapter summarises the history of electron gun design, particularly for material processing applications. The emission of electrons from a cathode is described and some of the important relationships are given. Beam quality metrics are introduced as a gauge for how well a tentative gun design meets the requirements of its potential application. The computing methods used in the present day design of electron guns are described. Details are given of the particular modelling software used in this research work.

2.1 Electron gun design

Electron beams have been a topic of research for over 100 years, and our improved understanding of how to generate and use them has led to the development of many essential technologies including valve electronics, CRT displays, microwave generation and radar, X-ray inspection and electron beam material processing. The earliest research into electron guns was primarily to understand the nature of ‘cathode rays’, and it was not until the late nineteenth century that the electron was discovered to have particle-like properties of mass and to carry charge (Thomson, 1897). At a similar time, it was also found that cathode rays produced X-rays when they impacted upon a target (Wilson, 1895), and the development of electron guns as X-ray sources began.

2.1.1 Cathodes

These early guns almost exclusively used gas discharges to produce free electrons, although Thomson experimented with different cathode materials, aiming to prove that the electrons produced by them were a fundamental building block of matter, i.e. common to atoms of different elements. It was established over the next decade that all atoms contain electrons in bound states – either in shells of atoms or within energy wells in solids. It was found there were several ways to cause electrons to be liberated from these states into a beam, including ultra-violet light or X-ray irradiation causing photoelectric emission, particle bombardment inducing

secondary emission, application of a strong electric field causing field emission and heating to produce thermionic emission. Emission from gas discharges is the product of some or all of these processes (Klemperer, 1959). However, through developments in vacuum technology, and for convenient use, thermionic emission rapidly became the most important method of free electron generation and was explored for refractory metal cathodes such as tungsten (Richardson, 1913) – a material still widely in use today for electron gun cathodes. The effect of electric fields on the beam current produced by cathodes gave the scientific foundation to electron emitter design (Child, 1911).

2.1.2 Thermionic Emission

The work function is described as the energy required to move a free electron from the bulk of the material to just outside the surface (Dushman, 1923). At absolute zero, the conduction band electrons occupy energy levels up to the Fermi level. There exists an energy barrier at the metal surface, which the electrons must overcome to escape the surface. The barrier is at a potential of the work function relative to the Fermi level. If the conduction band electron energies are elevated by, for example, heating the material, some of the conduction band electrons will gain sufficient energy to overcome the surface energy barrier. The energy of the electrons is in a distribution, and the high energy tail of this in a thermionic emitter, although containing only a tiny proportion of the total electrons available in the conduction band, represents those electrons that have sufficient energy to escape the surface. This is illustrated in Figure 2-1. Only electrons at energies greater than the material work function (i.e. to the right of the dotted vertical lines) will be able to escape the surface.

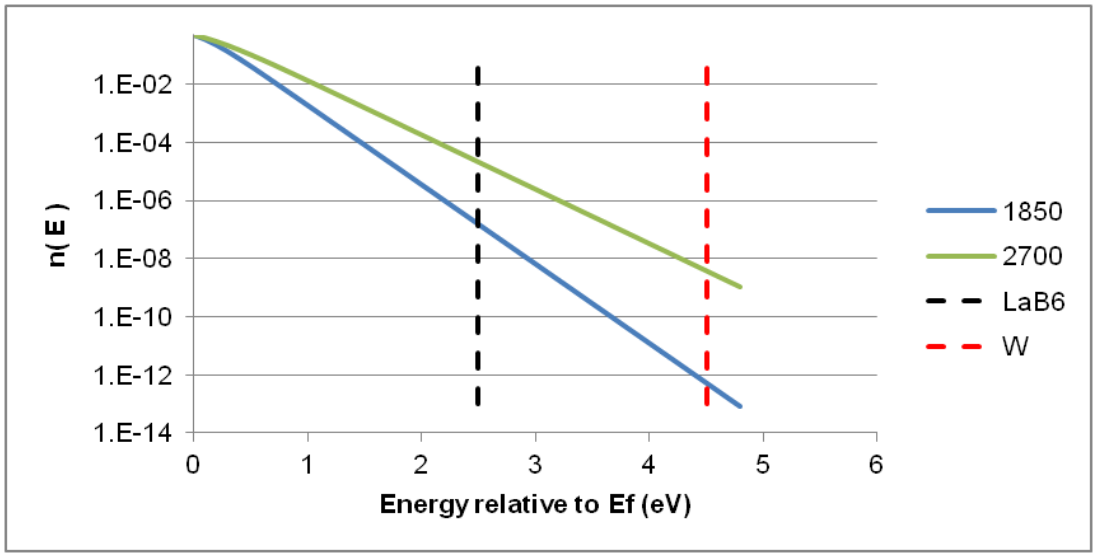

Figure 2-1 Graph showing the energy distribution of electrons relative to the Fermi level at a temperature of 1850 K and 2700 K, typical operation temperatures for lanthanum hexaboride and tungsten whose work function values are shown.

The probability of electron escape is very small, even at elevated temperatures. However, the density of electrons in the cathode is of the order of 10^{28} m^{-3}, assuming 1 per atom. The density of electrons in the beam has been found from equating the beam current to the number of electrons per second across a parallel beam:

$$\rho = \frac{\frac{electrons\ per\ second}{velocity}}{\pi r^2} = \frac{i}{\pi r^2 e\sqrt{2V^* \frac{e}{m}}} \qquad \text{Eq 2-1}$$

where

r is the parallel beam diameter, m

i is the beam current, A

e, m are the electron charge and mass, C and kg respectively

V^* is the relativistically corrected beam acceleration voltage, V

$$V^* \sim V(1 + V.10^{-6}) \qquad \text{Eq 2-2}$$

where

V is the accelerating potential, V

Considering a typical material processing electron beam, with 100 mA beam current and accelerated at 60 kV, and for simplicity assuming this is a parallel beam of, say, 2 mm diameter, the electron density in the beam can be calculated to be of the order of 10^{14} m^{-3}, which is a factor of 10^{14} less than in the cathode. Consequently, only a tiny fraction of the conduction band electrons at a particular temperature are required to have energy sufficient to overcome the work function potential barrier in order for the cathode to generate the required beam current.

The different types of emitter are categorised by how the electrons overcome the energy barrier at the surface i.e. in a photo-emitter an electron receives energy from a photon when the cathode is illuminated, and in a field emitter the energy barrier is lowered by a strong, localised external field of greater than 10^{8} Vm^{-1} so that it becomes more probable that electrons can tunnel through this barrier.

The conducting electrons within a metal are mobile within the material. Should they escape the surface of the material, they will experience an electrostatic force due to an image charge being created, which will attract them back to the material bulk. With no further measures, the escaping electrons will be attracted back to the metal surface. Consequently, hot metals, for example, are surrounded by a cloud of electrons that have been emitted and are about to be re-absorbed at the surface. The electrons can be attracted away from the surface if the electric field attracting the electrons to the surface can be reversed by applying a potential difference across a space defined by the metal (now a cathode) and an anode. Richardson, and later Dushman, (Dushman, 1923; Richardson, 1913) derived a description of the maximum quantity of electrons, expressed as a current density, that would escape from a surface elevated to a defined temperature.

$$J = AT^2 e^{\frac{-\emptyset}{kT}} \qquad \text{Eq 2-3}$$

where

J is the emission current density, A m^{-2}

A is Richardson's constant, 1.202 x 10^{6} $Am^{-2}K^{-2}$, which is corrected for each material

T is the cathode temperature, K

ϕ is the work function, eV, 1 eV = 1.602 x 10^{-19} J

k is Boltzmann's constant, 8.6173 x 10^{-5} eV K^{-1}

Also $\frac{\emptyset}{k}$ is the work function expressed as electron temperature, K

2.1.3 Thermionic cathode materials

Barium and strontium oxides are semi-conductors and have low work functions of approximately 1.3 eV whereas platinum has a high work function of 5.9 eV. However, it is the relationship between the work function expressed as the electron temperature and the material melting point temperature that determines an important factor for assessing the practicality of using a material as a thermionic cathode. Tungsten has been used widely because, although its work function is relatively high at approximately 4.5 eV, its melting point is very high, it being a refractory metal, at 3695 K.

Within this work, data was extracted from (Haynes, 2016). Work functions were converted to electron temperature units, and were plotted for a number of metals, barium oxide and lanthanum hexaboride, against their melting points, see Figure 2-2. With this plot, identification of potential candidate materials as thermionic cathodes could be carried out clearly. Assuming the Richardson constant is 1.2 x 10^{6} $Am^{-2}K^{-2}$ for all materials, a line of constant emissivity at the melting point can be plotted on this chart by re-arranging the Richardson equation, so that the work function expressed as an electron temperature is equated to a function of the melting point and the emissivity at the melting point.

$$\frac{\phi}{k} = -T_m \ln\left(\frac{J}{AT_m^2}\right) \qquad \text{Eq 2-4}$$

where

T_m is the material melting point, K

Although the Richardson constant is usually corrected by a factor between 1% to 140% depending on the material and surface properties, the emissivity dependence on temperature is largely dictated by the exponential term in the equation. The work function required to give an emissivity at the material melting point of 5 x 10^4 Am^{-2} (i.e. 50 $mAmm^{-2}$) is shown as a dotted line on the plot, Figure 2-2. Materials with emission intensities lower than this would generally not give a bright enough electron source to design an electron gun for practical use, or would have to be operated so close to their melting point that lifetimes would be too short due to evaporation. These materials are plotted above the dotted line, as they have higher work functions or lower melting points. Materials with lower work functions or higher melting points are plotted below the dotted line, and these are generally good candidate materials for thermionic cathodes.

Other factors for determining the viability of using a material as a thermionic cathode include the evaporation rate (as described in section 2.1.4) and the chemical stability in the operating environment.

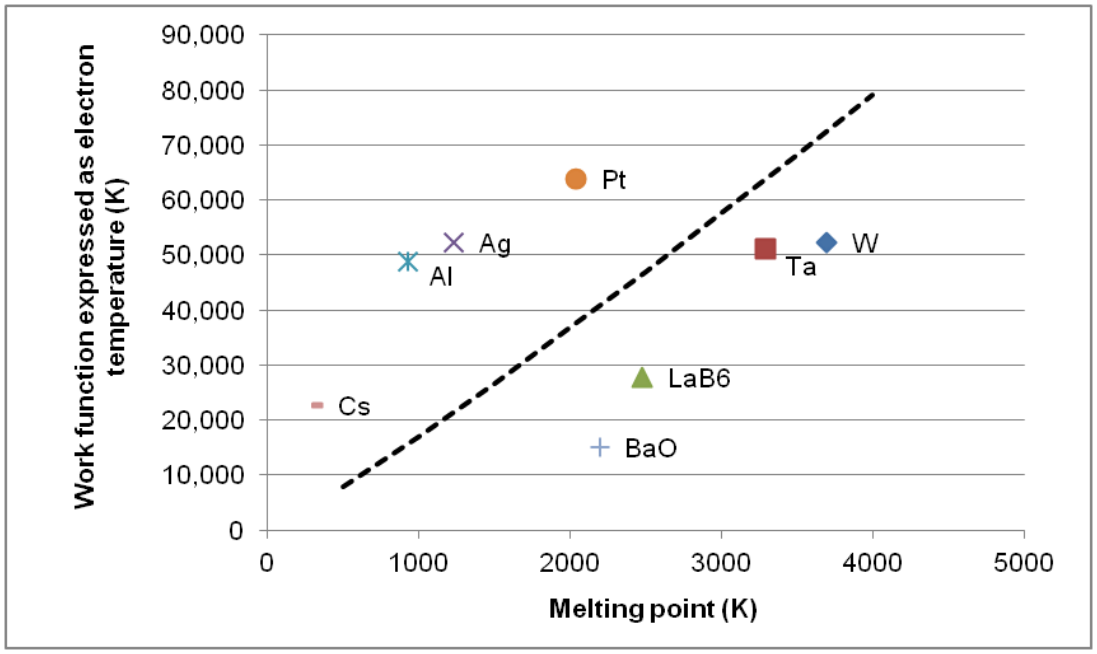

Figure 2-2 Work function plotted against the melting point of materials - practical thermionic emitters are shown below the line of constant emissivity at melting point (dotted) where the emissivity at their melting points is greater than 5 x 10^4 Am^{-2}.

2.1.4 Cathode evaporation

A wide number of materials can be used for thermionic emission. The important factors in choosing a material are the operating temperature, the emissivity of the cathode, the chemical stability of the material and the surface regression rate (due to evaporation) at the required temperature. To maximise the brightness of the generated electron beam, the material should have a low work function and consequently a high emissivity. This allows operation at a lower temperature for the same emission area. However, to reach the higher levels of emissivity required for intense electron beams used for materials processing, the material must remain chemically stable at high temperature, and not evaporate at too high a rate as this would change the critical dimensions of the cathode and thus lead to a short cathode lifetime (Tsong and Mueller, 1970). The application for the gun will largely determine the allowable tolerance on the cathode dimensions. In applications where the beam characteristics do not need to be closely reproduced, the through-life cathode evaporation could be 50 µm – inferring a tungsten lifetime of some 300 hours. However, for focussed electron beams for the applications of interest in this work, cathode dimensional tolerance is

frequently required to be better than 5 µm (Bakish and White, 1964) inferring a tungsten cathode lifetime of at most 30 hours. During the 1950's a number of high emissivity materials were identified (Lafferty, 1951). For example, lanthanum hexaboride is today a common material for electron gun cathodes.

Within this work a useful plot, Figure 2-3, was compiled that showed the surface evaporation rate vs cathode emissivity with data that was gathered from a number of publications (Davis et al., 1986; Iiyoshi et al., 1996; Jones et al., 1927). Due to the lower work function of lanthanum hexaboride compared to tungsten and tantalum, it produces a high electron emission at a lower temperature. At emission temperatures it has a low rate of evaporation, indicating that this material offers a long cathode life.

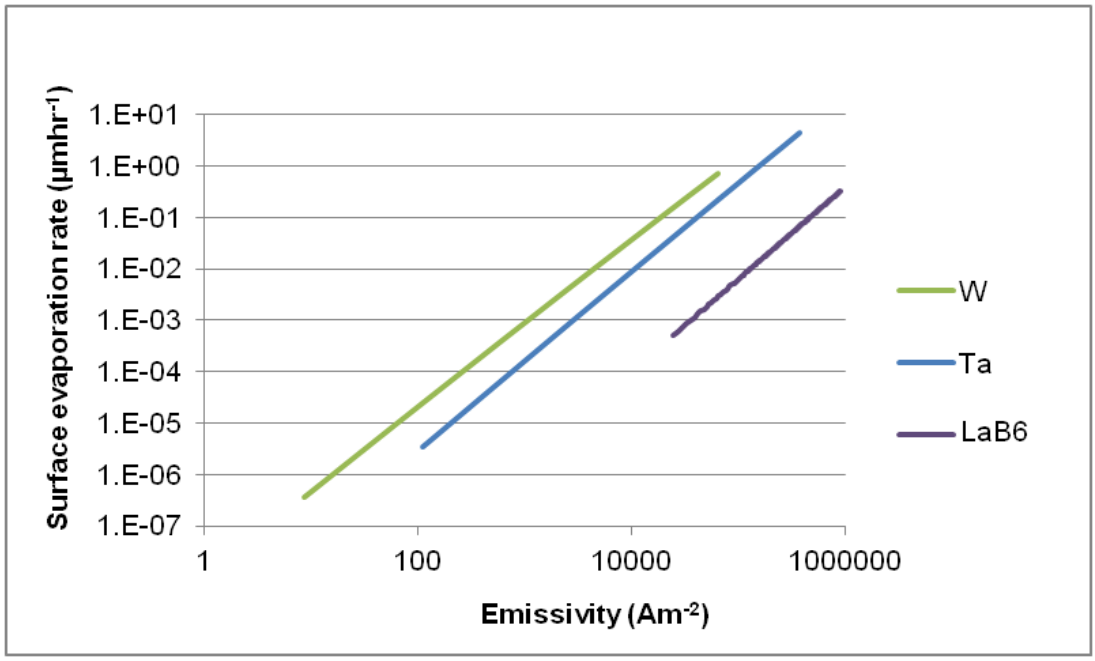

Figure 2-3 Comparison of surface evaporation rate vs emissivity for tungsten, tantalum and lanthanum hexaboride.

2.2 Space charge limited emission

In the design of electron guns it has often been found beneficial to limit the beam current to less than the thermally saturated current predicted by Richardson (Eq 2-3). This limitation occurs when the electric field is insufficiently strong such that the slow moving electrons near the cathode

surface form a space charge field that produces an additional potential barrier preventing the full current from being extracted. Only the higher energy electrons can overcome this barrier. In this way, irregular emission levels due to variances in the cathode surface, such as crystal orientation or chemical contamination, can be evened out. The phenomenon was first described by (Child, 1911) who produced an equation describing the current drawn from an unsaturated cathode (i.e. more current could be drawn with increased electric field strength at the surface) as a function of the electric field in a planar diode in vacuum. This law was enhanced by Langmuir and Fry (Fry, 1923; Langmuir, 1923), who derived an equation for the energy distribution of the electrons overcoming the potential barrier in front of an unsaturated cathode.

$$J = \frac{4}{9}\varepsilon_0\sqrt{\frac{2e}{m}}\frac{V^{\frac{3}{2}}}{d^2} \qquad \text{Eq 2-5}$$

where

ε_0 is the electric constant, 8.854 x 10^{-12} Fm^{-1}

$\frac{e}{m}$ is the charge to mass ratio of the electron, Ckg^{-1}

V is the voltage across the planar diode, V

d is the distance between the plates, m

Electron guns where the beam current is controlled by the cathode temperature (Eq 2-3) are usually diodes, and those where the beam current is controlled by the potential on a third electrode (Eq 2-5) are usually triodes. These are the main two types of electron guns for material processing. The differences in their operation are illustrated by the models described below.

A model of the cathode region of a diode gun is shown in Figure 2-4. The model is axi-symmetric and only the right hand side of the cross section of the cathode region is shown. The turquoise region represents the cathode and in this case the work function of lanthanum hexaboride and a temperature of 1650 K was entered into the modelling software to allow the

emissivity to be calculated, given the electric field near the surface. With this particular geometry a beam current of 33.4 mA was produced, and the 20 beamlets that together carried this current are seen to be near parallel as they leave the cathode.

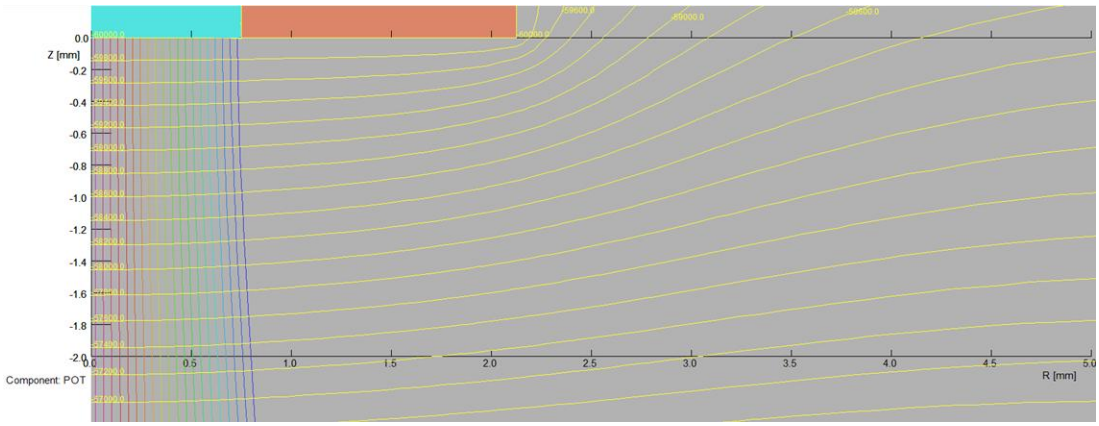

Figure 2-4 Finite element model showing the right hand side cross section of the cathode (turquoise) region of a diode gun. The equi-potential lines are shown in yellow and the beamlet trajectories colour coded by radial position of launch from the cathode surface.

Space charge played only a minor role in modifying the electric field near the cathode and therefore had an insignificant effect on the beam current emitted and has negligible effect on the electric field further from the cathode as the electrons are accelerated and their charge becomes less dense. A plot of space charge density for the diode gun examined is shown in Figure 2-5 and the highest space charge of -7.82 mCm^{-3} was within 0.1 mm of the cathode surface.

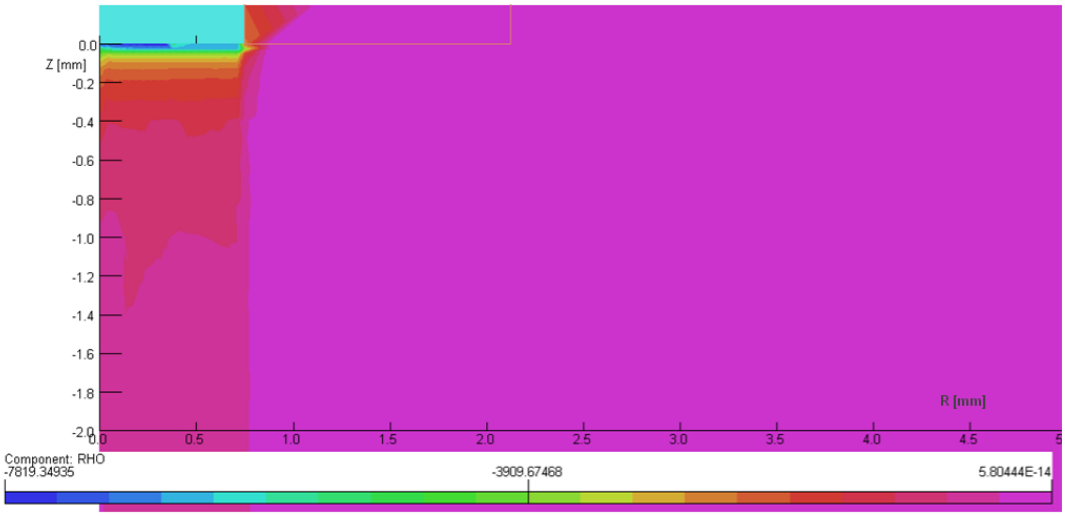

Figure 2-5 A plot of the space charge in the cathode region of a diode gun. The highest space charge of -7.82 mCm^{-3} was within 0.1 mm of the cathode surface.

For a triode gun a very similar model was created with the addition of a small, annular control electrode put in front of the cathode. The cathode temperature was increased to 1850 K to ensure that the emission would be controlled by the bias potential. A sweep of bias potential was carried out and the gun modelled at each level. From this was found the bias potential required to give a similar beam current to the diode gun with a cathode at 1650 K. It was found that at a bias potential of -60.46 kV a beam current of 32.6 mA was produced, i.e. a very similar current to that produced by the diode configuration with the cathode at a lower temperature. The equi-potential lines and beamlet trajectories are shown in Figure 2-6.

It can be seen that the -60 kV equi-potential line had a triple point on the cathode. Beamlets launched from a radius greater than the radius of the triple point did not form part of the beam but instead were in a region of reversed electric field and were accelerated back onto the cathode surface. In this way the bias field irised the cathode, allowing only the central area to contribute to the beam.

In addition, the equi-potential lines in front of the cathode were more widely spaced than can be seen for the diode gun in Figure 2-4, as the electric field was reduced. This reduced the emission from the surface as

predicted by Child's law (Eq 2-5), and space charge was increased in this region.

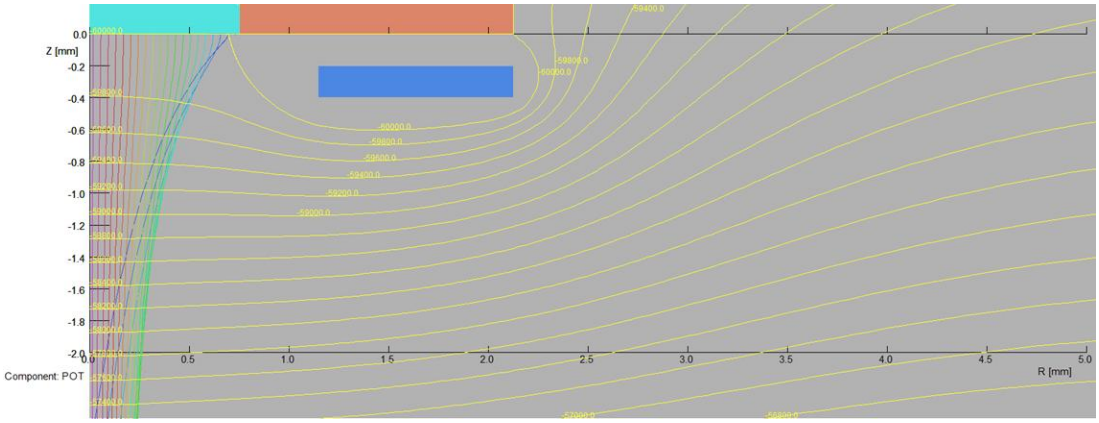

Figure 2-6 Finite element model of the cathode region of a triode gun. The bias voltage of -60.46 kV was applied to the annular bias electrode (shown in blue) whilst the cathode was at -60 kV.

The space charge for the triode gun can be seen in Figure 2-7. It was considerably higher than for the diode gun by a factor of greater than 6 at a maximum value of -49.1 mCm^{-3}.

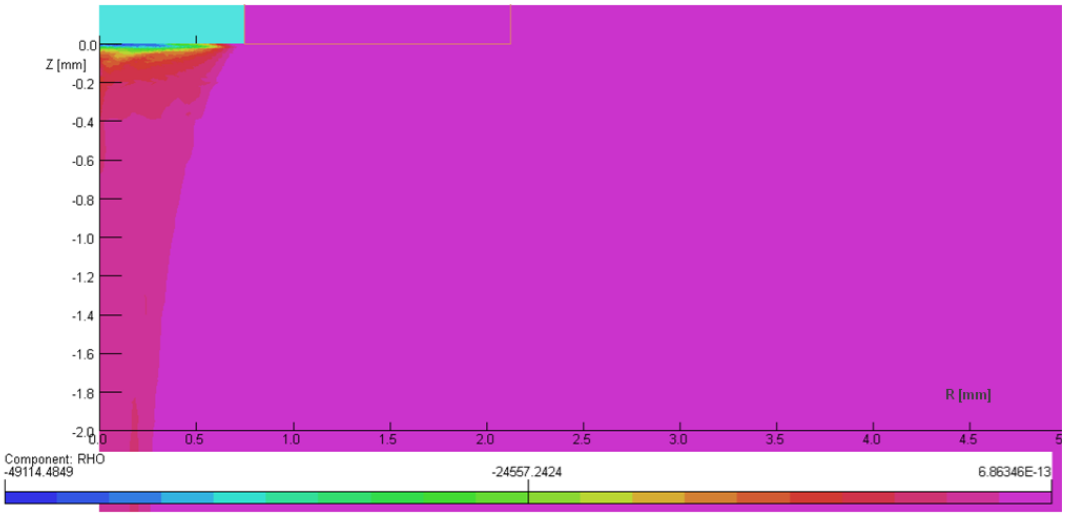

Figure 2-7 A plot of the space charge density in the cathode region of a triode gun. The highest space charge density was within 0.1 mm of the cathode surface but was more than 6 times greater than for the diode gun.

The distribution of the space charge modified the electric field such that emission across the triode cathode was no longer even. This can be illustrated by the sampled beam current density at a plane spaced 0.1 mm

from the cathode surface. This comparison is shown in Figure 2-8. Whereas the diode beam current density sampled across the beam radius was even, as no surface irregularities have been modelled, the triode beam current density at the centre was greater than 6 times the beam current density at the edge of the beam. This effect can be used to provide an intense electron source from a triode, however this benefit is countered by the strong curvature of the field in a triode near the cathode, which can lead to beam aberration and a reduction in beam intensity at the work piece.

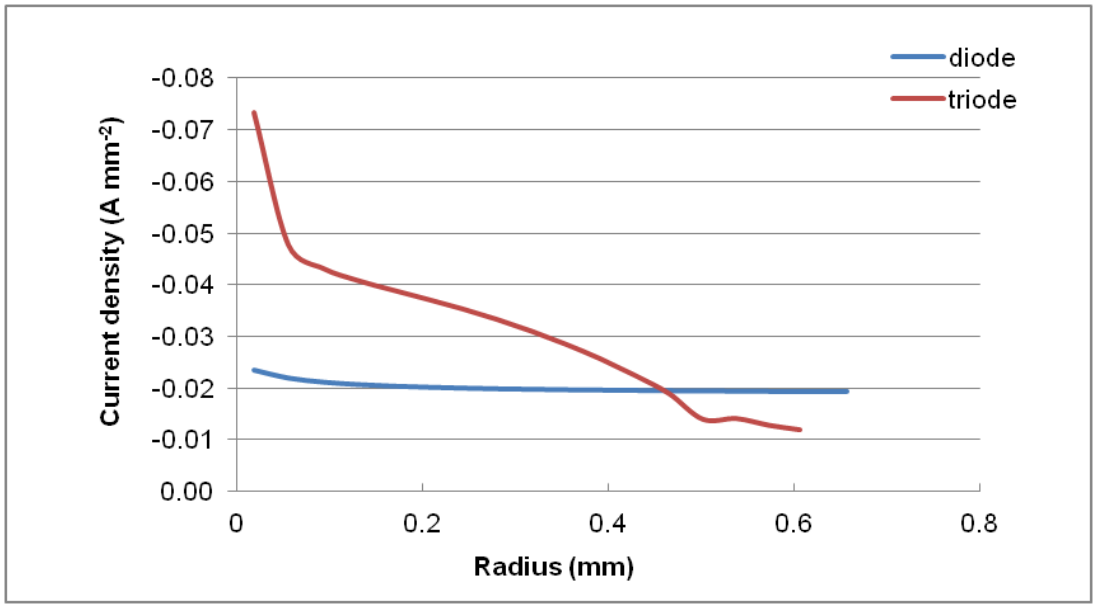

Figure 2-8 The beam current density sampled at a plane 0.1 mm from the cathode surface - comparing a diode with a triode gun.

Space charge plays an important role in the emitted current and beam envelope shape from triode guns but has only a minor role in determining the emitted beam current for diode guns. Space charge can influence the beam envelope shape from diode guns though, as the beamlet trajectories are very sensitive to changes in electric field near to the cathode surface.

2.3 Beam brightness and emittance

For many applications, intense beams are required, e.g. thick section and narrow fusion zone electron beam welding, and are only possible to produce with intense and parallel beams, or X-ray generation where the resolution of the X-ray equipment is in part dependent upon the intensity of

the focussed electron beam. Brightness is defined as the ratio of beam intensity to solid angle and with perfect electron optics remains invariant along the beam path from the cathode to the focal position. For deep section welding, which for electron beams refers to beams penetrating metals several hundred millimetres thick, the beam is also required to maintain its intensity throughout the penetration depth. Thus the beam must have low angle.

The combination of high beam intensity with low angle is quantified as beam brightness. This combined quality can also be described by the similar metrics of beam emittance and beam parameter product, and these are described below.

In a thermionic emitter the range of the electron energies coming from the cathode is termed the thermal velocity spread. It causes a spread of trajectories through the electron gun and focussing optics and has the effect of fixing the maximum beam brightness that could be obtained from a cathode of a defined size and temperature. This result can be illustrated readily for a saturated planar diode where the electron paths are not curved, see Figure 2-9. The electric field E is in the Z direction. The electron, e^-, velocity vector, v_e, can be resolved into a component from the acceleration field, v_v, and a component from the average thermal energy of the electron, v_t. This value can be calculated by considering the distribution of the high energy tail of electrons escaping the cathode surface and is related to the cathode temperature (Septier, 1967).

The vector additions of these two velocities for a range of electron temperatures defines a beam half angle, *Ang*.

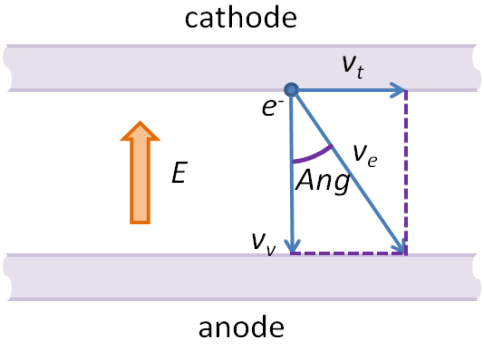

Figure 2-9 An electron leaving the cathode in a planar diode will be accelerated to a velocity by the acceleration potential in the Z direction, and will have an average thermal velocity in the radial direction, defined by the cathode temperature.

The electron beam brightness is a fundamental property of a gun and remains the same value from the cathode to the work piece, neglecting any degradation by aberration introduced by electron optical elements. It is defined as the ratio of the beam intensity to the solid angle, and so tends to infinity as the beam tends towards being parallel. Fundamentally, the beam cannot be parallel due to the thermal velocity spread described above.

The intensity at the cathode can be calculated from the emission current density, dependent on temperature and material properties as described by the Richardson – Dushman equation, see Eq 2-3. Consequently, the maximum beam brightness obtainable from a cathode can be derived from the average transverse velocity, which will be determined by the cathode temperature, Eq 2-6, and the average axial velocity, which will be determined by the accelerating potential, Eq 2-7:

$$\frac{1}{2}mv_t{}^2 = kT \qquad \text{Eq 2-6}$$

$$\frac{1}{2}mv_v{}^2 = eV \qquad \text{Eq 2-7}$$

where

v_t is the transverse component of the electron velocity, ms^{-1}

v_v is the axial component of the electron velocity, ms^{-1}

For small angles we can compute the solid angle of this beam:

$$\Omega_{\min} = \frac{\pi kT}{eV} \qquad \text{Eq 2-8}$$

So the highest brightness from a gun with these cathode characteristics is given by:

$$B_{max} = \frac{J}{\Omega_{\min}} \qquad \text{Eq 2-9}$$

where J and Ω have been computed for the cathode temperature. This is a useful result, as assuming the beam brightness is invariant (i.e. not lowered by electron optical aberration) it allows the minimum achievable beam spot size to be calculated at the work piece if the beam current and beam angle are also known. It should be noted that the beam brightness will increase with cathode temperature due to the exponential term in the emissivity, Eq 2-3, dominating over the increase in transverse velocity.

The beam parameter product is used in laser beam processing (ISO, 2005), and has started to be adopted in electron beam processing by some users. It is defined as:

$$BPP = \frac{\theta d_f}{4} \qquad \text{Eq 2-10}$$

where

θ is the total included beam angle, rad

d_f is the beam diameter at focus, mm

As, for small angles

$$\Omega = \frac{\pi\theta^2}{4} \qquad \text{Eq 2-11}$$

Therefore, brightness, the ratio of beam intensity to beam solid angle, is a function of beam parameter product and beam current:

$$B = \frac{i}{\pi^2 BPP^2} \qquad \text{Eq 2-12}$$

There are various methods to define the beam diameter. For symmetrical laser beams the D4σ definition is used widely (ISO, 2005),

which is the width of 4 standard deviations. For electron beams it is more common to use the full width at half maximum, which is a measure less prone to variation due to low current fringe beam or electrical noise.

Emittance is a measure of the distribution of beam angle and current density over the beam cross section (Lawson, 1977; Koleva et al., 2001). It can be defined in a number of ways but the most common one is to consider it to be the area of an ellipse that contains the beam when the particles intersecting a sample plane are plotted in phase space. For example, with the particle momentum vector angle vs its X position, see Figure 2-10, which plots beamlet trajectory data extracted from a gun simulation where the beam was accelerated in the Z direction. Each point plotted was a beamlet, which carried an associated current. The beam was diverging as the trajectory velocity vector angle generally (but not always) had the same sign as the X position. Some of the beamlets had a current level that was very low, such that they may not be considered significant if they were determining the emittance. As the model was axi-symmetric, the result was the same in the Y direction. In this case the units of emittance were in mm mrad, and this was a measure of the transverse emittance in the X direction. The longitudinal emittance is a measure of the momentum distribution in the same direction as the beam acceleration.

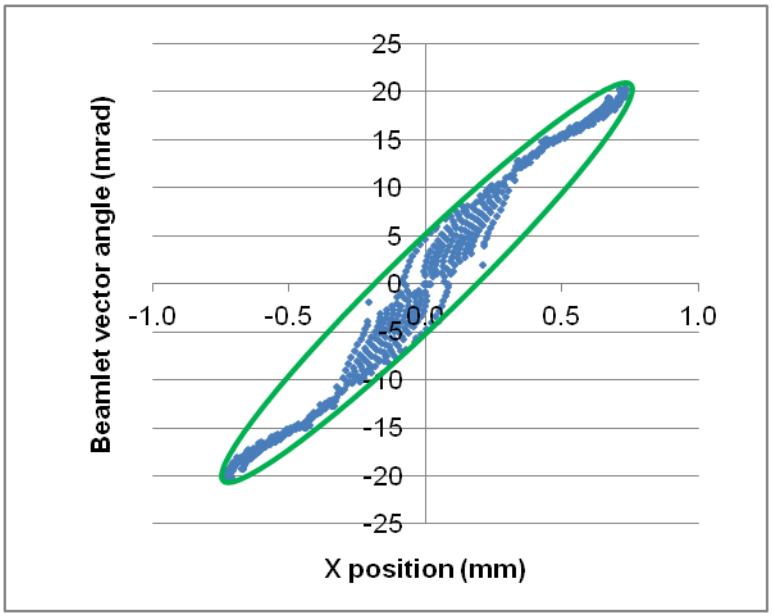

Figure 2-10 A beam sampled at a Z position and plotted in phase space. The green ellipse has an area equivalent to the beam emittance.

In a similar manner to brightness and beam parameter product, emittance remains invariant for a fully accelerated beam and is an inherent characteristic of the beam resulting from the gun design. As the accelerating potential is increased, the Z momentum increases and the vector angle (plotted on the vertical axis) tends to get smaller leading to a reduction in the ellipse area and therefore a lower emittance.

The emittance is a useful characteristic for beam accelerators, where the desired beam is parallel, as it provides a quantified measure of the non-parallel nature of the beam. However, material processing beams are seldom required to be parallel, as they are normally focused to give a higher intensity. Also, the power levels involved make practical measurement difficult as this requires sampling of the beam at two Z positions to determine the angular components of the beam over its cross section.

2.4 Gun design methods

2.4.1 Non-computational methods

Successful gun design requires an appreciation of electron emission (as described above) and the focussing of electron beams that can be

achieved as they are accelerated. Early cathode ray tubes and electronic valves used electron guns designed using simple geometric shapes for the electrodes. The invention of the electron microscope (v. Borries and Ruska, 1939) gave impetus to the refinement of electrode designs to maximise their resolution. Further to this, high current and high voltage electron guns were being developed for applications in radio and television – for example the klystron tube (Varian and Varian, 1939). High voltage and high power electron beams for welding applications were first demonstrated during the late 1940s and 1950s by Steigerwald in Germany, Stohr in France and Wyman in the USA – and were developed from transmission electron microscopy and oscilloscope equipment designs (v. Dobeneck, 2007), see Figure 2-11:

Figure 2-11 The first purpose built electron beam materials processing machine designed by Dr K. H. Steigerwald for Zeiss AEG in 1951 for "welding, joining processes, drilling, material-removing processes, engraving, material modification and refining" (by permission, pro-beam).

This machine operated at 125 kV and generated beams of up to 3 kW power. Its first use was for drilling jewel bearings for watch and clock making, but wider use of this type of equipment for welding and micro-machining was investigated from 1952 onwards.

Electron gun perveance is a quantified measure of the importance of space charge to the electron flow. It is a constant for a given geometry. It relates the beam current to the accelerating potential and is derived from Eq 2-5:

$$I = PV^{\frac{3}{2}} \qquad \text{Eq 2-13}$$

where

P is the perveance given by:

$$P = \frac{4}{9}\varepsilon_0\sqrt{\frac{2e}{m}}\,\frac{1}{d^2} \qquad \text{Eq 2-14}$$

where

d is the distance between the cathode and anode, m

The design of guns to give higher current beams at the same accelerating voltage, that is to say higher perveance designs, required new approaches to avoid beam aberration due to the mutual repulsion of the electrons, particularly as they are first emitted from the cathode. In particular, the Pierce gun geometry was developed that used focusing electrostatic fields to overcome beam spreading caused by space charge (Pierce, 1954).

The design optimisation of gun electrode shapes in order to produce bespoke beam characteristics required, at this time before the availability of significant computing power, the plotting of fields using an electrolytic tank as a physical analogy to the gun electrode space. Metal foils were used to form the electrodes and an AC current was passed between them. The voltage of the tank was probed to establish distribution of potential. This method was unable to simulate the beam space charge, and was therefore only effective for guns of low perveance. Using these simple design tools, low power electron guns became available to industry – particularly for aero engine manufacture, nuclear fuel encapsulation and for metal melting and refinement (Bakish and White, 1964).

As computing power became available, the first electron optical software for the design of guns and optics was developed initially for accelerator experiments – notably at Stanford University (SLAC) in USA (Herrmannsfeldt, 1988) and Rutherford Appleton Laboratories (RAL) in UK (Biddlecombe and Simkin, 1983). Computer analysis of electron gun designs allowed design of guns producing higher beam powers. Highlights included developments during the 1970's and 1980's by Steigerwald, Sciaky and TWI (v. Dobeneck, 2007).

2.4.2 Present day electron gun modelling software

The design of electron guns, lenses and deflection systems has advanced significantly since the introduction of computer modelling of electrostatic and electromagnetic systems. In particular, development of high power guns used for welding and melting, where space charge plays a significant role in determining the beam qualities, has depended upon accurate modelling. The programs from SLAC and RAL have been developed further in scope and capacity, taking advantage of computer hardware developments, and are now available as EGUN and the Opera software packages respectively. There are now many other electron gun analysis programs available, such as MICHELLE, CST and CPO.

The modelling software used in this research was the Opera 2D modeller and the space charge solver module (Cobham, 2012a). This choice was made as the author had many years experience in using this software for electron gun design, and a good degree of confidence in the accuracy of simulation. The vast majority of electron guns used for material processing are axi-symmetric and can be effectively analysed in 2-D, saving computing time. The exceptional gun types requiring 3-D modelling are those producing sheet beams for evaporators and guns using an array of cathodes, for example. The modelling of a gun geometry using this software is carried out in the following steps:

2.4.2.1 Geometry model

Electron guns usually comprise of metal electrodes separated by a vacuum gap. The surface of the metal electrodes becomes a boundary to the vacuum space where the electric field is distributed. In some cases, dielectric material may be within the gun region, and this must be modelled as it will affect the distribution of potential and the electric field. The initial stage in simulation involves drawing the geometry of the gun electrodes. The software operator can manually enter the geometry, or import these from a drawing file. The model is divided into regions, where each region can be assigned different electrical properties, in particular electrical permittivity. The software can model in 2-D for XY symmetry or axi-symmetry, so at this stage the software option for axi-symmetric modelling is normally selected for electron guns. Essentially, the geometry consists of a number of coordinates connected together by lines which may be curved. Each region is divided into a mesh where the crossing points of the mesh and the centres of the triangles formed are a set of points where the field will be resolved. The mesh can be varied in its resolution so that high resolution can be used near the beam, especially near the cathode, whereas further from this region lower resolution will not compromise accuracy of the simulation, see Figure 2-12.

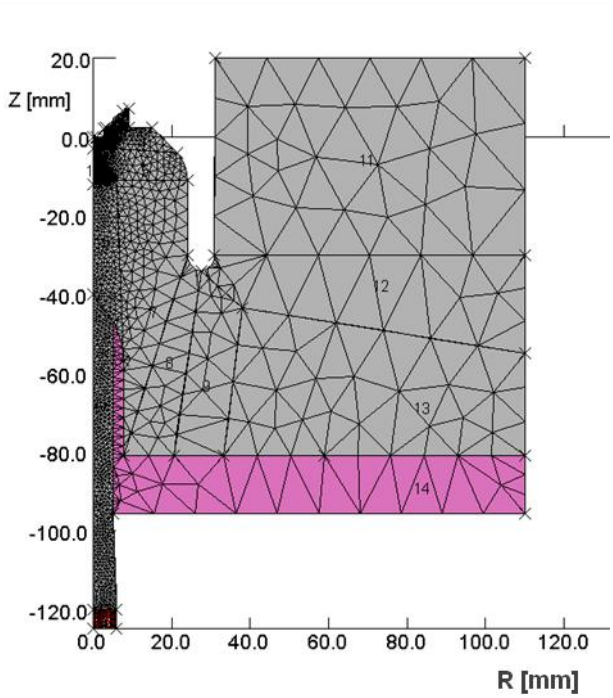

Figure 2-12 Half section of modelled gun geometry showing meshed regions.

2.4.2.2 Boundary faces

The boundary of an electron gun model is the gun electrodes which can be set to a defined potential. This sets all of the nodes along the face to be the same potential. Typically, the anode and gun enclosure is at 0 V, and the gun is at -60 kV to -150 kV. If the gun is a triode, the bias potential on the grid electrode must be set as a boundary condition as well.

2.4.2.3 Cathode definition

The cathode is defined as one face, normally one that is a boundary of fixed potential. The cathode is represented by a number of beamlet emissions distributed along the face. Each beamlet represents the beam current emitted from an area of the cathode defined by the emission point spacing. At this stage, the cathode is defined as a one-dimensional Langmuir-Fry model (Fry, 1923), with a single beamlet emission at each position, see Figure 2-13. The parameters for modelling the cathode are the material work function and its temperature. There are many different cathode models, the simplest using Child's law for emission current calculation. However, this is not representative of thermionic emission in many cases, as

the reversal in electric field immediately in front of the cathode, caused by space charge accumulation, can lead to beamlets being launched but then being returned to the cathode surface. The one-dimensional Langmuir-Fry model looks in front of the cathode face at a position defined by a sampling distance to measure the electric field to calculate the beamlet current. The sampling distance is typically 50 µm. The beam will be launched not necessarily at the cathode surface but rather at the furthest forward position that has the same potential as the cathode surface. The emitter parameters are stored in a separate file with the same route name as the geometry file.

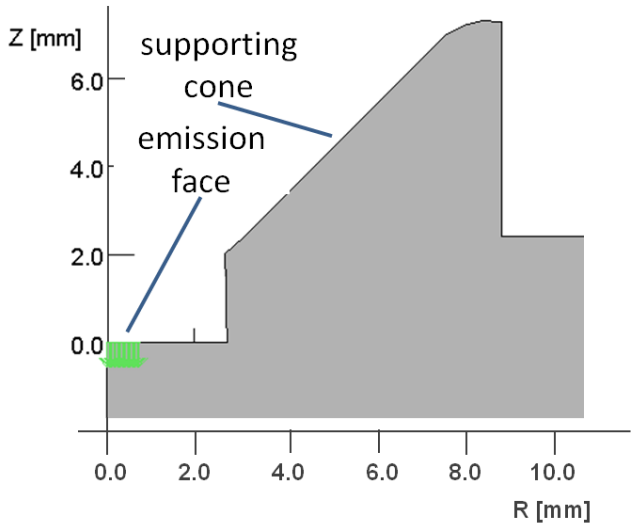

Figure 2-13 Definition of the cathode face – detail in cathode region shown.

2.4.2.4 Solution

The space charge solver is run and the geometry and emitter file opened by it. The solver initially finds a solution to the Laplace equation at all the nodes in the model, which describes the potential distribution in the absence of charges. Thus the potential distribution and its gradient, the electric field, are found. The beamlet currents from the cathode can then be calculated, and their trajectories plotted through the model. The space charge solver then recalculates the potential distribution, but this time using Poisson's equation to take into account the presence of the space charge in the electron beam. The beamlet emission currents are recalculated and trajectories re-plotted, and this process is continued for a number of iterations until the solution is converged.

Following this it has been found to be more accurate to use a model of the cathode that introduces thermal velocity spread, see Figure 2-14. This is achieved in the model by producing a set of trajectories from each emission point where the normal and tangential velocities are sampled from a Maxwellian distribution – this being a close approximation to the Fermi-Dirac distribution in the high energy tail of the energy distribution of electrons, see section 2.1.2 . The model is re-solved using this more complicated cathode with usually fifty to several hundred times as many trajectories, starting from the solution using the simpler cathode with a single trajectory at each point.

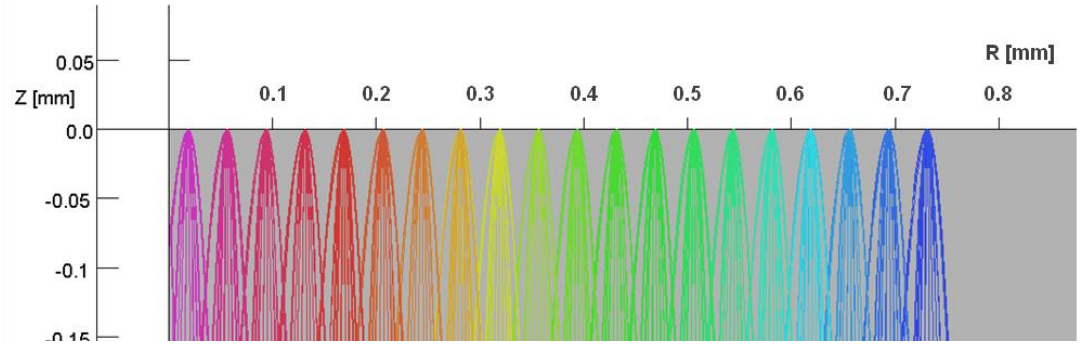

Figure 2-14 Cathode with normal and tangential velocity sampling from a Maxwell energy distribution. The trajectories are coloured to indicate their radial position of emission.

2.4.2.5 Post-processing

The post processor allows examination of the solution files. It is possible to map the potential distribution, the electric field distribution and space charge, for example. It is also possible to plot and interrogate the trajectory file – this can be seen in the cathode region in Figure 2-15.

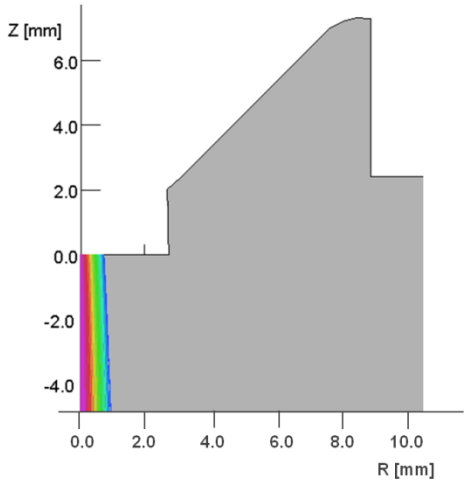

Figure 2-15 Beamlet trajectories leaving the cathode face. The trajectories are coloured to indicate their radial position of emission.

Most relevant for this work is to capture the trajectories at a plane after they pass through the anode so that the beam quality can be analysed. The post processor will generate a text file which lists, for each beamlet intersecting a sample plane, its position, vector and current. Figure 2-16 shows the model solution with a trajectory plot (very close to the axis) and equi-potential lines, in this case with a 1.5 kV spacing.

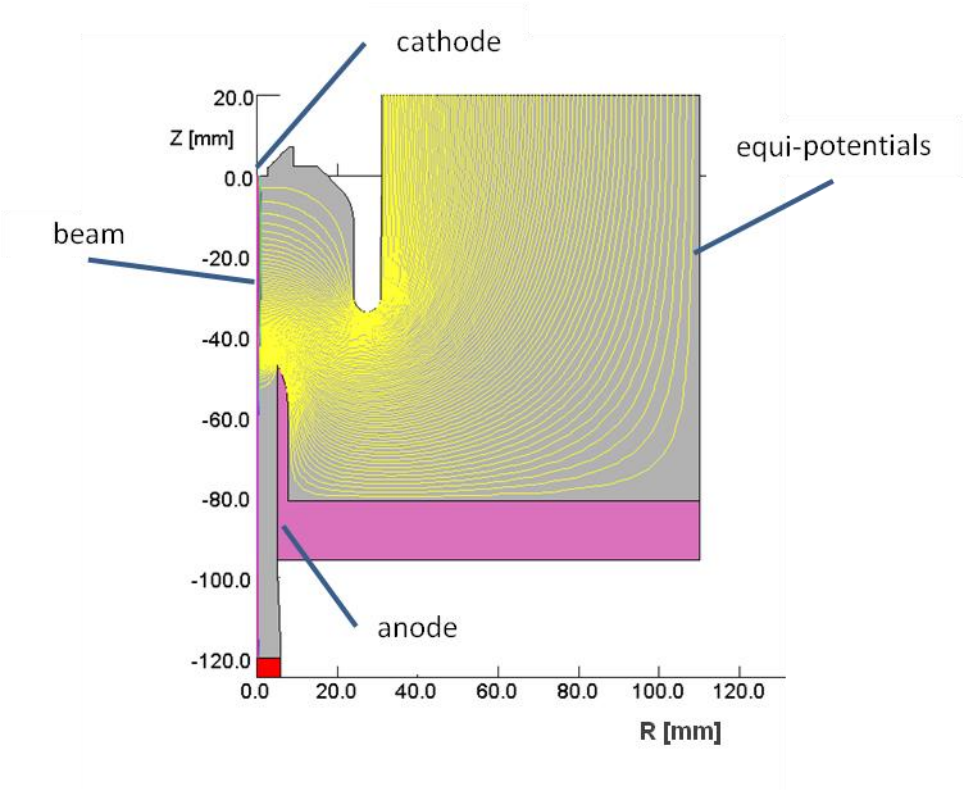

Figure 2-16 Solved model showing equi-potential lines and beam trajectories.

2.5 Quantified metrics of the electron beam characteristics

Some fundamental properties of the beam produced by an electron gun model can be extracted from the beamlet data, sampled for the fully accelerated beam after the anode. These are described below.

2.5.1 Electron source position and focus lens calculation

The electron source position, which is important for electron optical design, was found using a current weighted average of all the beamlets, back projected from their position and velocity vector at the sample plane to where they intercept the Z-axis, see Figure 2-17. This source position is either apparent (if it is behind the cathode) or real (if it is in front of the cathode).

$$z_{src\_imean} = \frac{\sum_{n=1}^{N} z_{src\_n} i_n}{\sum_{n=1}^{N} i_n} \qquad \text{Eq 2-15}$$

where

i_n is the current assigned to the nth beamlet, A

N is the total number of beamlets

z_{src_n} is the position where the n[th] beamlet projected backwards crosses the Z axis in mm, given for each beamlet by

$$z_{src} = z_{pos} - \frac{v_z}{v_r} r_{pos} \qquad \text{Eq 2-16}$$

where

r_{pos}, z_{pos} are the coordinates in mm of the beamlet captured from the model data at the sample plane

v_r, v_z are the velocity components of the beamlet in the radial and axial directions in mms^{-1}.

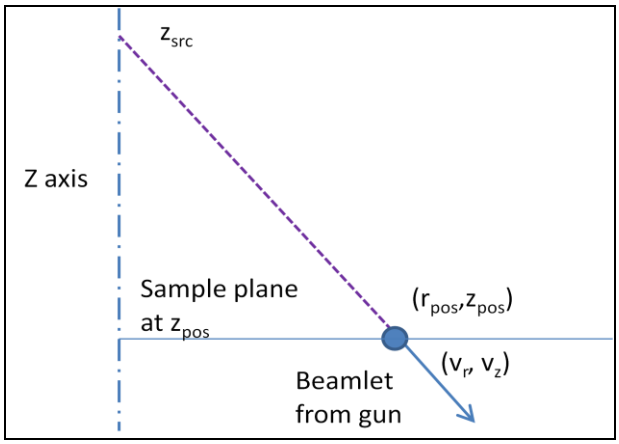

Figure 2-17 Back projection of one of the beamlets at the sample plane to find the beamlet source position - the current weighted average of all the Z axis intercepts is used to define the overall beam source position.

Electron beam guns for material processing normally project their beams some distance to the work piece, for example 500 mm. Typically, at least one electromagnetic lens is used to focus the beam. There may be other electron optical components in the gun column as well. In principle these can all be modelled. To retain accuracy, enabled by using a high resolution mesh, the number of nodes in a lens model is necessarily very high. This would normally make the computation time long, and probably too long for the optimisation algorithm to be efficient. However, there are a number of ways to overcome this problem. If the lens focal length can remain

constant (i.e. the gun source position remains constant) then the magnetic field does not need to be remodelled for every solution. Trajectory plotting can be carried out through the same magnetic field, and there is negligible effect from space charge when the beam is fully accelerated. Additionally, if the gun source position varies from one model to another, which would be typical, it may also be possible to simply scale the magnetic field of a single lens solution in order to adjust the focal length. However, choosing the scaling factor for the magnetic field may require some iterations which will take additional computing time. Especially within the context of this work, where many solutions will be carried out during the optimisation process, an alternative means of determining the beam characteristics at the work piece was developed.

For the types of electron gun used in material processing, electron lenses are invariably electro-magnetic solenoid coils. These can be shrouded with a magnetic soft material which boosts the magnetic field produced. Liebmann developed empirical formulae to estimate the focal length of such lenses in electron microscope applications (Liebmann, 1955).

$$f = \frac{24(S+D)V^*}{(NI)^2} \qquad \text{Eq 2-17}$$

where

f is the focal length of the lens in mm

S is the pole piece gap in the shroud in mm

D is the internal bore diameter of the shroud in mm

NI is the lens coil current excitation in A-turns

V^* is the relativistically corrected acceleration potential in V given by Eq 2-2

In addition, the spherical aberration introduced by such a lens (Septier, 1967) has been shown to be given by:

$$r_s = \frac{1.25(1+M)r_l^3}{(S+D)^2} \qquad \text{Eq 2-18}$$

where

r_s is the radius of confusion at the focal plane, mm

r_l is the radius of beam at the lens centre plane, mm

M is the lens magnification

For the work carried out, it was checked that the spherical aberration was insignificant in determining the spot size, and then the focal length of the lens and its position relative to the gun and work piece was used to calculate the landing position of the beamlets at the beam focal plane.

The optimum lens coil excitation was determined initially by calculating the virtual (i.e. behind the cathode) or real (i.e a beam cross over in front of the cathode) electron source position. The image distance from the lens centre plane to the focus position, e.g. at the work piece, is known from the gun column layout. Consequently, the Newtonian optic equation can be applied

$$\frac{1}{f} = \frac{1}{u} + \frac{1}{v} \qquad \text{Eq 2-19}$$

where

u is the distance from the lens centre plane to the calculated electron source in mm

v is the distance from the lens centre plane to the beam focus position e.g. at the work piece in mm

The required focal length of the lens was given by

$$f = \frac{(z_l - z_{src\_imean})(z_f - z_l)}{z_f - z_{src\_imean}} \qquad \text{Eq 2-20}$$

The radial distance of each trajectory at the focal position is calculated from similar triangles, see Figure 2-18, by

$$r_f = \frac{r_l(z_f - z_{cross})}{(z_l - z_{cross})}$$ Eq 2-21

where

r_f, z_f are the coordinates of the trajectory at the beam focal position in mm e.g. at the work piece surface

r_l, z_l are the coordinates of the trajectory at the lens centre plane in mm. r_l is found from:

$$r_l = \frac{(z_{src} - z_l)}{(z_{src} - z_{pos})} r_{pos}$$ Eq 2-22

z_{cross} is the position in mm where the trajectory crosses or virtually crosses the Z axis near to the beam focal position, given by re-arrangement of the Newtonian optics equation:

$$z_{cross} = z_l - \frac{f(z_l - z_{src})}{f - (z_l - z_{src})}$$ Eq 2-23

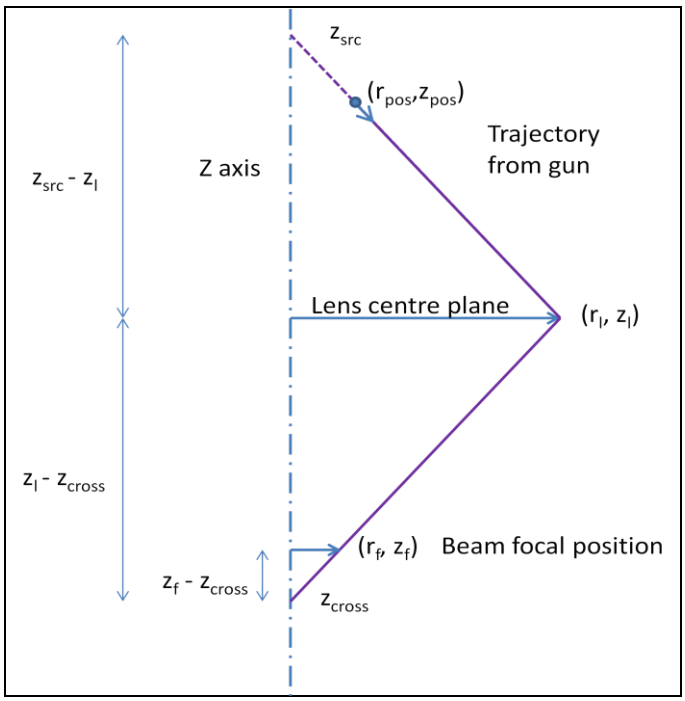

Figure 2-18 Projection of a trajectory from the gun with a position and velocity through a mathematical lens to a radial position at the beam focal plane.

Consequently, knowing the position of the lens and the required focal plane position, the radial coordinate of each trajectory at the required beam

focal plane could be calculated and using the beamlet current associated with each one, a beam intensity plot could be calculated. This was achieved by distributing the current from any two trajectories adjacent on the cathode to a midpoint between them at the beam focal plane. An example of a ray plot from the trajectory analysis is shown in Figure 2-19.

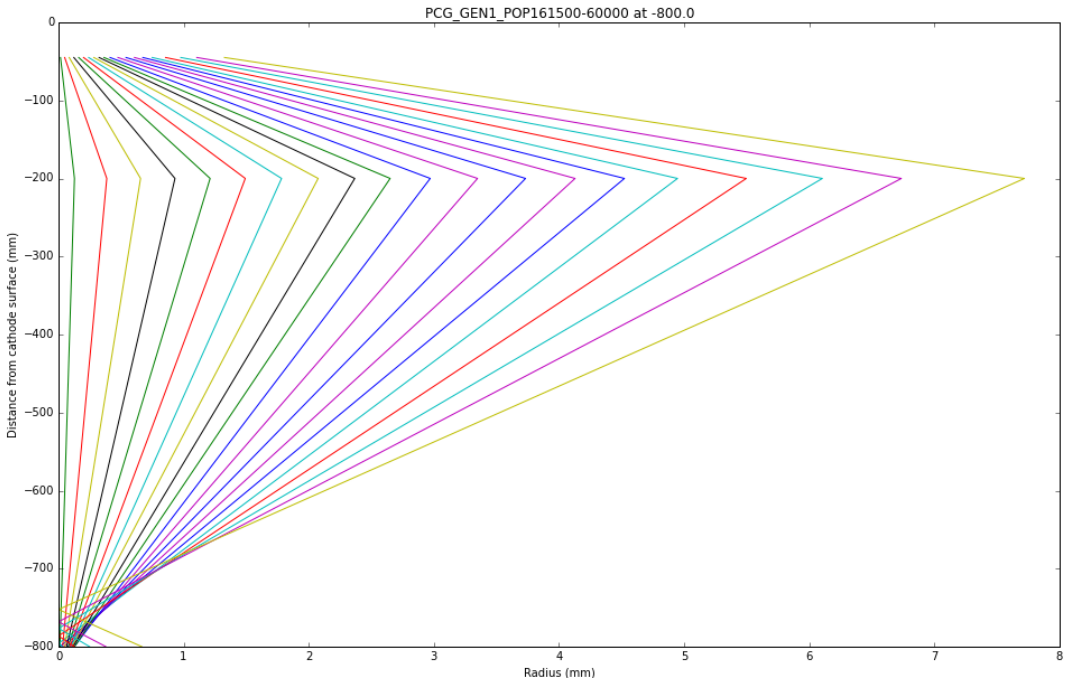

Figure 2-19 An example of a ray plot produced by projecting the beam from the sample plane in the gun region through a mathematical lens to the required focal position.

In electron optics, the circle of confusion is defined as the minimum waist in the beam envelope. Using the method described above, it was often found that the circle of confusion did not exactly correspond with the image plane. This was due to the spherical aberration introduced by the lens, or inherent in the characteristics of the beam generated from the electron gun, causing the Z position of the circle of confusion to be closer to the lens plane than the Z position of the image plane. The algorithm to find the optimum lens focal length was enhanced by introducing a search for the minimum FWHM value at the working distance for a range of focus settings. In this way, the lens strength was adjusted about the calculated value in order to minimise the beam width at the required working distance. This was found to give more consistent values for the beam width.

Three dimensional mapping of the beam intensity profile gives more intuitive results from the modelling, and it was found possible to convert the axi-symmetric results to three dimensions. As the model of the electron gun is two dimensional and axi-symmetric, each beamlet is representing a cylinder of beam current in three dimensions. As the radial position increases, the current assigned to the beamlet is spread across a larger area, and so the intensity decreases with the square of radius. To enable three dimensional intensity plots, the axi-symmetric beam intensity graph was converted through rotation into a map of the beam cross section. This is shown in more detail in the following section.

Visualisation of the model outputs has been found to be very useful in understanding and communicating results. However, within the context of this work, quantified measures of the beam characteristics were required to enable scoring of gun designs as part of the optimisation process and these are described in the following section.

2.5.2 Beam characteristics extracted from the model

Some fundamental characteristics of the beam from the modelled gun were extracted from the beamlet data using equations derived as follows.

2.5.2.1 Source radius

As the current weighted average Z position of the apparent or real electron source was calculated as described earlier in this section, the current weighted average radius of the beam at the source in mm was calculated from:

$$rad_{src\_imean} = \frac{\sum_{n=1}^{N} \frac{v_{r\_n}(z_{src\_n} - z_{src\_imean}) i_n}{v_{z\_n}}}{\sum_{n=1}^{N} i_n} \qquad \text{Eq 2-24}$$

where

v_{r_n}, v_{z_n} were the radial and axial velocity components of the n^{th} beamlet in mms^{-1}

2.5.2.2 Source intensity

The source intensity, in Amm^{-2}, was estimated from the source radius and the total beam current as follows:

$$Int_{src} = \frac{4\pi rad_{src\_imean}^2}{\sum_{n=1}^{N} i_n} \quad \text{Eq 2-25}$$

This was an estimate as the radius of the source was approximated to twice the current weighted average radius calculated above.

2.5.2.3 Beam divergence angle

The beam divergence angle, in radian, was calculated in a similar manner using a current weighted average method:

$$Ang_{imean} = \frac{\sum_{n=1}^{N} i_n \tan^{-1}(\frac{v_{r\_n}}{v_{z\_n}})}{\sum_{n=1}^{N} i_n} \quad \text{Eq 2-26}$$

For some types of electron gun the beam divergence angle is an important parameter e.g. where a near parallel beam is required.

2.5.2.4 Source brightness

The source brightness was estimated from the ratio of the source intensity and the beam divergence solid angle as follows:

$$B = \frac{Int_{src}}{2\pi(1-\cos(2Ang_{imean})} \quad \text{Eq 2-27}$$

This was an estimate as the total beam divergence angle was approximated to twice the current weighted average beam divergence angle calculated above, and the source intensity was approximated as described above.

2.5.2.5 Source position variance

The variance in the source position gave an indication of how closely clustered the source positions were for the beamlets. The perfect gun design would have had a source position variance of zero. This value was calculated as follows:

$$z_{src\_var} = \frac{\sum_{n=1}^{N} i_n (z_{src\_n} - z_{src\_imean})^2}{\sum_{n=1}^{N} i_n} \quad \text{Eq 2-28}$$

2.5.2.6 Beam divergence angle variance

This parameter was only useful for beams where the divergence angle of the beamlets was required to be the same e.g. for a gun that produced a parallel beam. It gave an indication of how similar were the divergence angles of the beamlets. It was calculated as follows:

$$Ang_{var} = \frac{\sum_{n=1}^{N} i_n (\tan^{-1}(\frac{v_{r_n}}{v_{z_n}}) - Ang_{imean})^2}{\sum_{n=1}^{N} i_n} \quad \text{Eq 2-29}$$

2.5.2.7 Current weighted average diameter of the focused beam

There were a number of possible ways to quantify the beam diameter at the work piece or beam focal position. The current weighted average diameter of the beam was calculated from the derived trajectory data and was found as follows:

$$CWAD = 2\ \frac{\sum_{n=1}^{N} i_n r_{f\_n}}{\sum_{n=1}^{N} i_n} \quad \text{Eq 2-30}$$

where

r_{f_n} is the radial position of the nth trajectory at the beam focal position in mm.

2.5.2.8 Full width half maximum (FWHM) and full width half power (FWHP)

The FWHM is the width of the beam spot at an intensity threshold of half of the peak intensity. It was found from the trajectory data and more specifically the intensity plot at the beam focal plane using a numerical method. It is widely used as a beam width metric, but is very sensitive to the peak intensity of the beam. A more useful measure is the FWHP, which is defined as the width of the beam containing half of the beam current. This was also found numerically from the intensity data at the beam focal plane.

Table 2-1 Summary of the beam characteristics derived from the model beamlet data.

Beam Characteristic	Calculation
Current weighted average source Z position	$z_{src\_imean} = \frac{\sum_{n=1}^{N} z_{src\_n} i_n}{\sum_{n=1}^{N} i_n}$
Variance in the current weighted average source Z position	$z_{src\_var} = \frac{\sum_{n=1}^{N} i_n (z_{src\_n} - z_{src\_imean})^{\,2}}{\sum_{n=1}^{N} i_n}$
Current weighted average beam divergence angle	$Ang_{imean} = \frac{\sum_{n=1}^{N} i_n \tan^{-1}(\frac{v_{r\_n}}{v_{z\_n}})}{\sum_{n=1}^{N} i_n}$
Variance in current weighted average beam divergence angle	$Ang_{var} = \frac{\sum_{n=1}^{N} i_n (\tan^{-1}(\frac{v_{r_n}}{v_{z_n}}) - Ang_{imean})^2}{\sum_{n=1}^{N} i_n}$
Current weighted average radius of the beam source	$rad_{src\_imean} = \frac{\sum_{n=1}^{N} \frac{v_{r\_n}(z_{src\_n} - z_{src\_imean}) i_n}{v_{z\_n}}}{\sum_{n=1}^{N} i_n}$
Estimated intensity of the beam source	$Int_{src} = \frac{4\pi rad_{src\_imean}^2}{\sum_{n=1}^{N} i_n}$
Estimated brightness of the beam source	$B = \frac{Int_{src}}{2\pi(1 - \cos(2Ang_{imean})}$
Calculated focal length of the lens	$f = \frac{(z_l - z_{src\_imean})(z_f - z_l)}{z_f - z_{src\_imean}}$
Current weighted average diameter of the beam spot at the focal plane position	$CWAD = 2\,\frac{\sum_{n=1}^{N} i_n r_{f\_n}}{\sum_{n=1}^{N} i_n}$
FWHM, FWHP	Derived by numerical means

2.5.3 Software code to derive beam characteristics

Software coding, to convert the trajectory intersect data into beam characteristics, was an essential step in providing a quantified assessment of the gun design. The software developed within this work used the concepts described in section 2.5.2. Initially, the real (i.e in front of the cathode) or

virtual position of the source (i.e. behind the cathode) was calculated using a current weighted average method on the trajectory data, see section 2.5.1. This position was used to find the object distance from a lens centre plane specified by the user. Although it was possible to simulate the lens field and plot the trajectories through it, this suffered from inaccuracies for the finite element modelling method used by Opera, and more accurate results were obtained using a mathematical model of the lens, which was accurate under the condition that aberration is small compared with beam focused spot radius – see Eq 2-18.

The software code developed could operate independently of the design optimisation code and could be used to assess a model or series of models. It also could be called from within the optimisation algorithm and the results yielded then used to derive a fitness score for the design, see Chapter 4.

2.5.3.1 Trajectory intercept data

The trajectory intercept data was the output from the modelling software that allowed assessment of the suitability of a gun geometry. During this work it was required that the gun was assessed over its working range of cathode temperature and electrode potentials. This required an algorithm to automatically generate this data for each of a number of geometries and to tabulate the beam characteristics.

Command files are scripts that execute a series of commands in Opera. Two command files were developed to first solve a series of model files listed in a text file, with the cathode temperatures and electrode voltages specified in an operating parameters file and the second command file to open the solved model, plot the trajectories and intercept these at a sampling plane, the position of which is also specified in the operating parameters file. The trajectory intercepts file was stored for later analysis.

The gun simulation software, in common with other similar programs, allowed a sample plane to be defined and then data was collected on the

beamlet trajectories that passed through this. This data was presented as a text file, as shown in Table 2-2. In this file the sample plane (intersection line) coordinates were given, and following this for each beamlet trajectory its current, position and velocity components in each direction. Despite being a 2-D modeller the software could model rotation of the beam – for example if it passed through a magnetic lens. The small Y position values and Y components of velocity were generated from rounding errors in the software. It should be noted that there is some inconsistency in the labelling of coordinates between the modeller and the trajectory intercept files. In the latter case Z always refers to the axial direction, and Y to a rotated radial axis perpendicular to X. In the former case Y and Z are interchangeable. The intersect line is actually defined in X,Z coordinates rather than X,Y as reported. The trajectory intercept file also gave the total current intercepting the sample plane.

Table 2-2 Example of a beamlet trajectory intercept file - the beamlet positions and velocity vector are given, and their assigned beam current.

Opening file for reading: C:\ dgnorm15_1600-60000_1.tracks							
Number of Intersections = 1000							
Intersection line :							
X1= 0.0 Y1= -110.0 X2= 6.0 Y2= -110.0							
Curvature= 0.0							
Current	X	Y	Z	Vx	Vy	Vz	POT
-2.534E-06	-5.892E-05	0.000E+00	-110	-4.918E+08	1.865E-16	-1.902E+11	0
-1.918E-06	-1.622E-04	5.752E-29	-110	-4.926E+08	4.015E-16	-1.902E+11	0
-1.905E-06	-2.076E-04	1.552E-28	-110	-4.930E+08	6.338E-16	-1.902E+11	0
-2.245E-06	-2.604E-04	2.689E-28	-110	-4.934E+08	9.041E-16	-1.902E+11	0
-5.018E-07	-3.137E-04	3.833E-28	-110	-4.938E+08	1.176E-15	-1.902E+11	0
e.g. 1000 rows of trajectory data of the format above							
-1.412E-05	-3.408E-01	1.364E-20	-110	-1.670E+09	1.977E-10	-1.902E+11	0
-1.865E-05	-3.413E-01	1.365E-20	-110	-1.673E+09	1.979E-10	-1.902E+11	0
Total current intersecting the line = -4.93809622990053E-03 [Amp]							
Integral of J = -0.016882322785503							
Closing connection to stream 1							

2.5.3.2 Beam characteristics output

Using the calculations described in sections 2.5.1 and 2.5.2 an algorithm was developed in Python to process the trajectory intercept files into beam characterisation data. This algorithm generated a table of data for each geometry, operated over a range of parameters – an example is given in Table 2-3:

Table 2-3 An example of the beam characterisation data derived from the trajectory intercept file.

Temperature (K)	1500	1550	1600	1650	1700
Bias (V)	-60000	-60000	-60000	-60000	-60000
total_current (A)	-0.0012	-0.0025	-0.0049	-0.0094	-0.0175
zsrc_imn (mm)	-74.6	-75.8	-82.4	-95.7	-111.9
zvar_imn (mm^2)	2221	2270	2662	9013	7271
rsrc_imn (mm)	-0.065	-0.067	-0.066	-0.062	-0.060
angdiv_imn (rad)	0.0069	0.0069	0.0069	0.0064	-0.0025
angdivvar_imn (rad^2)	7.18E-06	7.51E-06	8.09E-06	1.58E-05	5.14E-05
Area (mm^2)	0.0524	0.0566	0.0547	0.0482	0.0459
Omega (sr)	0.0006	0.0006	0.0006	0.0005	0.0001
Brightness ($Amm^{-2}sr^{-1}$)	-38	-73	-151	-386	-4850
f_lens (mm)	155.0	154.2	150.2	142.0	131.7
foc_d_imn (mm)	0.440	0.460	0.468	0.472	0.506
foc_fwhm (mm)	0.064	0.017	0.177	0.363	0.082
foc_fwhp (mm)	0.392	0.425	0.413	0.398	0.433
Max_diameter_at_-275 (mm)	4.34	4.31	4.22	4.06	3.81

The large change in brightness seen as the beam current increased was due to the beam current increasing and the beam angle decreasing, brightness being proportional to the ratio of these characteristics.

2.6 Beam characteristics at the work piece

Practical measurement of electron beams can be carried out with probe devices. There are many types of beam probe. They essentially sample current from either a small spot or from a narrow strip across the beam cross section.

As the beam for processing guns tends to be intense and of high power, the beam probe device is designed to be in the beam path for only a very short time, e.g. tens of microseconds so that the energy absorbed is kept to values well below 1 J and the beam path across the probe is traversed quickly.

Typical examples of probes include a spinning wire probe that rotates a wire across the beam, slit probes that collect the beam passing through a narrow slit (e.g. 0.1 mm wide) as the beam is deflected across it and pin-hole probes that that collect a 'pixel' from the cross section of the beam as the beam is deflected in a raster pattern over the probe, see Figure 2-20.

The pin-hole device will give the closest results to those generated by a three dimensional intensity map of the beam in the modelling software. This is useful for comparing performance of gun designs in the real world with modelled gun designs. Pin-hole probes have some limitation in the beam power that can be examined and in their resolution, which is determined by the diameter of the pinhole. At higher beam powers the more robust slit probes are more commonly deployed.

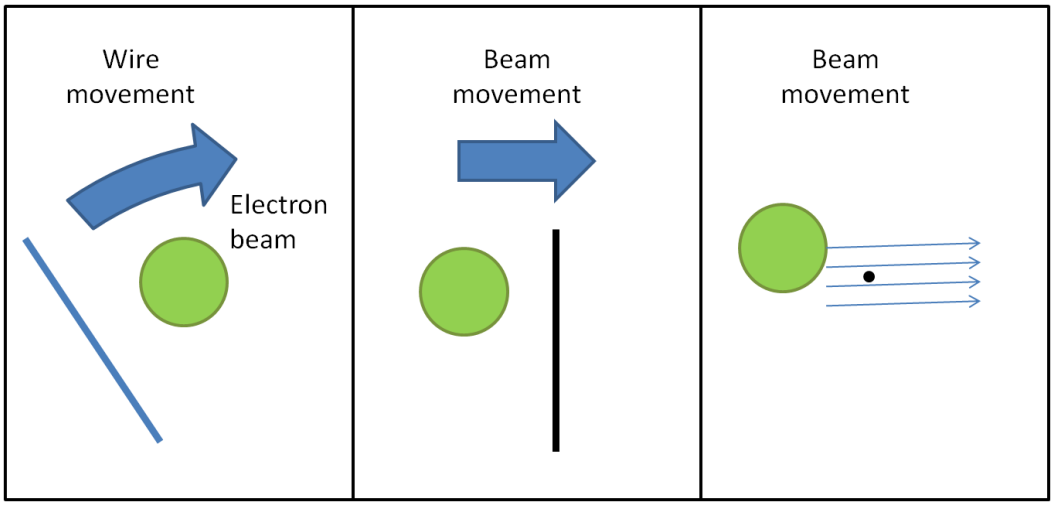

(a) A spinning wire probe - the collected signal will be an integral across a angularly swept chord of the beam

(b) A slit probe - the collected signal will be an integral across a swept chord of the beam - this may be linearly or angularly swept

(c) A pin-hole probe - the collected signal will be an intensity map of the beam cross section limited in resolution by the pin-hole diameter

Figure 2-20 Three methods of practical beam probing

2.6.1 Current density distribution measurement

There is no standard established for the measurement of electron beams although one does exist for laser beams as described in section 2.3. To avoid variation in measurement of beam width due to electrical noise, the FWHM measurement is normally used for electron beams.

Comparison of wire or slit probe measurements with computed results is best achieved by converting the intensity map generated into a probe trace by performing the swept integral of the beam with the appropriate probe width and motion relative to the beam. The FWHM measurement can then be made upon this derived signal.

The ray plotting algorithm developed in this work generated intensity data at primarily the focus position in Z but also at any other Z positions to allow the beam spot to be examined at focus and above or below focus. The intensity of the trajectories is captured in radial bins with a fixed interval so that there are sufficient bins to give detailed resolution. It was found that 40 bins gave a reasonable resolution, see Figure 2-21. This plot is for a 40 mA beam from a triode gun simulation and ray plot analysis.

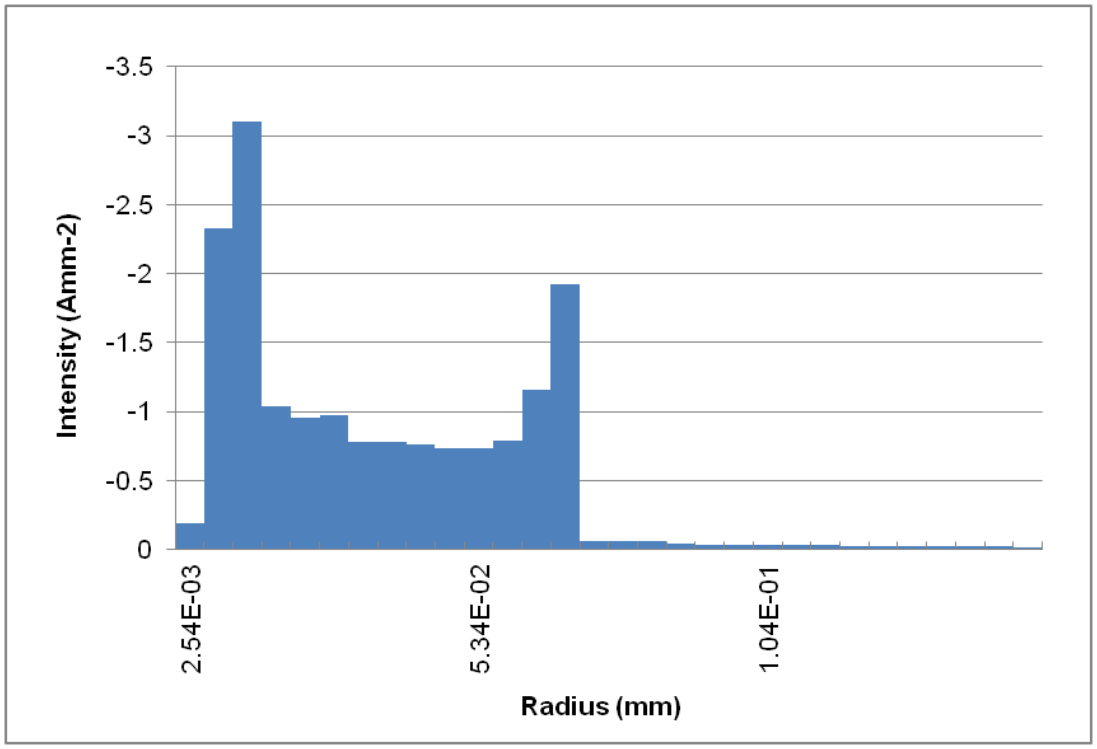

Figure 2-21 Example of a radial intensity plot from data collected by the ray tracing algorithm.

The data was directly plotted on a graph and also output to a data file for further processing. The graph gave a view of the radial intensity of half the beam. This was better presented as a 3-D map of beam intensity where the radial intensity is plotted as the vertical axis and the radial data is mapped onto an XY patch. The patch was divided into small elements and the calculated radial position of each element was used to look up the radial intensity.

The data generated from this gave a visually more intuitive plot, see Figure 2-22. The visualisation tool also allowed intensity data collected at different Z positions to be scrolled through, or similarly to allow beams focused at different Z positions to be examined through focus. This is similar to the view a machine operator would have as they looked at the beam whilst adjusting the lens focal length, by changing the coil current.

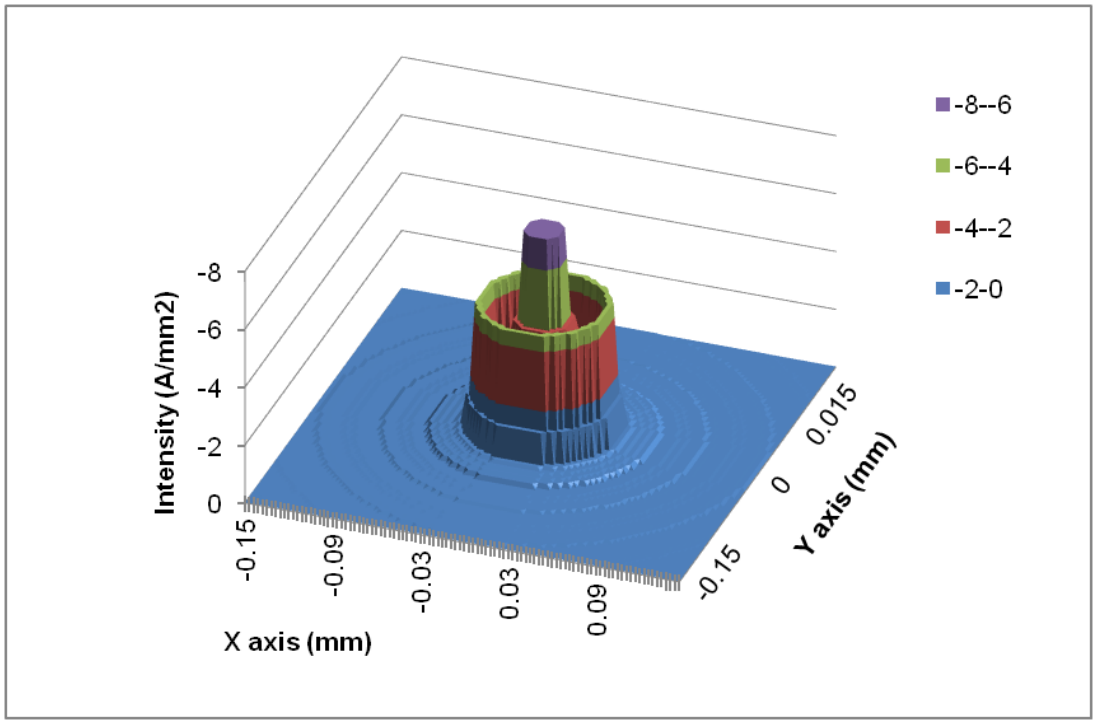

Figure 2-22 XY Intensity plot of the same data presented in Figure 2-21

It was possible to simulate probing of the beam. A pin-hole probe would allow a similar visualisation of the probe data to Figure 2-22. The probe resolution will be defined by the diameter of the pin-hole over which the beam is deflected in a raster pattern. Simulation of this for a 30 µm hole diameter is shown in Figure 2-23 for the same intensity data presented in Figure 2-22. It can be seen that much of the beam detail is lost even with this relatively small hole diameter, which is difficult to produce and maintain in practice.

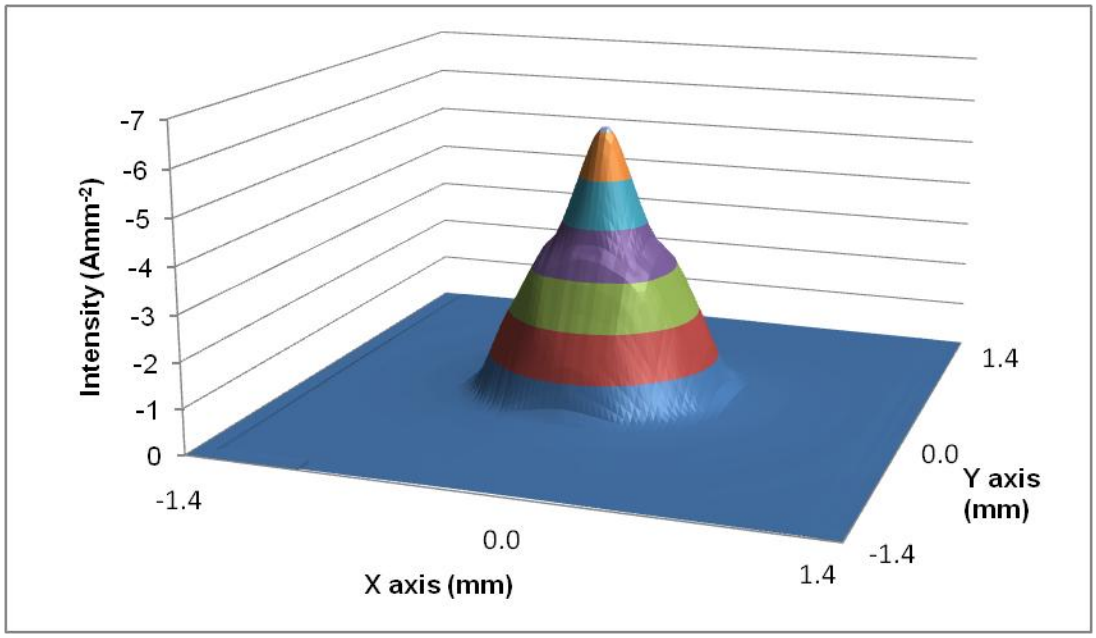

Figure 2-23 Simulated pin-hole probe measurement data for a 30 µm diameter hole showing lack of fine structure to the beam.

However, this type of probe is not typically capable of probing high power electron beams above ~10 kW as the beam dwells on the probe for too long, causing melting. At these beam power levels it is necessary to use a linear probe, either a wire or a slit probe. In these devices the beam is only on the probe for a short time and for a single transit. The data is collected as a signal, the time base of which is determined by the transit speed of the beam across the probe. The signal collected does not immediately give the intensity plot detail as the linear probe integrates across a long thin strip area as the beam is swept across the probe.

The simulation was carried out by entering the probe slit or wire width and its speed. This was then used as an integral interval and the data was integrated in strips. The intensity data was converted to current by multiplying by the area of the discrete elements, and the currents summed together over the probe area. The position axis was converted into a time base by dividing by the speed. The plot from this was representative of the signal from a probe looking at the example beam modelled, see Figure 2-24. Figure 2-24 (a) shows the trace that would be received if this beam was probed with a 0.1 mm wide slit or 0.1 mm diameter wire. As the probe radius

is comparable to the radius of the beam, much of the internal structure of the intensity map is effectively filtered to give a smooth trace. Figure 2-24 (b) shows the same intensity map being probed with what is practically the smallest possible probe slit or wire width of 0.02 mm. A little more detail is apparent, indicative of the more structured intensity map.

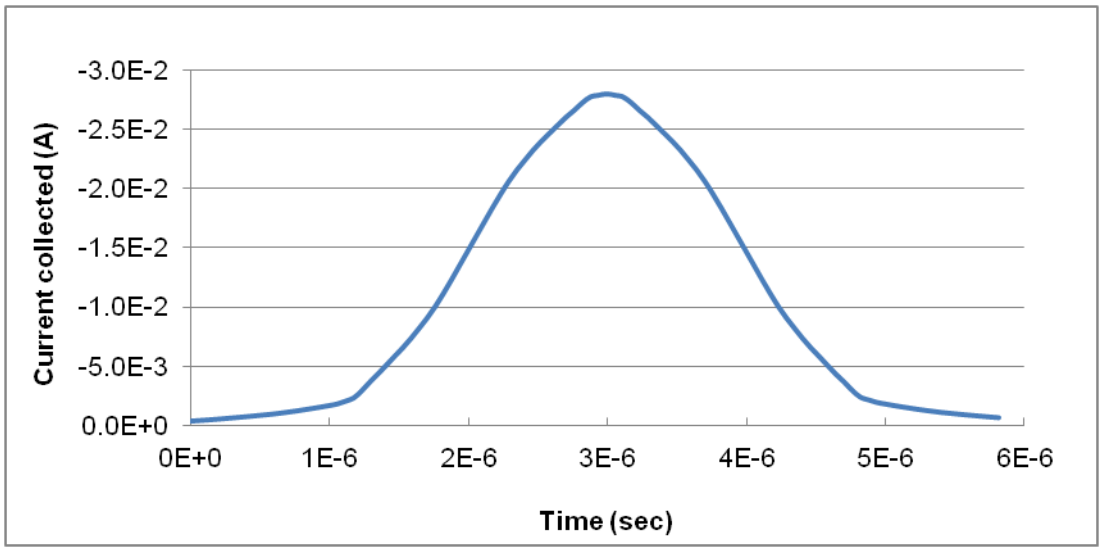

(a) A 0.1 mm wide probe trace

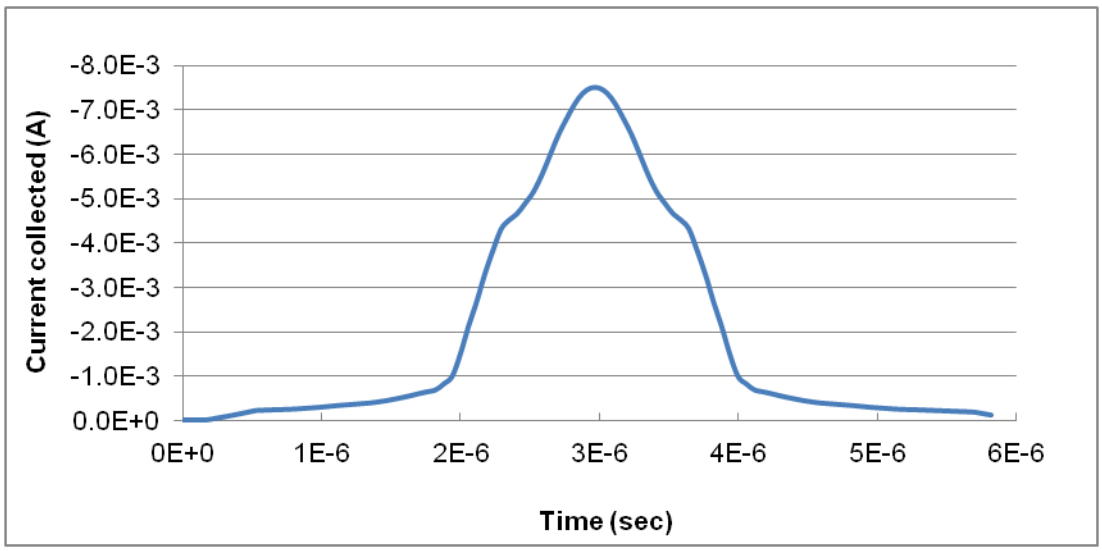

(b) A 0.02 mm wide probe trace.

Figure 2-24 Intensity plot converted into the current collected by probe with a transit speed of 5×10^4 mms^{-1} for the example data shown in Figure 2-22.

Measurements were made of the FWHM and FWHP of these pulses to allow direct comparison with probe data. In this simulation, it was

necessary to include the probe width to provide the correct pulse shape. In the calculation of the beam width from the pulse width, half of the probe width was subtracted from the measured value as an estimate of the contribution of the probe to the measured value. This estimation becomes more significant if the beam width and probe width are comparable. Subsequently, a probe was used with a width significantly less than the beam width, within limits of practicality.

For rotary wire probes the angular sweep of the probe - beam transit would need to be taken into account, and this would become more significant if the radius of the probe arm supporting the wire was small.

If the assumption is made that the intensity distribution of a beam that has been measured is axially symmetric, it is possible to work in the opposite direction - i.e. to reconstruct an intensity map from the probe signal collected. This is carried out by deconvolving the probe trace to obtain an intensity map. If a number of traces are collected with the probe at different angles to the beam no assumptions need be made about symmetry. It is possible to reconstruct the intensity map using the inverse Radon function (Elmer and Teruya, 2001), in a similar manner to medical X-ray tomography, for example. In the referenced work, where no assumptions were made about symmetry, it was necessary to measure the beam at 17 different probe angles, each one was a 0.1 mm slit, in order to be able to reconstruct the intensity map with reasonable integrity i.e. without false artefacts being generated by the algorithm due to a lack of data. For high power beams this is possible, but takes time and requires many probes or a motorised probe to generate the required number of different angles.

Intensity maps from the simulation can be highly structured. However, when these were converted to probe traces that could be measured in practical trials, much of the beam structure was smoothed out. In order to generate quantified measures of the beam diameter, the use of metrics such as the FWHM, FWHP and CWAD are favoured, although it is clear that the intensity structure within the beam could cause these to be misleading. This

is particularly the case for FWHM which can be strongly influenced by the peak intensity, whereas FWHP and CWAD provide more robust measurements of the overall beam width.

2.6.2 Determination of apparent electron source

A useful method for verifying electron gun modelled beam characteristics with real world data has been developed in this work that used measurements of the lens current to give sharp focus at a range of working distances. By then applying equations Eq 2-17 and Eq 2-19 it was possible to determine the apparent electron source position.

This method worked as follows. A beam was generated at the same gun electrical operating parameters. The beam probe was moved to known working distances from the lens centre plane and the lens current found for sharp focus. A number of these readings could then be plotted. For a fixed lens and for the gun operating at a fixed accelerating potential, Eq 2-17 can be rearranged as

$$f = \frac{L}{I^2} \qquad \text{Eq 2-31}$$

where

L is a constant combining lens characteristics with the accelerating potential, mm A^{-2}.

Substituting into Eq 2-19 we then obtain

$$I^2 = \frac{L}{u} + \frac{L}{v} \qquad \text{Eq 2-32}$$

where

u is the distance of the apparent source of the gun at the operating point under investigation to the lens centre plane, mm

v is the distance from the lens centre plane to the beam focus position, i.e. the beam probe position, mm

So a straight line plot was obtained plotting I^2 against $\frac{1}{v}$, with a gradient of L and which intercepted the vertical axis at a value of $\frac{\mathrm{L}}{u}$. This is illustrated in Figure 2-25, where data was plotted for focal distances from the lens centre plane of between 300 mm and 550 mm. The gradient of the plot (L) was 45.79 mm A^{-2}. The straight line plot was extrapolated to intercept the vertical axis at a value of 0.187 A^2. This yielded a value for the apparent electron source position of 245 mm from the lens centre plane.

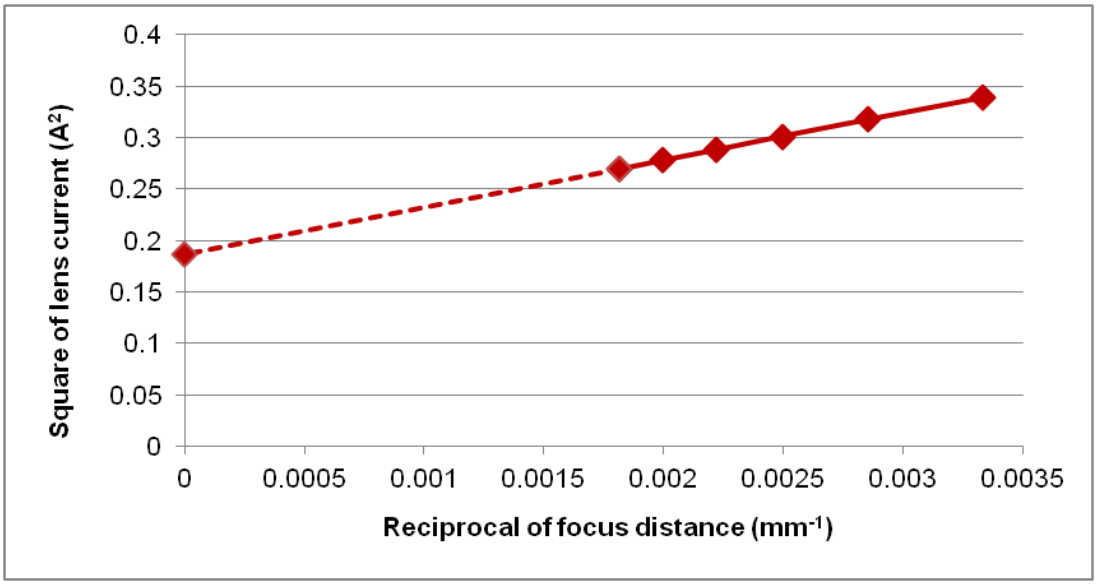

Figure 2-25 Plot of the square of the lens current against the reciprocal of the focal distance to a beam probe. The gradient is the constant L, and the intercept at the vertical axis is the ratio *L:u*.

Using this method it has been possible to indirectly measure the apparent electron source position and readily compare modelled beam characteristics with measured data to verify the model accuracy.

Chapter 3: Investigation of optimisation methods

This chapter reviews a variety of optimisation methods and investigates how evolutionary methods can be applied. Evolutionary parameters are described and tests show how these may be optimised for problems of different complexity.

3.1 Design Optimisation

During the past 20 years many variants of optimisation techniques have been developed for design and optimisation problems (Bianchi et al., 2009). These techniques have been shown to be effective where the problem to be solved can only be tackled by a trial and error method. The techniques have been successfully applied in many diverse fields (Fonseca and Fleming, 1995) including architecture and civil engineering (Nguyen et al., 2014), aerospace engineering design (Zhu et al., 2016), economics and logistics (Ponsich et al., 2013), geophysics (Sen and Stoffa, 2013), cryptology and data clustering (Bacquet et al., 2011) and electrical engineering (Song, 2013).

The typical characteristics of a design problem for optimisation are that, in order to meet the requirements for finding a solution to the problem, there will be many real-world variables and it is not possible to directly map these to the solution. Further, any functional relationship between these variables and the solution is an unknown type. That is to say, it could be continuous or non-continuous with a single optimum solution or multiple sub-optimum solutions. In short, the solution function is unknown.

It is also a requirement that for any set of input variables the solution can be evaluated. This is usually executed by using a computer simulation which itself is a model of the real-world problem. Each candidate solution is evaluated and scored so that the optimisation technique can be implemented. It is vital that the evaluations can be quantified in terms of their suitability to meet the requirements. Where the solution space is large, i.e. there are many input variables which interact in a complex way, heuristic algorithms such as genetic design, ant colony and particle swarm

optimisation are used. These techniques have often been adjusted in order to avoid the optimisation process from becoming trapped in local optima, to ensure they explore all of the solution space or to allow them to converge more efficiently. In contrast, response surface modelling techniques such as Kriging (Hawe and Sykulski, 2007b; Lebensztajn et al., 2004) have been deployed for some problems, most typically those with fewer variables.

A number of optimisation techniques have been reviewed and these are described below. They typically draw inspiration from optimisation methodologies found in nature.

Simulated annealing is an optimisation method that is analogous to cooling metals from a high temperature, which form a variety of crystal structures or states. Each of these is a potential solution with a different thermodynamic free energy (Kirkpatrick and Vecchi, 1983). A metal will normally find its lowest energy state when it is cooled slowly. For this algorithm, the energy term is the score for the solution. More optimum solutions have lower energies. The algorithm looks for other candidate states and computes an acceptance probability – that is the probability of making a transition to them. This calculation is dependent upon the energy difference of the two states and upon the temperature parameter, which is gradually reduced each iteration. The algorithm explores the problem space broadly at first when the temperature is high, and transitions between largely different energy states is possible. However, as the temperature is lowered the algorithm tends to find nearby states and optimisation occurs more locally.

Particle swarm optimisation (PSO) has been inspired by the swarming of insects, flocking and murmuration of birds, schooling of fish and herding of cattle (Clerc, 1999; Bratton and Kennedy, 2007; Higashi and Iba, 2003; Fourie and Groenwold, 2002). The axes in the problem space are the transformed input variables of the candidate solutions. The position of a particle in this space uniquely describes a candidate solution. Its movement through the solution space is directed by its own immediate history, as it seeks to direct itself towards further improvement, and by some of its

neighbours' velocities. Although visualised in three dimensional space, most problems will have many input variables and so the solution space will be multi-dimensional. Initially, a random swarm of particles is created. Then with each iteration the particles move through the problem space along a stochastically determined vector but with some dependence upon their previous velocity, their best known position so far and the best known position of all of the swarm, or a sub-group within it. PSO has been very successfully applied in many engineering optimisation problems and has many variants.

Many optimisation problems involve finding the shortest route between a number of destinations, or can be transposed into this form. Ant colony optimisation (Dorigo et al., 1999) draws an analogy with how ants find the optimum route from their colony to food. The solution is encoded into a series of paths, which when strung together make the route that the ant follows in moving from the colony to the food. The length of each path is representative of the cost. Choosing each path is in part stochastic, but is also influenced by how many ants have recently used that path. The optimal solution is one represented by the shortest route. The encoding within the algorithm lends the technique to finding optimum sequences, combinations or routes.

Genetic design algorithms (Franz, 2006) use an evolutionary technique to attempt to find an optimal design. Variables for the candidate solutions are encoded into a set of genes and a form of ‘natural selection’ is used to optimise solutions. The processes of inheritance, genetic cross-over, mutation and survival of the fittest are applied to a population of candidate solutions. The population is normally generated initially as a random set of solutions and then with each generation the fittest (i.e. those members of the population scoring highest) are stochastically paired to parent the next generation. The process continues until an optimal solution is generated.

The simplex (Dantzig, 1990) and complex methods (Box, 1965) started to be investigated almost 70 years ago. They are variants of linear

programming techniques and formed the basis of much of the work carried out for the military in operations research. They have been applied to many problems of logistics and production where an optimal solution needs to be found within a number of constraints. The constraints are converted into inequalities that describe the vertices of a shape called a polytope. The polytope will contain all feasible solutions and the solution method is to move the worst vertex towards the centroid of the shape, and to continue this action until the solution has converged. The methods in their original form can collapse onto a local minima solution, and are best applied to problems known to have a continuous solution contour.

Where there are multiple objectives (measures of fitness) it is likely that no one solution will optimise all of these (Andersson, 2001). Consequently, there are a set of optimal solutions that are equally weighted. If a representative sub-set of these is plotted in objective space, a Pareto front is displayed (Hawe and Sykulski, 2007a; Xiao et al 2014). All solutions on the front are equally optimal and none of them could be improved in one objective without another objective being diminished. Selecting one of the solutions can then only be carried out by applying another measure of fitness, or by a subjective choice. Solutions not on the front are non-optimal and are dominated by those closer to the front, which are more optimal.

3.2 Related Work

Mathematical analysis techniques have been applied to optimise the curvature of cathodes in electron guns (Lewis et al., 2004), and these have been shown to be effective. It may be possible to develop further these techniques to look at the combined shape of the gun electrodes and cathode, however the complexity of the problem space, and the number of possible combinations, may extend computing times beyond reasonable durations. Interesting developments in artificial life studies have developed techniques for a design process that explores the design constraints in meeting requirements (Bedau et al., 2000; Sims, 1994). These show promising potential – especially for the design of electron guns where incremental

improvements may not progress towards the best design, or where (as will normally be the case) less constrained variation in geometry offers a very large number of design options to be tested.

Kriging is a method originally developed for geo-statistical modelling, in particular estimating the distribution of gold deposits from a limited number of bore hole samples. It has been applied (Hawe and Sykulski, 2007b; Lebensztajn et al., 2004) to electromagnetic problems to interpolate between known values in order to find an optimum value – for example to optimise the pole piece profile to produce a required magnetic field distribution. This is most suitable for investigating minor changes to geometry, where the variation is reasonably constrained and where the solution is continuous.

No one optimisation method has been found to be universally better than any other (Wolpert and Macready, 1997). However, this is not to say that for a particular problem type there are not more efficient optimisation methods and less efficient ones. The suitability of the method can be assessed by the time taken to evaluate the design.

In the case of an electron gun analysis, the evaluation requires a model to be built, but more specifically for the model to be solved. The extraction of electron beam characteristics takes about 1% of the model solution time within the space charge solver, which presently requires a time of the order of minutes. This time is sometimes called the cost of evaluation, and for electron guns, where a finite element model of each design must be iteratively solved, this cost can be regarded as reasonably high. Some optimisation techniques allow exploration of potential solutions that could be solved in parallel offering very substantial improvements in efficiency– for example, in genetic design algorithms, a generation of solutions can be solved simultaneously. Similarly, in particle swarm optimisation methods all of the swarm of particles (different gun geometries) can be evaluated in parallel for one time step.

Surrogate modelling is a technique applied to problems with a high cost of evaluation. They can be simplified models giving a response curve for variables, or they can be data driven (Jin, 2011). There is an overlap with Kriging, as a similar response curve is predicted and used to more rapidly home in on the optimum solution. Surrogate models may also be constructed from neural networks trained from solution data. They are most effective when the number of variables is reasonably low. The difficulty in applying them to electron gun design is that the response curve is not known and in all but the most trivial design changes there is little data to support the generation of a surrogate e.g. by training a neural network.

3.3 Genetic algorithm trials

3.3.1 A simple evolutionary optimisation demonstration

An evolutionary optimisation algorithm must employ some of the genetic processes on a population of designs. These include selection of the fittest, random gene mutation and gene swapping.

A simple illustration of the, perhaps, counterintuitive effectiveness of selection of the fittest has become known as Dawkin's Weasel after (Dawkins, 1986). The starting point for this work is the infinite monkey theorem, first put forward by a French mathematician in the early twentieth century (Borel, 1913). In more modern times it is popularly restated as being: that given eternity, a monkey will produce the works of Shakespeare (or any other text, an infinite number of times).

Dawkin's Weasel was a demonstration in two parts. Firstly a computer program was rewritten in this work to try to randomly generate a target sentence (from Hamlet, "Methinks it is like a weasel"), see Figure 3-1 (a). Secondly, the ability to randomly mutate a seed sentence (mutation), and to select the sentence most closely resembling the target (selection of the fittest) was added to the program. There was no gene swapping in this algorithm. This second program operated by taking a seed sentence, mutating it 20 times to populate a generation with a mutation probability of

0.05 for each character, choosing the sentence most closely representing the target, then used this as the seed for the next generation, until the target sentence was generated, see Figure 3-1 (b). This process is called cumulative selection from a randomly mutated population.

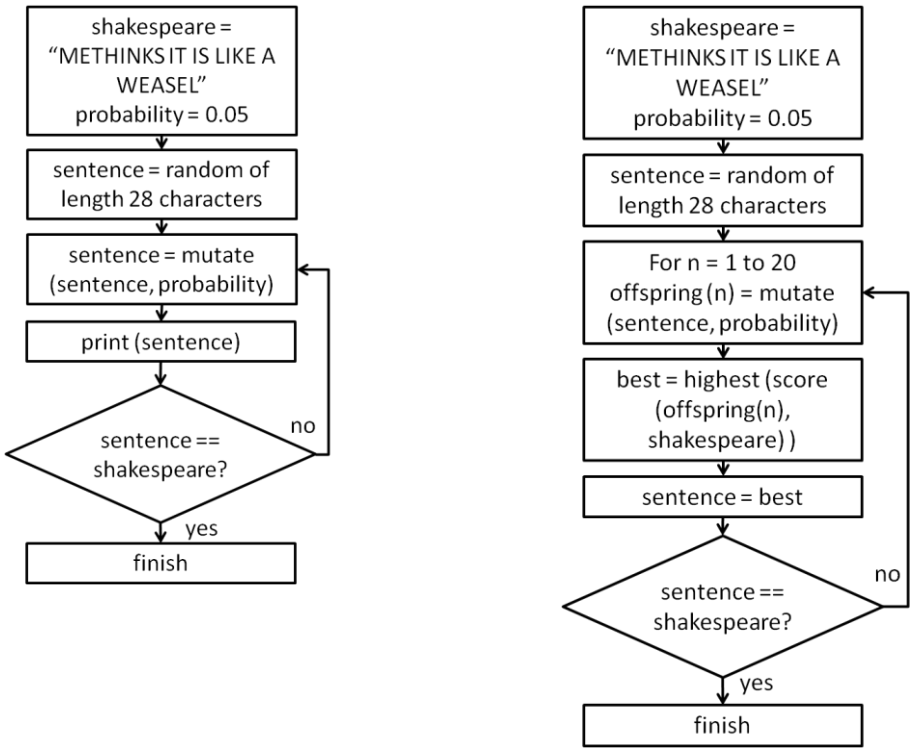

(a) Random sentence generator program (b) Dawkin's weasel program

Figure 3-1 Software flow diagram for random sentence generator and Dawkin's weasel program.

The two programs used for this demonstration within this work are given in Appendix A and Appendix B, and they are a re-scripting of the originals. In the first case, the program generated about 10000 sentences per second, checking each one against the target. However, the large number of permutations available (10^{40}) means that at the given rate the program will only be 50% likely to successfully generate the target after $5x10^{39}$ attempts, taking 10^{28} years. (The universe is estimated to be 10^{10} years old.) The second program successfully generated the target sentence after scoring 7500 attempted sentences, in a time of less than 1 second. Samples of the evolution of the sentence are shown in Table 3-1.

The example demonstrates that even for a relatively simple problem, evolutionary processes are highly effective at finding a solution compared with random trial and error methods.

Table 3-1 Evolution towards a target sentence using random mutation and cumulative selection.

Calls to score function	Highest scoring sentence of generation
0	KRWZEPBSPLFRALWLUUZOHYWSSNZL
300	KRWZEFBSMIBMASILLUZ HYWSANZL
600	KPKHVFBSWIBRQSILO E HYWVANZL
900	KPKHVFDSKIBRQSILOKE ZYWAAS L
1200	KETHINTSKI RQSILOKE AYWDAS L
1500	YETHINTSKIJRISMLOKE AGWDAS L
1800	WETHINTSFIJKIS LOKE AMWDASEL
2100	WETHINTSFIJKIS LIKE A WDASEL
2400	WETHINTS IJKIS LIKE A WAASEL
2700	WETHINTS IJFIS LIKE A WFASEL
3000	METHINTS IFHIS LIKE A WHASEL
3300	METHINCS IONIS LIKE A WHASEL
3600	METHINCS IONIS LIKE A WHASEL
3900	METHINCS IINIS LIKE A WHASEL
4200	METHINCS IITIS LIKE A WBASEL
4500	METHINCS IT IS LIKE A WVASEL
4800	UETHINCS IT IS LIKE A WEASEL
5100	METHINCS IT IS LIKE A WEASEL
5400	METHINCS IT IS LIKE A WEASEL
5700	METHIN S IT IS LIKE A WEASEL
6000	METHINQS IT IS LIKE A WEASEL
6300	METHINQS IT IS LIKE A WEASEL
6600	METHINQS IT IS LIKE A WEASEL
6900	METHINQS IT IS LIKE A WEASEL
7200	METHIN S IT IS LIKE A WEASEL
7500	METHINKS IT IS LIKE A WEASEL

In this example, the solution was a known target, but in real optimisation problems the solution will be unknown, and only the fitness threshold (i.e. the score to be achieved for the process to be complete) has been defined. However, this does not alter the optimisation process as the only reference to the target sentence was to derive a fitness score. It was

also pertinent that none of the letters were locked at any generation, so it was quite possible that some mutations will score less than the parent design if a correct letter in the correct location was mutated to be an incorrect letter.

With this simple example of an evolutionary optimisation program, there were two evolutionary parameters: population size and mutation probability. Within this work, the efficiency of an optimisation process was assessed by the number of calls made to the fitness function. This was then mapped against the two evolutionary parameters to show the best combination of these. If the number of calls to the fitness function exceeded 100,000, the optimisation with those parameters was terminated, and 100,000 recorded against that combination of parameters. The results of these trials are shown in Figure 3-2. This shows that the most efficient evolutionary parameters for this program were a population size in the range 20 to 50, and a mutation probability in the range 0.03 to 0.1. The minimum number of calls in this set of experiments was 3000, which was made when the probability was set to 0.085 and the population size was set to 40. Although there would be variation if the trials were repeated, because of the random nature of the mutation, the large number of combinations carried out indicates a clear trend towards combinations of evolutionary parameters that gave the most efficient solution algorithm. The trials showed that as the mutation probability was increased, it was necessary to have a larger population for the algorithm to be efficient. They also showed that lowering the mutation rate below 1% made the algorithm inefficient. It was concluded from the demonstration that cumulative selection is an extremely powerful tool for optimisation, with the right choice of evolutionary parameters.

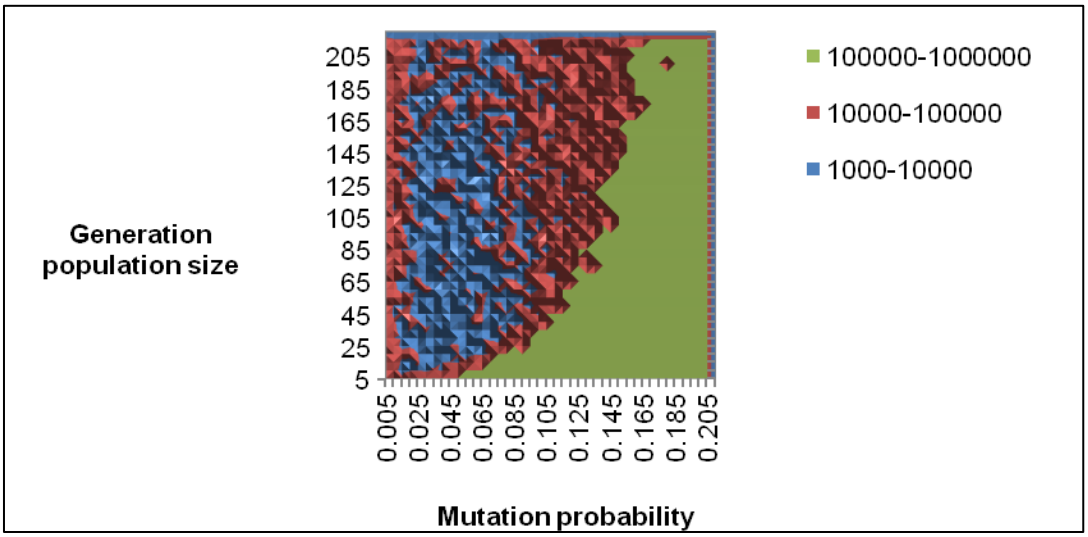

Figure 3-2 The relationship between the total number of calls to the fitness function and the population size and mutation rate for the Dawkin's weasel evolutionary program.

3.3.2 An evolutionary algorithm applied to a geometrical problem

More advanced genetic design algorithms were explored for a simple problem with similarities to electron gun optimisation. Within this work, an analogous design problem to electron guns has been used to examine the effect of different parameters on the evolutionary optimisation process. The analogous problem chosen is one of shape fitting. The main parameters for the evolution process were the parent group size, the offspring group size, the probability of gene mutation and the scale of gene mutation. These parameters generally determine the efficiency of the optimisation process, i.e. the time taken for optimisation and the exploration of the problem space. Although many publications quote the evolution parameters used, there is little justification for the choices taken (Karafotias et al., 2014).

The problem chosen for optimisation was the development of the closest fitting shape to a target design. In this case, a candidate shape was to be submitted to the fitness function and a score returned which indicated how close it was to a (hidden) target shape. No information was given about how close or how far any individual vertex was from the target, only the accumulated score for all vertices. This fitted the concept of a trial and error type of solution. It was considered a useful test case as the optimised solution is a 2-D shape – similarly a gun design is represented by a 2-D axi-

symmetric geometry. The optimum gun design is not hidden, it is simply unknown.

The objective of this trial was to determine the most efficient settings of the evolutionary parameters for solving a shape fitting optimisation, which it was anticipated would give an indication of the best evolutionary parameters for electron gun design problems. The fitness scoring for the shape was computed very quickly with several hundred scores being generated each second, compared with a gun solution and trajectory analysis taking several minutes each, and this allowed a wide range of evolutionary parameters to be explored.

Coding of the problem for evolutionary optimisation required shapes to be described in a genetic format that could be operated upon by the evolutionary processes. The genetic description of the shape was an ordered set of coordinates of the vertices. The fitness test applied to the shapes generated by the optimisation algorithm was to take the root of the sum of the squared differences between the target shape ordered coordinates and those of the shape being assessed, with a lower value indicating the fitter solution, i.e. the shape most closely resembling the target.

The optimisation algorithm included the following steps. First a target shape was randomly generated. A population of random shapes was generated and each of these was given a fitness score. The top scorers were selected and the rest of the population discarded. The top scorers then produced offspring by random selection of two parents, gene swapping by slicing out a segment where each slice was made at a random position in the genome, gene mutation by random selection of a position in the genome (a vertex in this problem) and then mutating this randomly within a range defined as the mutation scale. This process continued until the population size was restored, following which the offspring population would be scored. The new parent group was selected as the fittest from the entire population of both parents and offspring. This new parent group then produced offspring and this process continued until a population member had a fitness score

within a preset tolerance level, i.e. the population shape was a close fit to the target shape. The algorithm is illustrated in Figure 3-3.

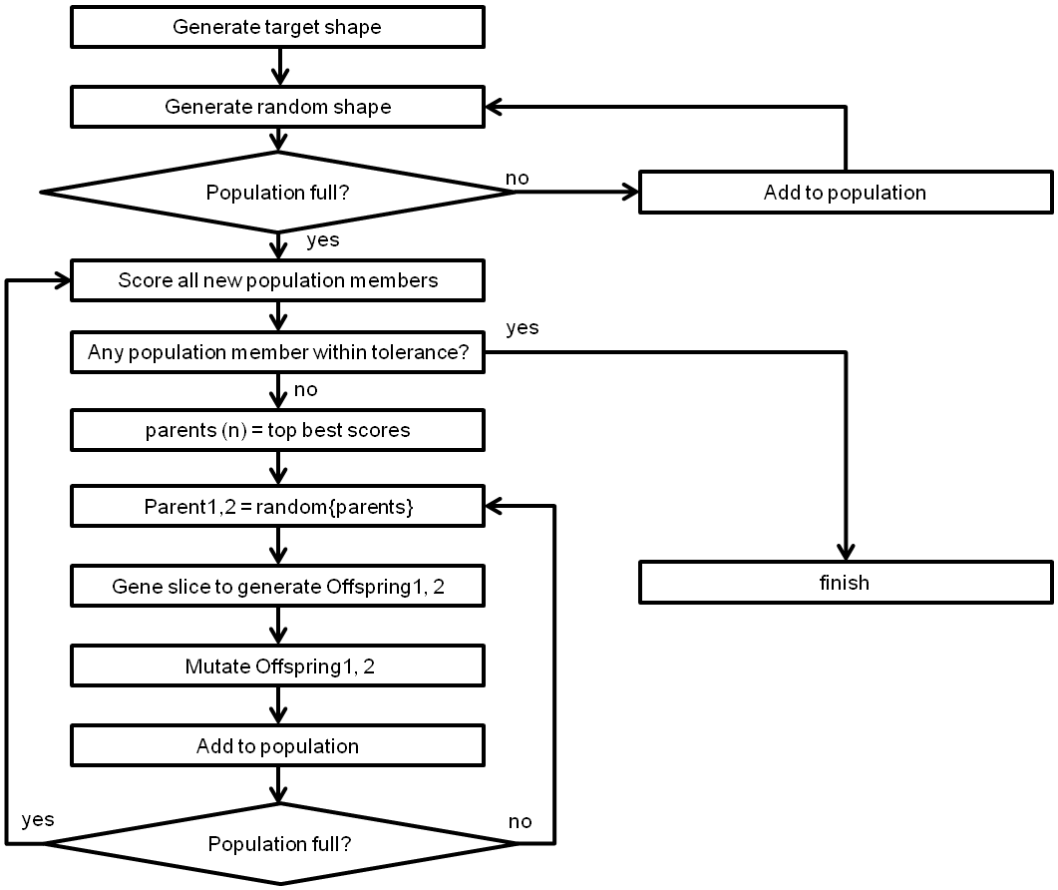

Figure 3-3 A flow diagram of an evolutionary algorithm for shape fitting.

The gene slicing and swapping algorithm generated two offspring from the randomly selected parents. A randomly selected section of the genome was cut out from each parent and swapped for the same section from the other parent. In the shape fitting algorithm this corresponded to swapping the coordinates of some of the vertices between the two parents genomes to create two offspring shapes. This is illustrated in Figure 3-4, where P_aX_n and P_aY_n are the X,Y coordinate pair, expressed as real numbers, for the n^{th} vertex of shape P_a. This method differs from typical implementations of genetic algorithms, where the encoding is binary and the slicing occurs at a random binary digit. This may cause the coordinate to be spliced part way through its binary representation and effectively to be mutated. Within this

work, as far as possible the mutation and gene slicing were kept independent to allow investigation of their settings separately.

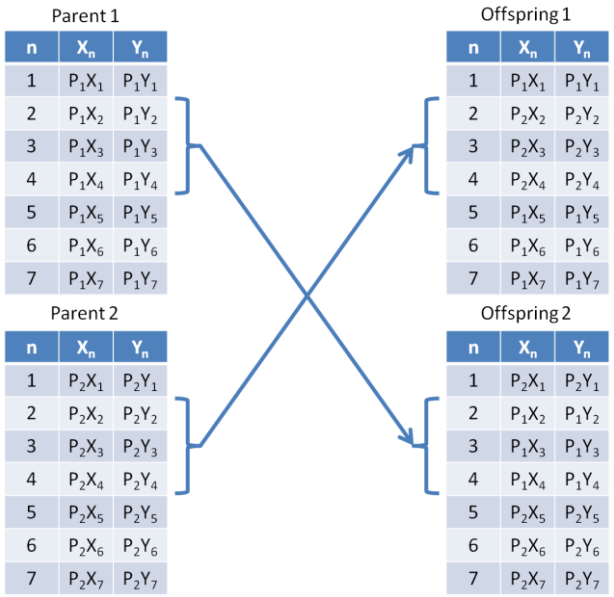

(a) Numerical representation showing an example where three vertices are swapped.

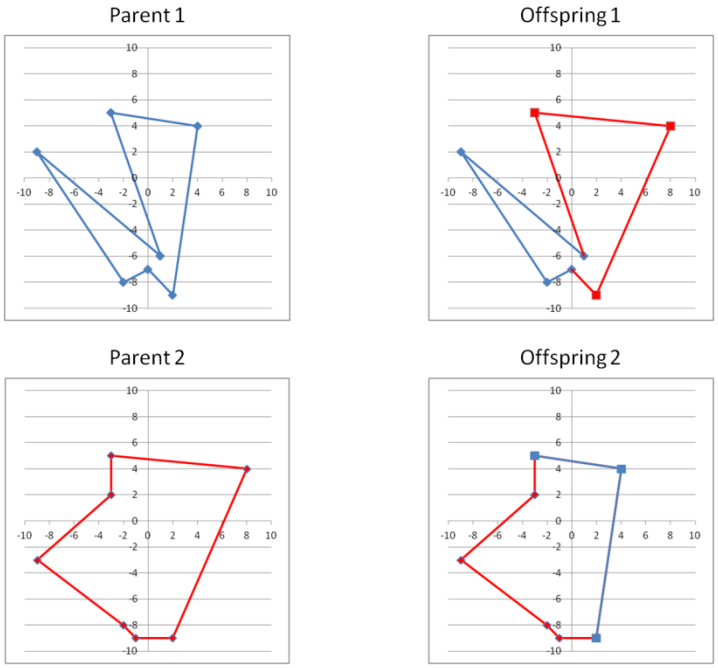

(b) Graphical representation for an example shape - three vertices are swapped between the parents, without mutation at this stage, to give Offspring 1 with four vertices from Parent 1 and three vertices from Parent 2, and Offspring 2 with four vertices from Parent 2 and three vertices from Parent 1.

Figure 3-4 The gene slicing and swapping algorithm generating two offspring from a pair of parents for seven vertices shapes.

The specific issues that could be investigated with this program were:

What are the optimum settings for population size, mutation rate and mutation scale?

How are these settings influenced by the problem complexity and the optimisation tolerance?

Trials were carried out for 3, 5, 8 and 10 cornered shapes, representing problems of increasing complexity. For shapes with more than 10 corners, the individual optimisations were taking too long to allow practical trials over a wide range of evolutionary parameters. Efficiency was measured by recording the total number of calls to the fitness function for each optimisation – scoring was carried out for all of the initial random population and each generation of offspring. In the analogous electron gun design optimisation, a call to the fitness function would require a model solution and trajectory analysis, taking up to one minute. In this case, a call to the fitness

function took under 1 ms, allowing a large number of trials to be carried out with different combinations of evolutionary parameters.

For three to ten cornered shapes, the number of offspring was varied from 2 to 100, the parent group from 2 to 30, the mutation scale from 0.05 to 1 (5% to 100%) and the mutation rate from 0.01 to 0.1 (1% to 10%). In total, the different combination of parameters led to 42,000 optimisations being executed for each shape. Each optimisation required from 338 calls to the fitness function (with evolutionary parameters giving the fastest solution for a shape with three vertices) to over 200,000 calls to the fitness function (with evolutionary parameters giving the slowest solution for a shape with ten vertices).

The results were analysed by plotting the minimum number of calls as a function of the number of offspring and number in the parent group for all variations of other parameters, see Figure 3-5 and the mutation rate and mutation scale, see Figure 3-6, both for ten cornered shape evolution. Also, sampling was carried out of the most efficient 1 % of optimisations for each shape and the modal evolutionary parameter settings were extracted – see Figure 3-7 and Figure 3-8.

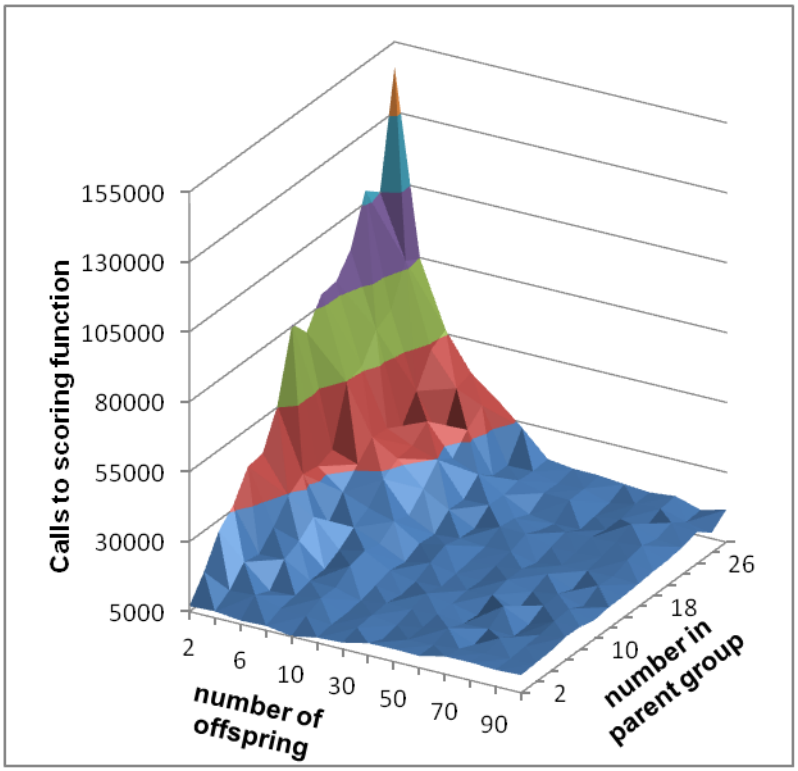

Figure 3-5 The minimum number of score function calls as a function of the parent group and offspring group sizes.

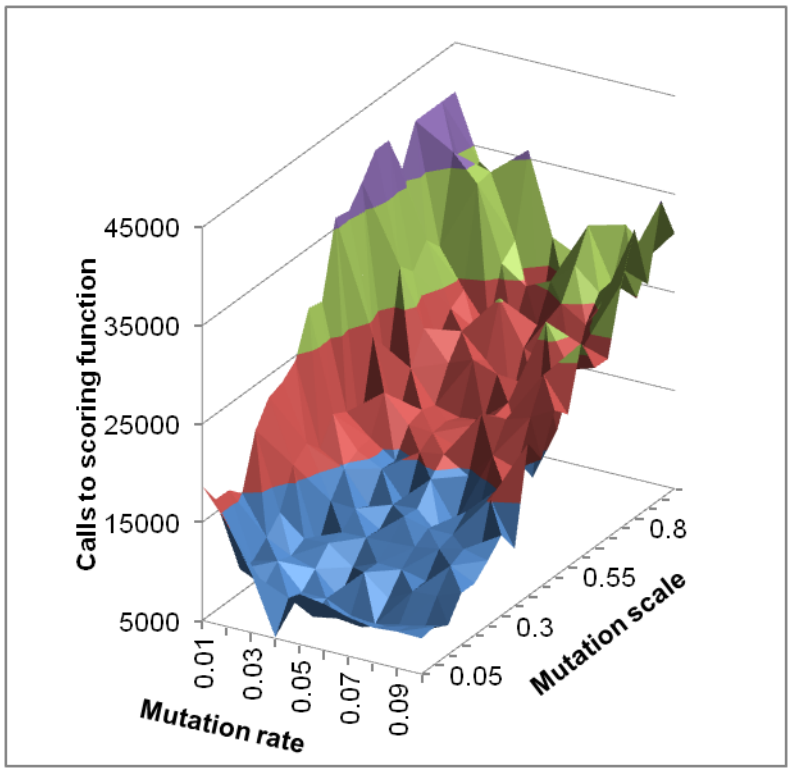

Figure 3-6 The minimum number of score function calls as a function of the mutation scale and mutation rate.

The results showed that a small parent group of two or four was most efficient over all the range of shapes. It was also clear that as the number of corners increased, the optimum values for mutation rate decreased. For three and five cornered shapes the optimum mutation scale was 0.15 dropping to 0.1 for eight and ten cornered shapes. For three cornered shapes the optimum mutation rate was 0.1, decreasing to 0.06 for eight cornered shapes and 0.05 for ten cornered shapes. This is shown in Figure 3-7 and Figure 3-8.

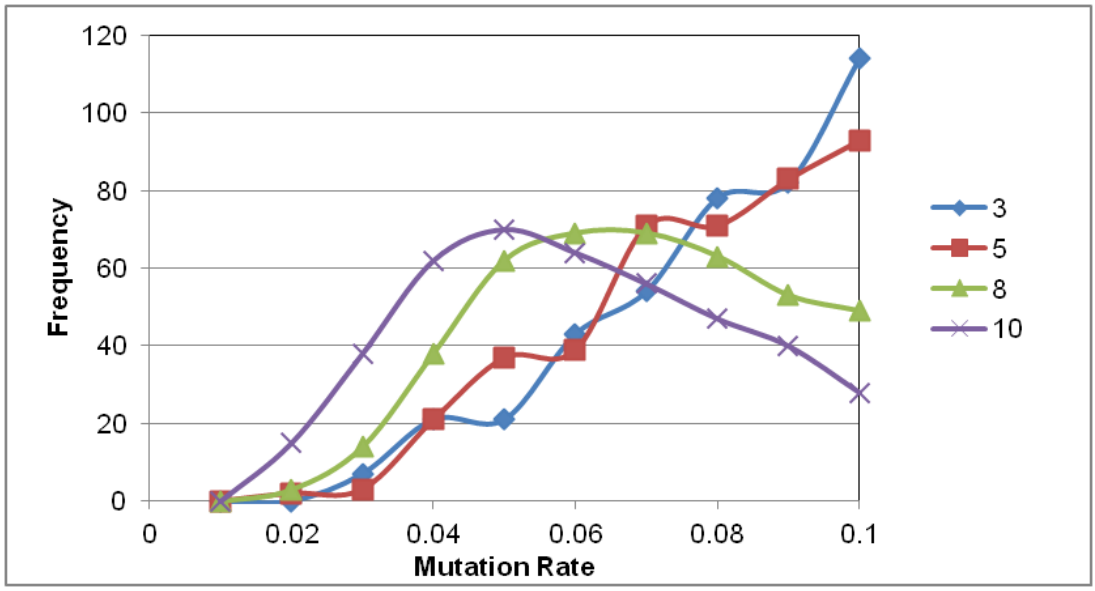

Figure 3-7 Histogram of the top 1% optimisation solutions showing decreasing mutation rate with increasing problem complexity.

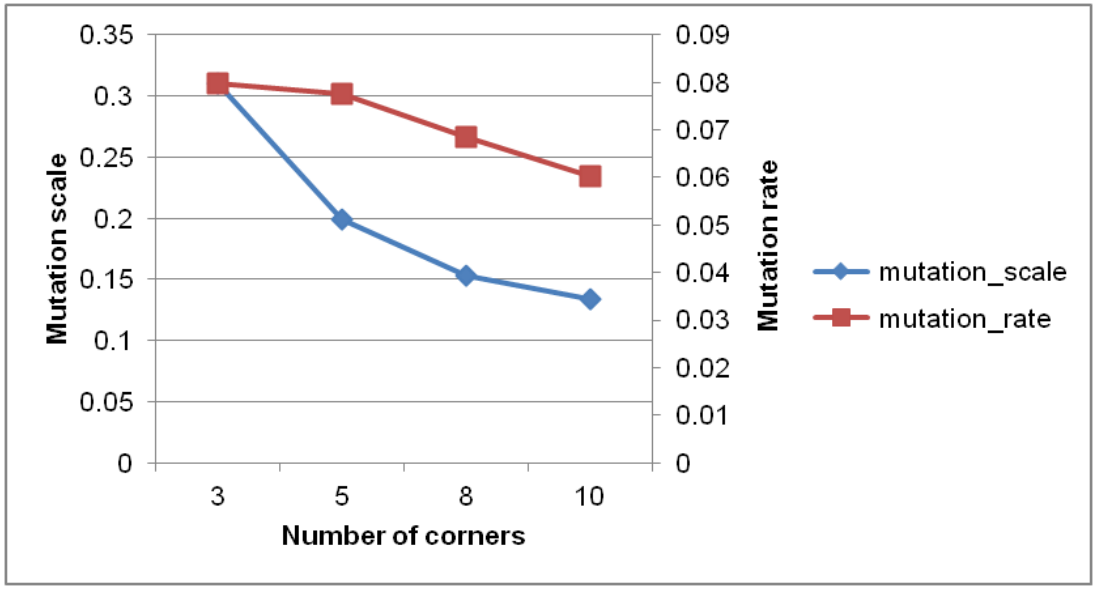

Figure 3-8 Modal values of mutation scale and mutation rate of the top 1% efficient optimisations.

Summary of trial

The problem addressed was to find the coordinates of the corners of a target shape. The fitness function was the inverse of the sum of the distances of mismatch between the potential solution corners and the target shape corners. This problem was useful for examining the effect of evolutionary parameters because it was dealing with coordinate values, as in

the electron gun optimisation. It was also scalable in terms of complexity – so the effect of increasing the number of corners in the target shape could be examined.

This trial has shown that as problem complexity increased the optimum mutation rate and scale for rapid optimisation will be lower. It indicated that values of mutation rate and scale should be used of less than 0.05 and 0.1 respectively. Regardless of problem complexity, parent groups of two or four were the most efficient, as were offspring numbers of ten or less.

These results were then used to indicate the best evolutionary parameters for an electron gun design problem.

This problem differs from electron gun design optimisation in that the fitness function had a single solution and varies smoothly, which would not be expected for an electron gun being scored on the electron beam optical qualities. However, tests carried out with this problem gave an insight into identifying the best evolutionary parameters for optimisation.

Chapter 4: Application of optimisation method to electron gun design

This chapter describes how the evolutionary algorithm was applied to optimising the design of electron guns, gives the rationale for introducing special adaptations and details of how these were implemented.

4.1 Model generation

To apply evolutionary design techniques it was necessary to encode the design into a genome. The genome was a collection of genes that describe the design. For an electron gun, designed in 2-D, a geometry was specified describing the anode, high voltage electrodes and the cathode. Within this work, a module within the Opera 2D software suite called the pre and post processor was used for creating the model. The geometric definition file was a series of definitions of face characteristics within a geometry. Each line within the geometry had a starting and stopping position and a degree of curvature. These parameters provided a means of describing the geometry as a series of real numbers that could be considered to be genes.

4.1.1 Model preparation

An example of an extract from the geometric description is given in Table 4-1, which is a set of commands to the Opera 2D software which would generate part of a model - in this case the anode electrode.

Each row in Table 4-1 described the next corner of an electrode, cathode or anode shape, and gave some parameters for the face created by the line between the two corners. The "DRAW" command has a number of parameters that characterise the region - see line 2. A full description of these is given in (Cobham, 2012b). The corner coordinates were given as real values, XP and YP. The keyword "CARTESIAN" indicated that these were in Cartesian notation. However, as the model was axi-symmetric, the XP value was interpreted as a radius from the axis, and the YP value was interpreted as a Z position. The subdivision of the line, which gave higher

mesh resolution, for curved lines for example, or for ensuring a region had high spatial resolution, was given by the parameter N.

The boundary condition for the model at that face was given by parameter F. In electron gun design the boundaries could be undefined, and in this case F was set to "NO". This would be the case on the axis, where the solver assumes axi-symmetry or on a boundary between different regions. Alternatively, the face could have been at a defined potential because it was describing a conducting surface such as the anode, in which case F was set to a value V. The keyword "FINISH" joined the current position to the first defined position of the region. The keyword "QUITDRAW" was used to indicate to the software that the parameters for the DRAW command for this region were complete. Each of the shapes within the gun design were defined in a similar manner to Table 4-1, and together these formed the complete gun model, and could be considered to be the genotype.

It can be seen that not all of the parameters were given for each line - this was a shorthand in the Opera software, which when exporting a model to a command file only stated the changed parameters for the command. For example, in line 6 only the TP ordinate was given and from this it was implicit that all other parameters for the region face were identical to those already defined on lines 4 and 5.

Table 4-1 Example of geometric description of the anode of an electron gun.

44	/ Region 1
45	DRAW SHAPE=POLYGON MATERIAL=4 N=0 SYMMETRY=0 PHASE=0 CONDUCTIVITY=0 PERM=1 DENSITY=0 VELOCITY=0 MIRROR=NO ROTATIONS=1 DX=0 DY=0 NX=1 NY=1 TMIRROR=0 TROTATION=0 XCENTRE=0 YCENTRE=0 ANGLE=0
46	CARTESIAN XP=1.71371716035381 YP=-38.7870937717372
47	CARTESIAN XP=1.14805533403224 YP=-28.7964448474328 CURVATURE=0 N=9 BIAS=0.5 F=V V=0 DVALUE=0
48	CARTESIAN XP=0.865224420871453 YP=-17.7130686970327 N=5
49	CARTESIAN YP=-10.0639781143621
50	CARTESIAN XP=5.57907297355124 YP=-10 N=8
51	CARTESIAN XP=8.21882816305192
52	CARTESIAN XP=10.0100906130702
53	CARTESIAN XP=10.1986445551774 YP=-23.4889126063961
54	CARTESIAN XP=10.5757524393918 YP=-30.5135876312976 N=9
55	CARTESIAN XP=11.0471372946598 YP=-38.6309898822949
56	CARTESIAN XP=100 YP=-38.7 N=93
57	CARTESIAN YP=-50 N=12 F=NO
58	CARTESIAN XP=3 N=98
59	FINISH N=12 F=V
60	QUITDRAW
61	GROUP NAME=ANODE ACTION=ADD MATERIAL=ALL NOT=NONE REG1=%INT(REGIONS)

The model data was prepared in the command file to be suitable for manipulation by the evolutionary processes, as described below in section 4.1.2.

The emitter surface was defined in a separate file for the Opera software. This file could be directly manipulated by the beam characterisation algorithm, which allowed, for example, modification of the cathode temperature. An example of the file, with a description of the entries, is given in Table 4-2:

Table 4-2 Description of an example Opera emitter definition file.

Line	Emitter Data						
1	0	0	0	0			
2	1	1.00E-02	1.00E-04	6.00E-03			
3	1	1550	2.69	120			
4	1	-1					
5	1	1	1.0				
6	1						
7	0						
8	1.00E-01	0.00E+00	0.00E+00	0.00E+00	0.00E+00	5.00E-01	20

Line 1 data is a leader of four 0's.

Line 2 specifies the emitter type (1), the maximum step length when calculating the trajectory path of the beamlet (1.00E-02 cm), the tolerance on the calculation (1.00E-04 cm) and the sampling distance (6.00E-03 cm).

Line 3 specifies the emitter type (1), the cathode temperature in K (1550 K), the work function in electron-volts for the cathode material (2.69 eV) and the Richardson constant multiplied by its correction factor for the cathode material (120 $Acm^{-2}K^{-2}$). Emitter type 1 is a Langmuir-Fry virtual cathode model emitter. The electric field at the surface has been found to underestimate the emission, so instead the field is sampled at the sampling distance away from the cathode surface and normal to it. This field value is then used to calculate the beamlet current and the beamlet is launched from the equi-potential line of the same value as the cathode surface.

Line 4 specifies that the particles emitted have 1 electron mass unit, and the charge of an electron (-1).

Line 5 - after 2 leading 1's the maximum allowable spacing of the emission points is stipulated in cm (1 cm).

Line 6 indicates for which segment (1) data is being given next.

Line 7 indicates the geometry type for the line segment data (0), which indicates axi-symmetry.

Line 8 gives the r,z coordinates of the end points of the cathode face segment in cm ((0.1,0), (0,0)) followed by the curvature of the face in cm^{-1} (0), the bias weighting for the distribution of emission points along the cathode face segment (0.5) and the number of emission points across this cathode face segment (20).

The assessment of a single gun geometry required examination of the model outputs at a number of cathode temperatures, and in some cases variation of electrode potentials.

In the case of a diode gun, the cathode temperature controls the beam current when the gun is operating in the temperature limited mode. At a limiting temperature the beam current no longer increases as the gun is operating in space charge limited mode. Variation of the cathode temperature allows investigation of this operation and characterisation of the electron beam produced over the operating range. Electrical potential changes could be used to simulate the gun geometry operating at different accelerating potentials. In the case of a triode gun configuration, the variation of cathode temperature and bias electrode potential can be used to investigate the gun peaking curve - and to find the points where the beam current is space charge limited.

4.1.2 Model analysis

The analysis of the model first required the model to be built in the pre-processor. This involved executing the command file to build the geometry with the correct potentials assigned to boundaries, adding a background region to fill the gaps between the electrodes and then meshing the model to generate the finite elements. The mesh and model data were stored. It was also necessary to construct a matching emitter file with the required cathode temperature. The model was then submitted to the solver module of the Opera suite. This process was achieved by building a list of model filenames to be solved and storing this. Also a list of operating parameter ranges to be solved with their associated step values were stored in a separate file. An Opera command file then read the model filenames in

turn to construct a series of models for each geometry using the operating parameter ranges.

A second Opera command file was used to sample the electron beam trajectories at a sample plane position defined to be in the region where the beam was fully accelerated, that is to say after the anode. This file read in the results of each model solution, and extracted a file containing the trajectory information. An example has been given in Table 2-2.

The trajectory intercept file was then submitted into the beam characterisation software developed within this work as described in section 2.5.3.

To initiate the design process, a model was created which contained all of the constrained geometries. The geometries could be constrained because of available design space, existing components or could be limited to reduce the solution space and reduce the time taken by the optimisation process to search within this space. Those features of the geometry that could be changed were altered to their extreme in two other models. Where the region face was totally constrained, there was no difference between the two geometries. It was also be possible to define the upper and lower extents to cover a very wide range of geometry types and size, where this range of design freedom was possible to be accommodated within the electron gun column dimensions.

The anode geometry described by the command file in Table 4-1 was one of two geometries that are shown schematically in Figure 4-1, the other being the matching geometry file describing the opposite extremity of change. These two geometries described the full range of design freedom. The area between the two geometries was the solution space to be investigated by the optimisation algorithm.

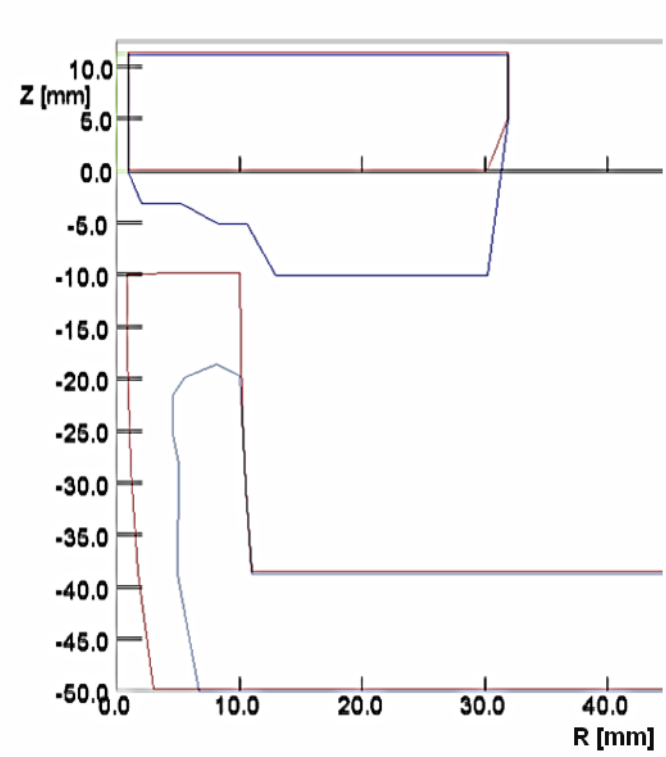

Figure 4-1 Schematic showing an example of two geometries that define the extent of change of the geometry of each electrode that will be allowable in the optimisation.

A software algorithm was generated to convert these two geometry files into a list describing which parts of the geometry could be changed and over what range. This algorithm worked in two stages. Initially both geometry files were modified so that all of the relevant face parameters were explicitly stated on each line. This was necessary as later, when the genetic algorithm changed lines, during mutation or when gene swapping, it was not desirable for changed parameters to be adopted by all subsequent lines where the parameter would have been set implicitly in the original model command file. The software then identified which lines had changed and the upper and lower bounds of the change - see for example Table 4-3. In this example only XP, YP and CURV parameters were optimised, although it was possible to add other parameters such as F and the potential it was set to, or N for subdivision of the face for accurate but not too slow solution times.

As this table described all of the lines that could have changed, variation between different geometries was described by lists of changes to the lines above, called the change genome, in combination with a list of

invariant geometry common to all designs, called the seed genome. The evolutionary processes were applied only to the change genome. For each population member this was merged with the seed genome to give a complete set of commands that would build the gun model. This could then be submitted for solution, the beam characteristics derived and the model score calculated - see section 4.2 .

Table 4-3 An example listing of the change genome showing the parameters that can change in the gun geometry between the upper and lower extents bounding the design freedom.

line	XPmax	XPmin	YPmax	YPmin	CURVmax	CURVmin
45	5.01	1.71	-38.63	-38.79	0	0
46	5.11	1.15	-28.02	-28.80	0	0
47	4.54	0.87	-25.21	-17.71	0	0
48	4.54	0.87	-21.46	-10.06	0	0
49	5.58	5.58	-19.74	-10	0	0
50	8.22	8.22	-18.49	-10	0	0
51	10.01	10.01	-19.59	-10	0	0
57	6.75	3	-50	-50	0	0
67	30.28	30.28	-10	0	0	0
68	26.25	26.25	-10	0	0	0
69	19.63	19.63	-10	0	0	0
70	13	13	-10	0	0	0
71	10.63	10.63	-5	0	0	0
72	8.25	8.25	-5	0	0	0
73	5.3	5.3	-3	0	0	0
74	2	2	-3	0	0	0

The range information carried in the change genome was used whenever a gene was mutated. The mutation was constrained within the limits for that position or line curvature and the scale of mutation was normalised to the range for that position or curvature.

As in the shape solving algorithm, gene splicing was implemented by swapping blocks of line changes from the change genome of parents, but lines were kept at the same position in the gene and the range information was therefore still valid.

The special adaptations that were made to evolutionary methods to allow them to be implemented for electron gun designs were:

- A change genome was constructed that contained only those parts of the design that can be changed and to which evolutionary processes can be applied
- A generic genome was constructed that described the rest of the design, and which when added to the change genome described a complete gun design
- The allowable range of any position or line curvature in the change genome was encoded within it (a) to constrain solutions within practical limits and (b) to scale any mutation to that range
- Gene splitting was only carried out between genes so that numbers were not split, so that mutation could be controlled independently.

4.2 Fitness test

Electron gun design is rarely aimed at optimising a single characteristic. When the design requirement specification called for optimisation of several characteristics simultaneously, this required the fitness test to be multi-objective. The optimised solutions were given by a series of trade-offs between the different objectives where improvement of any one objective would have diminished another, called a Pareto frontier, see section 3.1. The Pareto frontier would only be fully explored if the optimisation process was left to run indefinitely.

Subsequently, if the weighting factors and objective functions were correctly defined, all solutions on the Pareto frontier were equally optimal and the choice of any one of these designs could only be made by introducing an additional criteria. The weighting factors applied to different design objectives defined the shape of the Pareto frontier when plotted in solution space. For the design of electron guns, it was only necessary to meet the design objectives, consequently once a design solution had achieved a target fitness score then the optimisation process was halted.

In practice, the evolution algorithm would arrive at one of these, and the optimisation process was stopped once the design requirements had been satisfied.

4.3 Algorithm implementation

The following steps were carried out to implement the design evolution process, see also Figure 4-2.

An initial population of electron gun design variants was generated by producing genomes made from a randomised set of change genomes combined with the generic genome.

Each of the electron gun designs was analysed using a finite element space-charge solver and electron trajectory vectors for beamlets from the cathode determined as they left the gun. For each of the electron gun designs, the electron trajectory data was used to produce beam quality metrics (brightness, intensity, angle and beam width) through calculation of the trajectory path mathematically traced through an electron lens to the work piece. The beam quality metrics were then used to derive a fitness score for the design. This score depended upon the requirements for the gun e.g. maximise the beam brightness and minimise the beam angle.

Those designs with the best fitness score were selected to produce a ‘parent group’. The next generation of designs was produced from this group by choosing two designs randomly and splicing a random section of one change genome into the other. The genome was only split between genes to avoid mutations caused by splits occurring within a gene. Random mutation of any one of the change genes was also implemented within this stage. The new change genomes were combined with the generic genome to produce the new generation of gun designs.

The parent group and the new generation formed a new population, which was then put through the same process until a threshold satisfactory fitness score was achieved.

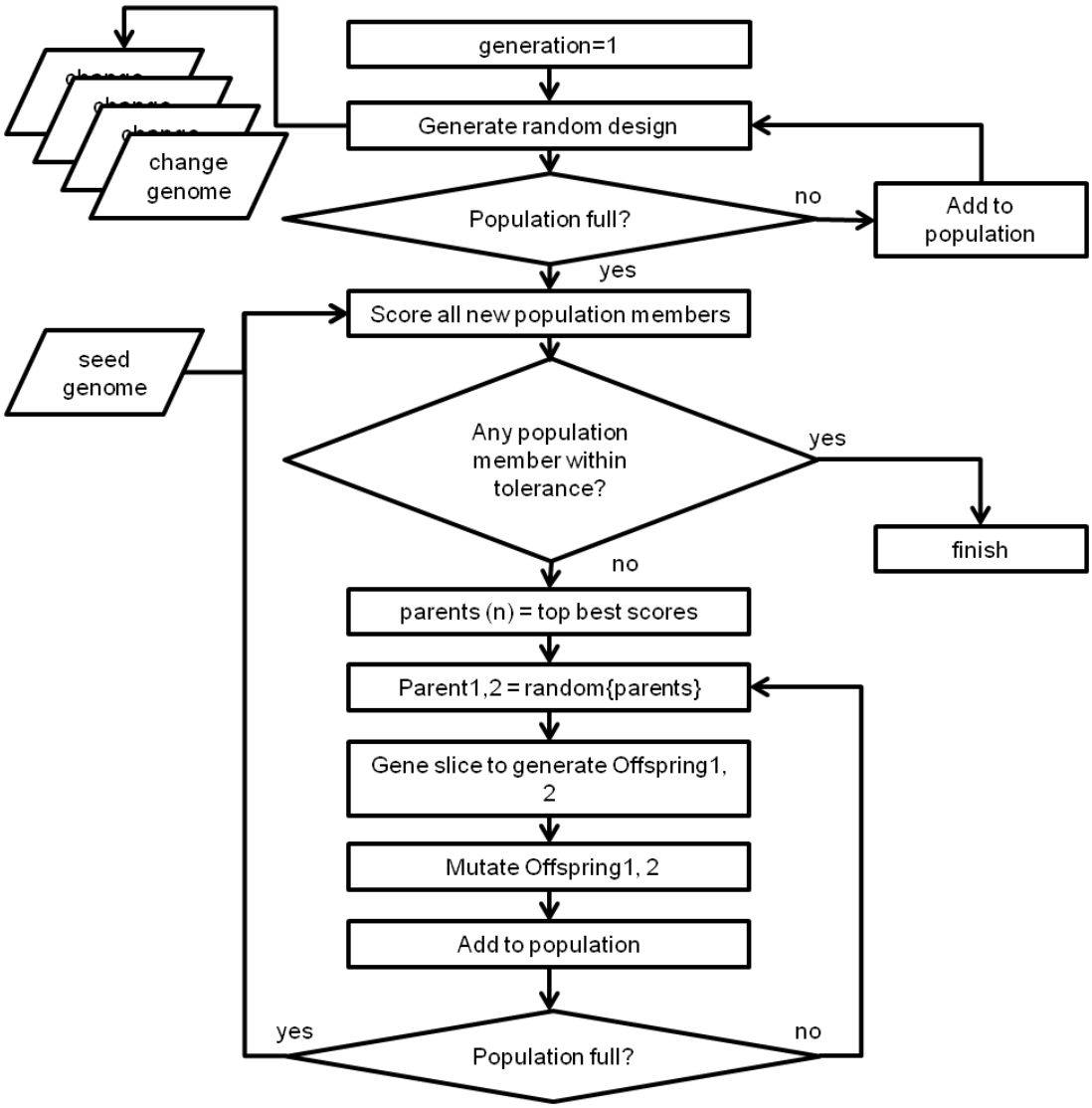

Figure 4-2 Flow chart of the gun model optimisation procedure using evolution.

The process therefore was designed to have a number of features anticipated to be of benefit to the particular challenge. At first, a good design genome was promoted to the population forming the next generation until its fitness score ranking was not high enough. This ensured that each generation's parent group was at least as good as the last, and is a process termed elitist selection. In later trials, this feature has been investigated, as there was concern that elitism may allow local maxima of the optimisation function to dominate, see Chapter 5.

By splicing the genes from two parents, a section of the design was copied to the child with the rest remaining the same as one of the parents. In

genetic algorithm terminology this was a two point crossover function. The splicing respected the database structure of the genome to avoid mutation of the design due to corrupting the database. This was achieved by ensuring that the data format as represented in Table 4-1 was maintained. However, some mutation in the form of randomisation of some of the variables within their mutation scale was introduced to a controlled level to ensure that the design space was adequately explored.

In summary, the evolutionary process was implemented with special adaptations to make it suitable for electron gun design using modelling software and working within practical physical constraints. These adaptations were the use of upper and lower bounds on the geometry to define the constraints and the range of mutation for any variable in the design, the automatic derivation of a seed and change genome to allow efficient implementation of genetic design processes and the writing of code to allow genetic algorithm parameters to be independently controlled.

Chapter 5: Electron gun model examples

In this chapter two examples are given of the operation of the optimisation algorithm for the design of electron guns. In the first case the optimisation was limited to changing the shape of just the anode, within dimensional constraints. In the second case a much wider design freedom was given so that both electrodes could be changed in shape over a wide range. The operation of the design evolution processes is described and the two cases compared.

5.1 Anode optimisation in a diode gun

The electron gun evolutionary design process was applied to a novel radio frequency (RF) excited plasma cathode gun design (Ribton and Sanderson, 2015; del Pozo et al., 2014). This type of gun design is a diode having a high voltage electrode and cathode at the same potential. The cathode is a plasma, but for simulation purposes the cathode surface was modelled as a lanthanum hexaboride thermionic emitter over a range of temperatures and therefore a range of emissivity, but in this case producing electrons with no thermal energy.

The gun design was required to produce an intense electron beam at focus and produce a reasonably low angle beam so that it could pass through an existing gun column with a constriction at the electron lens. Therefore the beam was required to be of high brightness. However, too low an angle beam would give poor electron optic magnification and too high a beam diameter would impinge upon the electron lens bore, so an optimum beam diameter of 4 mm at the lens position (150 mm from the cathode) was chosen. These requirements are summarised in Table 5-1:

Table 5-1 RF plasma gun beam requirements.

Metric	**Requirement**
Diameter at 150 mm from cathode	Ideally 4 mm
Brightness	> 5000 $Amm^{-2}sr^{-1}$

Weighting factors were used for each of the metrics as the design fitness test needed to combine the scores from each requirement into a single score in order to allow ranking of the design variants in the population. The scoring function, which utilises the quantified beam characteristics from the design simulation, is described in the following pseudo-code:

```
Over the cathode temperature range 1450 – 1600K and for 30 kV and 60 kV accelerating potentials:

score = add Log(brightness)*beam current

If beam current <20 mA

If 1/(beam diameter 150 mm from cathode – 4) >10

Add 10

Else

add abs(1/(beam diameter 150 mm from cathode – 4))
```

The evolution parameters used in this trial are presented in Table 5-2:

Table 5-2 Evolutionary algorithm parameters.

Parameter	Value
Parent group size	4
Offspring group size	6
Mutation scale	0.1
Mutation probability	0.07

The designs were labelled with a generation number and a population number, e.g. Gen_1_Pop_5 was the 5th offspring produced in the first generation. A log was kept of the scoring – this is shown for the 1st generation in Table 5-3 and for the 10th generation in Table 5-4.

Table 5-3 1st generation population ranked scores.

Model	Score
Gen_0_Pop_1	2.37
Gen_1_Pop_6	2.10
Gen_1_Pop_4	2.10
Gen_0_Pop_3	2.09
Gen_1_Pop_5	2.09
Gen_0_Pop_0	2.03
Gen_1_Pop_7	2.02
Gen_1_Pop_8	2.02
Gen_0_Pop_2	2.01
Gen_1_Pop_9	2.01

Table 5-4 10th generation population ranked scores.

Model	Score
Gen_10_Pop_4	11.59
Gen_6_Pop_4	3.57
Gen_8_Pop_6	3.57
Gen_9_Pop_5	3.57
Gen_10_Pop_6	3.57
Gen_10_Pop_7	3.57
Gen_9_Pop_7	3.23
Gen_10_Pop_5	3.03
Gen_10_Pop_8	2.89
Gen_10_Pop_9	2.65

The progress of the automatic design algorithm was monitored through the plotting the best fitness score of each generation. This is presented in Figure 5-1:

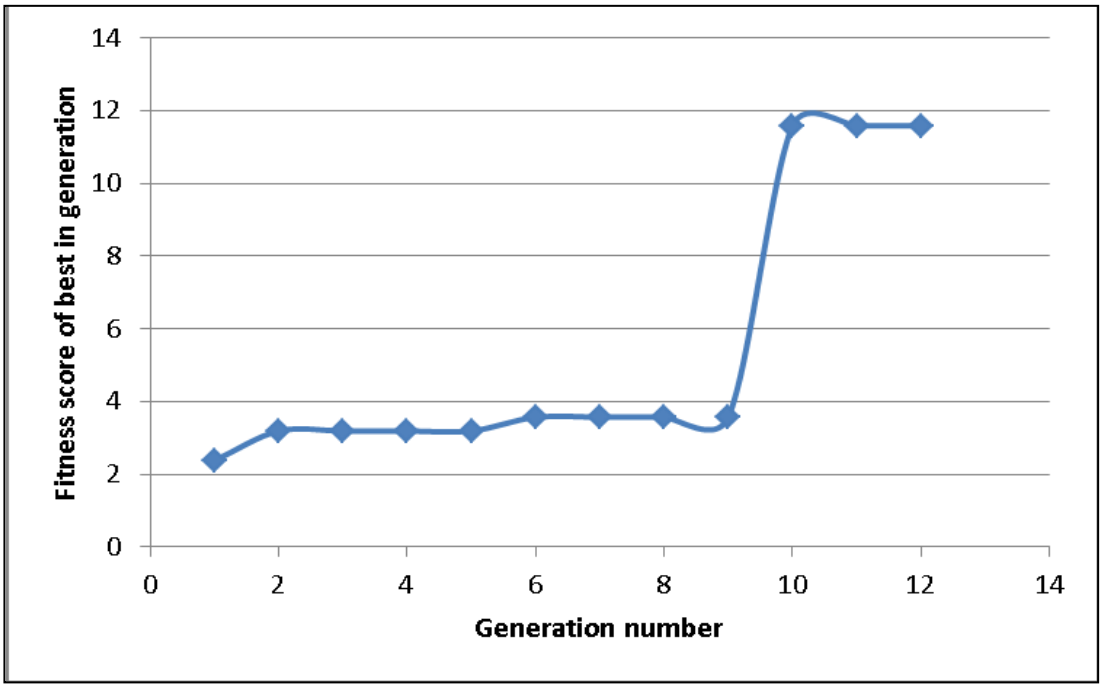

Figure 5-1 The best fitness score in successive generations.

It can be seen that in successive generations the score never decreases and is at least the same as the previous generation. This is a consequence of employing elitism, and this was examined in more detail in the example given below. It also can be seen that the evolution had a step change at generation 10. This raised concern that the problem space may not have been adequately explored in this example. This was in large part due to the nature of the scoring function, which was also modified in the following example by using error spread functions.

5.2 Low voltage gun electrode optimisation

In this section, a description is given of the evolutionary design of a low voltage electron gun to be operated at high powers. The design generated is compared with a gun developed using the Pierce methodology, which was also designed to operate at low voltage and high power.

A 30 kV high power diode gun design evolution was investigated. Normally a higher acceleration voltage, typically in the range 60 kV to 150 kV, has been used for high power electron guns for thick section welding. For example a 150 kV, 60 kW gun can be used to weld more than

200 mm thick steel. However, very narrow fusion zones of less than 1 mm, produced by intense and parallel beams that could only be generated at a higher acceleration voltage, are less desirable in thick sections. This is partly because precise joint fit up can become difficult to achieve. In addition, a deep and narrow keyhole can be unstable and prone to necking and reopening. This can lead to missed joint defects or cavities in the weld. Moreover, the lower the acceleration voltage the easier X-ray shielding becomes, which can make the equipment and its deployment simpler and cheaper.

Low voltage, high power electron guns have been widely used in vacuum electronics for devices such as klystrons and travelling wave tubes. An example is given in (Frost et al., 1962) where it is described that the initial electrode designs were calculated using the Pierce method (Pierce, 1954) and were then refined using electrolytic tank experiments as described in Chapter 2.

The objective of this investigation was to determine if the design approach used for vacuum electronics could be adapted to be valid for a low voltage gun suitable for electron beam welding.

The work was carried out in the following steps:

- Definition of two models describing the extents of the geometry range to be investigated.
- Definition of the scoring function for a low voltage EB welding gun.
- Preparing and running the design evolution with two population sizes and with or without elitism.
- Comparison of evolution outputs.
- Assessment of the characteristics of the beam produced by the optimised low voltage EB gun design.

5.2.1 Model extents

The extents of geometry within which the evolutionary algorithm would operate were defined as, in one extreme, parallel flat electrodes, 20 mm

apart. In the other extreme, the geometry was defined as two nested cones, with a 5 mm separation measured in the Z axis direction. These are shown in Figure 5-2, where the cathode is green, the gun electrode blue and the anode is red.

The surface of the gun electrode and the anode was defined by a series of points in a geometric progression of greater radii. This gave more geometrical detail close to the cathode where it was expected that there would be a strong influence of geometry on the beam characteristics. Those nodes that change position between Figure 5-2 (a) and (b) define the range of geometry to be explored by the evolutionary algorithm.

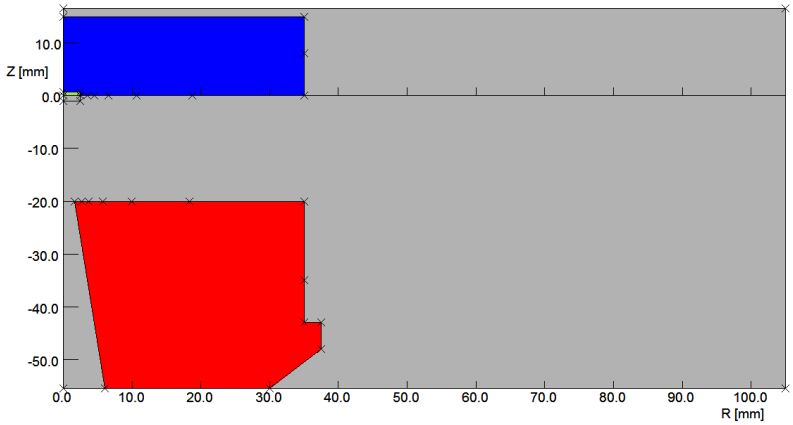

(a) Lower extent of geometry

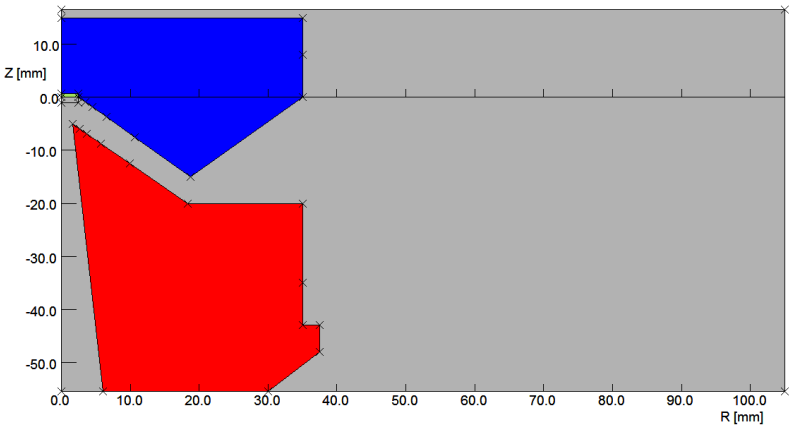

(b) Upper extent of geometry

Figure 5-2 Definition of the geometry extents with two models

In preparation for the evolutionary algorithm the two model files were processed – first to give the change file listed in Table 5-5. In addition, the models were listed explicitly, in such a way that they could be adjusted by the evolutionary algorithm.

Table 5-5 The change file listing for the geometry extents illustrated in Figure 5-2.

Line in command file	XPmax (mm)	XPmin (mm)	YPmax (mm)	YPmin (mm)	CURVmax (mm^{-1})	CURVmin (mm^{-1})
55	3.515625	3.515625	-0.93751	0	0	0
56	4.53125	4.53125	-1.87501	0	0	0
57	6.5625	6.5625	-3.75002	0	0	0
58	10.625	10.625	-7.50003	0	0	0
59	18.75	18.75	-15.0001	0	0	0
70	1.6	1.6	-4.99999	-20	0	0
71	2.64375	2.64375	-5.93749	-20	0	0
72	3.6875	3.6875	-6.87498	-20	0	0
73	5.775	5.775	-8.74998	-20	0	0
74	9.95	9.95	-12.5	-20	0	0

The manner in which the two extents were described meant that only the Z coordinate of the points on the faces of the electrode and anode were changed. The distance over which the nodes were different from one extent model to the other defined the range of that coordinate position to be

investigated. It should be noted that in the Opera command files (which were text macro files used by the evolutionary algorithm to build individual gun models) the Z coordinate is named YP, and this naming convention has been used throughout.

An additional measure taken with the preparation of this optimisation was to include a finely and regularly meshed region in front of the emitter in order to accurately model the space charge in this region of the gun. This region was only 0.5 mm thick and was included in the model definition of the cathode.

5.2.2 Scoring function

One of the problems that can occur in modelling the gun and then deriving beam characteristics is that the trajectory plotting algorithm in the Opera post-processor does not normally detect when a trajectory passes through a surface, see Figure 5-3. This can lead to designs scoring well that would be impossible to realise practically.

This problem was avoided by specifying a conducting material for the anode - the trajectory plotting stopped whenever a trajectory met this material, so that they would not extend beyond the anode to the sampling plane used to assess beam quality. It was necessary to ensure that the scoring function in part optimised for high current after the anode at the sampling plane to ensure the designs where the beam did not impinge on the anode scored more highly and were favoured.

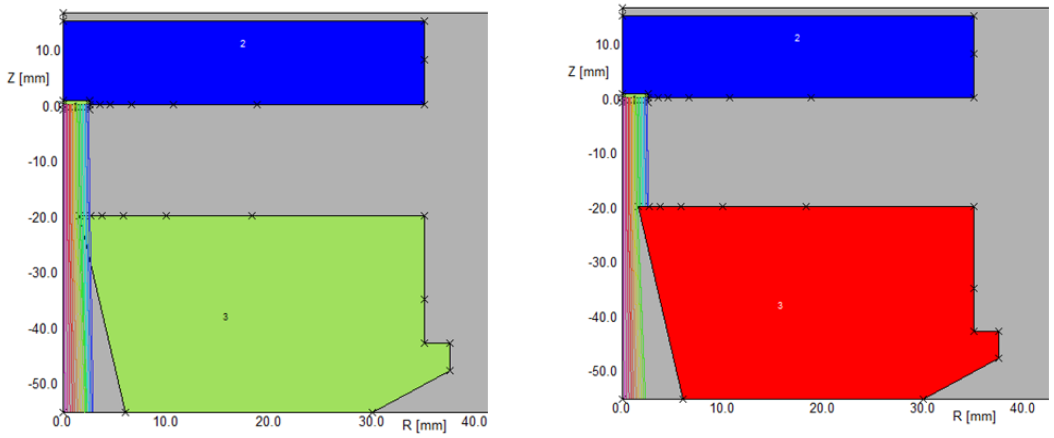

(a) Normal materials allow trajectories to pass through the anode

(b) Use of a conducting material halts the trajectories that impinge on the anode

Figure 5-3 Trajectory plotting in the post-processor could lead to non-practical geometries scoring highly as the trajectories could pass through the anode.

The scoring function for this design was defined as follows:

- for all currents >10 mA, FWHP < 0.8 mm
- for all currents >10 mA, maximum beam diameter in lens is 20 mm
- for all currents >10 mA, lens focal length > 50 mm
- at cathode temperature of 1600 K, beam current > 1 A

Any specific design of gun was modelled for a range of cathode temperatures and then the score was derived over the operating range of the gun. This was encoded into the model_evolve script following the algorithm shown in Figure 5-4, where

total_current is the beam current in A

s is the score in arbitrary units

foc_fwhp is the FWHP of the beam at the work piece surface in mm

lens_diam is the maximum beam diameter at the centre plane of the lens in mm

f_lens is the calculated lens focal length in mm to focus the beam at the work piece surface

temperature is the cathode temperature in K for the specific model data

g1, g2, g3 & g4 are relative gain factors between the different functions in arbitrary units

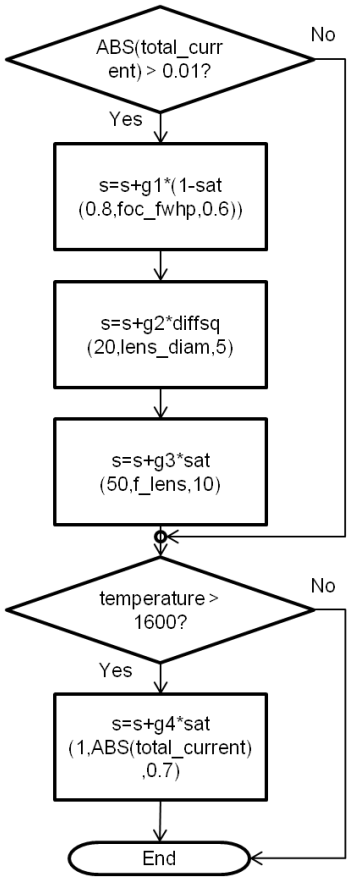

Figure 5-4 The scoring function algorithm for a low voltage, high power EB welding gun.

Two error spread functions were used called sat and diffsq, illustrated in

in

Figure 5-5. The aim of these was to allow the score to progress towards a maximum rather than jumping once a threshold was reached. It was envisaged that this would improve the efficiency of the evolution algorithm in exploring the problem space.

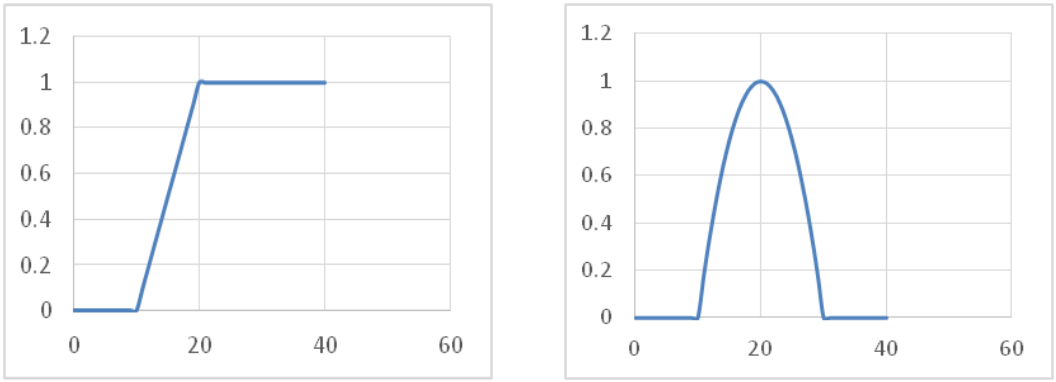

(a) The sat function: threshold at 20 with a range of 10

(b) The diffsq function: centred on 20 with a range of 10

Figure 5-5 Error spread functions used in the scoring algorithm.

5.2.3 Model evolution

Four different evolutions were carried out using the same scoring function. For each of the four evolutions, elitism was toggled on or off, and the number of offspring was changed from 12 to 24. The mutation rate was maintained at 7% and the mutation scale at 10%. A parent group of the 8 highest scoring individuals was selected from each generation. The model evolutions completed 20 generations within 5 hours to 10 hours on a single core i5 processor laptop.

The scores for the parent group of the last generation from the evolution are shown in Table 5-6. When elitism was enabled it can be seen that there was a high incidence of cloning – the clone designs are highlighted in the table.

Cloning happened as the parent group was likely to consist of mostly the same individual designs from one generation to the next, especially in later generations. Consequently, there was a higher likelihood that a clone offspring was produced. If this happened to be a clone of a parent, it was likely it was promoted into the parent group for the next generation. There was generally an even higher likelihood of cloning if the two clone parents gene swapped without mutation as this would produce another clone.

Table 5-6 Parent group scores of last generation.

	12 offspring		24 offspring	
	Model name	**Score**	**Model name**	**Score**
Elitism	Gen_12_Pop_12	22.89456	Gen_13_Pop_12	22.64782108
	Gen_11_Pop_18	22.87686	Gen_15_Pop_8	22.64782108
	Gen_12_Pop_16	22.63198	Gen_17_Pop_18	22.64782108
	Gen_15_Pop_15	22.63198	Gen_12_Pop_8	22.63398685
	Gen_17_Pop_15	22.63198	Gen_14_Pop_9	22.63398685
	Gen_9_Pop_13	22.52363	Gen_15_Pop_26	22.63398685
	Gen_13_Pop_17	22.52363	Gen_16_Pop_11	22.63398685
	Gen_6_Pop_14	22.36306	Gen_16_Pop_13	22.63398685
No elitism	Gen_18_Pop_8	23.57578	Gen_18_Pop_22	23.71866438
	Gen_18_Pop_15	23.50613	Gen_18_Pop_25	23.55861005
	Gen_18_Pop_14	23.35567	Gen_18_Pop_18	23.39785312
	Gen_18_Pop_9	23.34075	Gen_18_Pop_21	23.38766775
	Gen_18_Pop_18	23.22605	Gen_18_Pop_24	23.35296694
	Gen_18_Pop_12	23.18526	Gen_18_Pop_19	23.31590849
	Gen_18_Pop_11	23.14629	Gen_18_Pop_16	23.27645892
	Gen_18_Pop_19	23.06651	Gen_18_Pop_12	23.27574531

Although elitism ensured the best score in a generation was at least as good as the previous generation, it seemed to be less efficient at optimising the design. It can be seen from Table 5-6 that in both examples of the population size, the score reached by the best optimisation was better without elitism.

Switching elitism off seemed to allow the algorithm to more efficiently explore the problem space, and to arrive at a higher scoring optimum.

The geometries of the optimum models produced after twenty generations are shown in Figure 5-6. It should be noted that there was no element of the score derived from high voltage stress reduction - there are consequently some sharp features on the optimum designs that if implemented would be likely to precipitate high voltage breakdown between the gun electrode and the anode. A practical implementation would also include a review of the design to reduce high voltage stress in the anode-electrode gap.

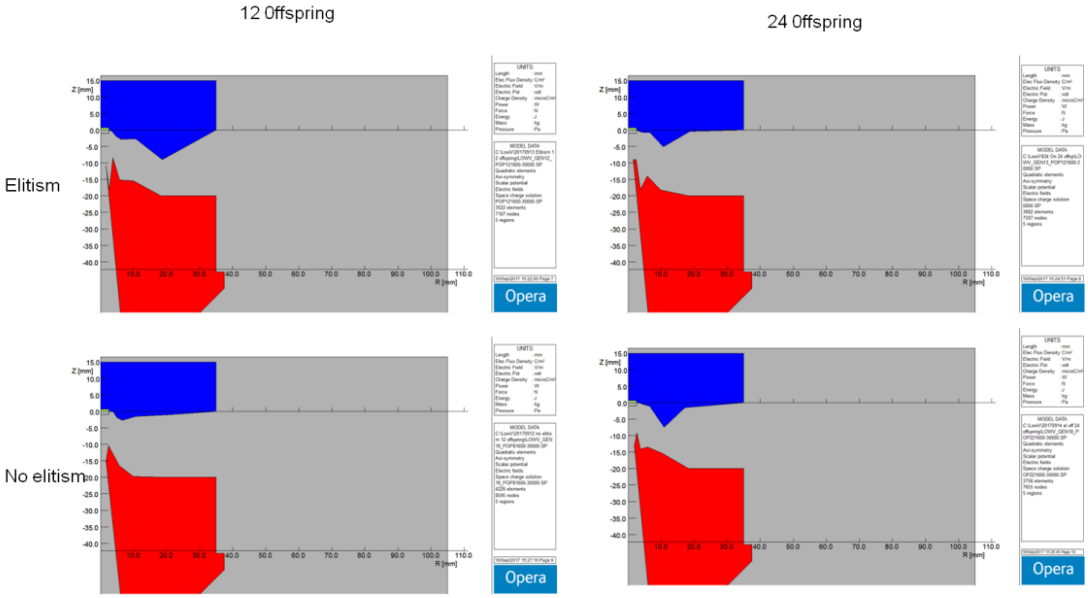

Figure 5-6 The four optimum designs produced by evolutions either with or without elitism and with 12 or 24 offspring each generation.

It is interesting to compare these with the Frost geometry – although this was a 2 kV gun and was physically smaller. The anode designs evolved are similar to the Pierce geometry – this leads to a beam compression from the cathode and a real beam cross-over positioned just beyond the anode.

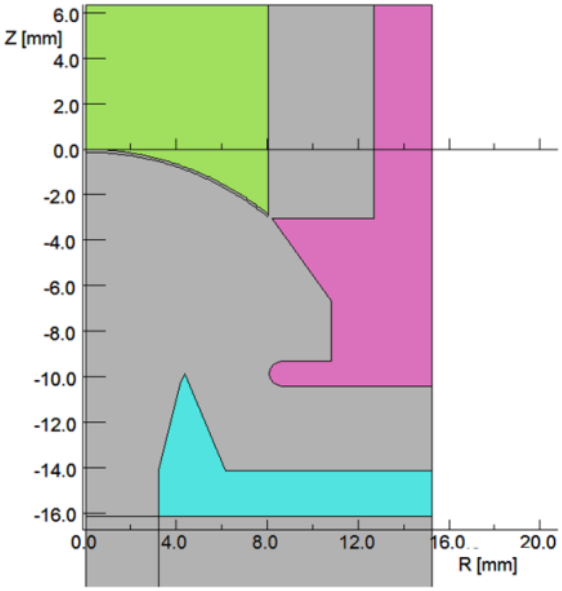

Figure 5-7 Pierce gun type 4A, 2 kV gun geometry for comparison (Frost et al., 1962).

5.2.4 Optimum design

The beam trajectory plots for the highest scoring gun design for the four cathode temperatures used to derive its score are shown in Figure 5-8. The beam characteristics derived from these trajectories is shown in Table 5-7.

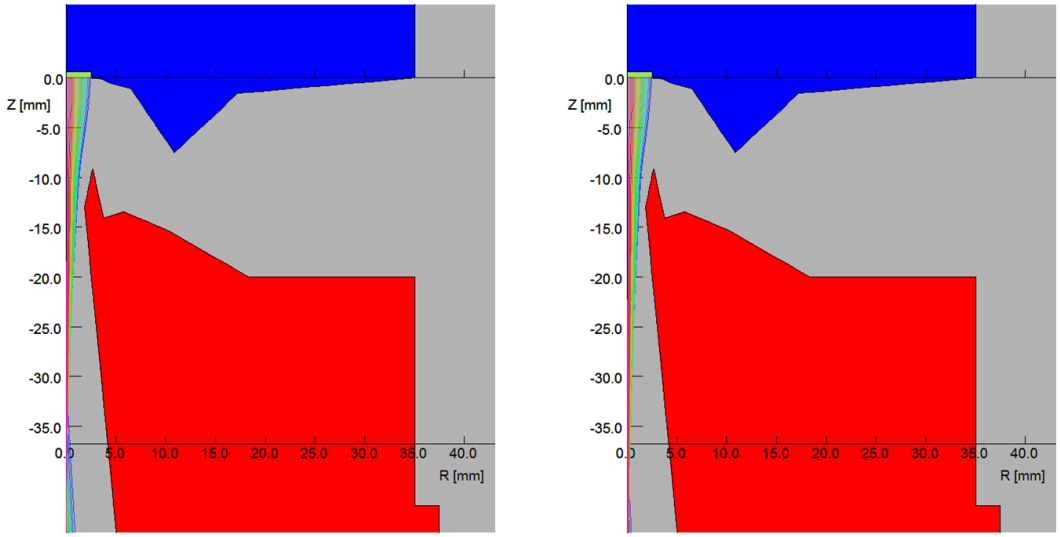

(a) 1500 K, 48.5 mA (b) 1600 K, 202.6 mA

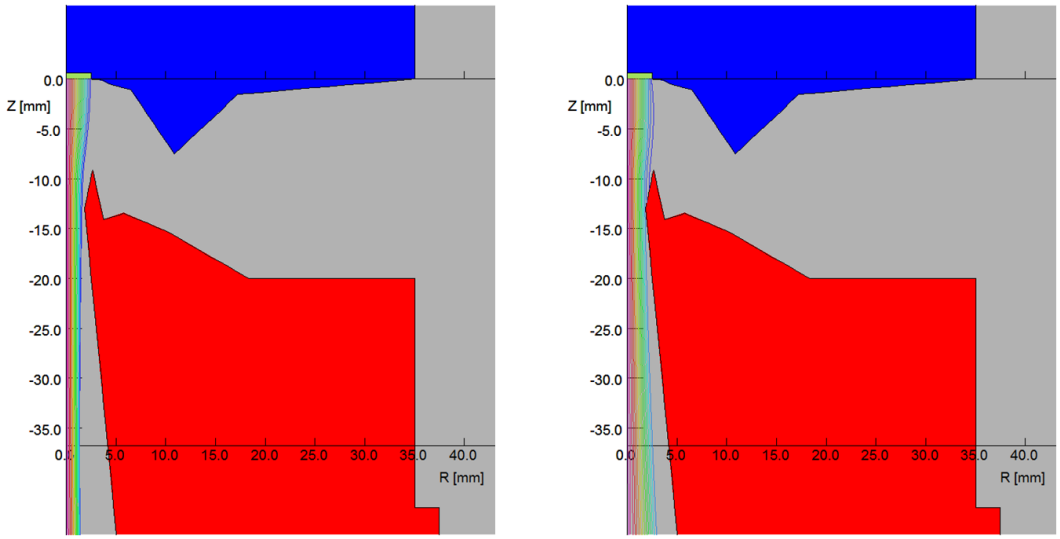

(c|) 1700 K, 721.7 mA (d) 1800 K, 1039.4 mA

Figure 5-8 The optimum gun geometry derived shown at the four cathode temperatures at which the beam characteristics were assessed - caption is the cathode temperature, beam current.

When the characteristics were derived it was assumed that the electron lens was 200 mm from the cathode and that the work piece was 200 mm from the lens centre plane.

The model shows that a beam current of 1034 mA at 30 kV i.e. 31.2 kW of beam power could be produced into a beam spot diameter (FWHP) of 0.16 mm.

Table 5-7 Table of beam characteristics for model "gen18_pop22".

Temper-ature (K)	total_ current (A)	zsrc_ imn (mm)	zvar_ imn (mm^2)	rsrc_ imn (mm)	angdiv_ imn (rad)	Angdivvar _imn (rad^2)	Area (mm^2)
1500	-0.0485	-37.2375	15.6326	-0.12114	0.036394	0.000259	0.184398
1600	-0.2026	-49.2197	83.9220	-0.18414	0.015875	0.00062	0.426089
1700	-0.7217	37.51364	804.649	-0.28235	0.01361	8.95E-06	1.001798
1800	-1.0394	5.131332	8.55752	-0.09654	0.039833	0.000138	0.117113
Temper-ature (K)	**Omega (sr)**	**Bright-ness ($Amm^{-2} sr^{-1}$)**	**f_lens (mm)**	**Foc _d_imn (mm)**	**Foc _fwhm (mm)**	**Foc _fwhp (mm)**	**Max_diameter _at_ -200mm (mm)**
1500	0.01663	-15.8334	89.7350	0.2977	0.183415	0.176629	20.65696
1600	0.00316	-150.186	85.1088	0.617679	0.198466	0.203915	16.05918
1700	0.00232	-309.559	112.917	0.65848	0.115595	0.084137	7.413413
1800	0.01992	-445.395	101.266	0.188246	0.180574	0.163628	22.41026

This evolutionary design was considered to be successful in that the score function had driven the evolutionary process in a practical direction, the gun design produced generated a beam over its operating range that had highly suitable characteristics for EB welding and the design was radically different in geometry from typical electron beam guns used for welding, but had some similarity to low voltage, high power guns used for vacuum electronic devices.

Chapter 6: Beam measurements and comparison

In this chapter comparison is carried out between the beam characterisation algorithm outputs with measured data from experiments carried out in the laboratory. This is given for a new type of diode gun geometry, where the characterisation algorithm was checked against measurements made in the laboratory with a slit probe device.

6.1 Verification of gun analysis and beam characterisation

As part of this research a new type of gun was explored using a laser beam to heat the thermionic cathode. The gun was operated as a diode with the cathode in the temperature limited mode. The focus of the initial tests was on the optical elements for the laser, its transmission into vacuum and the power requirements for the laser. However, one of the experimental objectives was to produce and measure the beam from the gun over a range of beam currents, and to assess its suitability for two applications: 3-D printing and turbo-charger impellor welding. As the beam would be projected through the anode it was necessary to ensure that the lens position and bore would be suitable for its transmission down into the work chamber where it could be measured.

Initially, the design of the gun electrode was from a previous gun geometry which had been employed at -150 kV accelerating potential. There was a choice of anode upstands available and the results shown are for the gun configuration that was selected from the available options. The specific geometry for which the analysis and measurements were carried out is shown schematically in Figure 6-1 and is termed the laser heated cathode diode geometry (LHCD). This gun was to be operated at -60 kV accelerating potential.

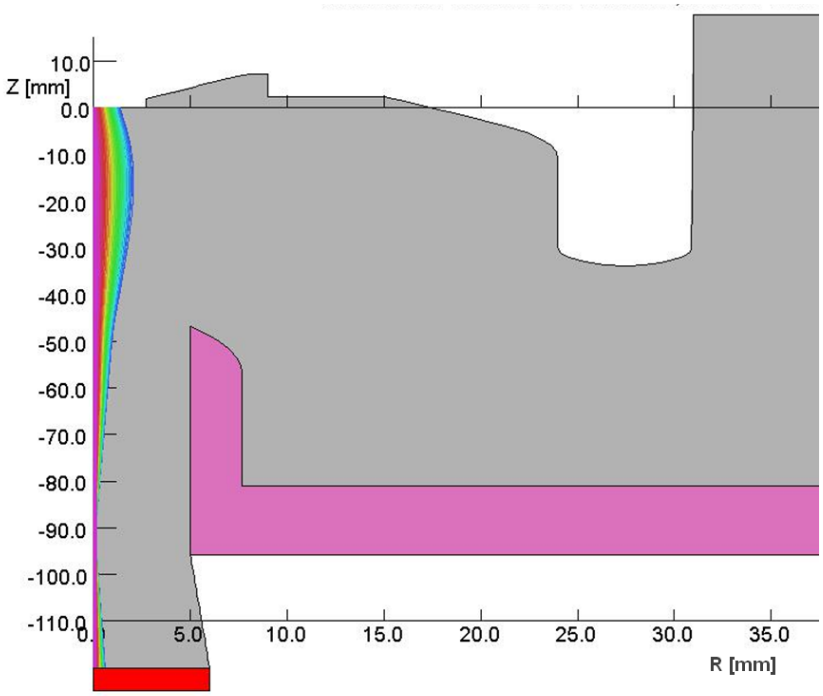

Figure 6-1 Laser heated cathode diode gun geometry with trajectories, colour coded by radial position of emission, plotted from the emitter through the resolved field of the electron gun.

The cathode is a sintered lanthanum hexaboride button which is mounted in a tantalum holder - see Figure 6-2. The holder and button were then ground flat with the aim of producing no features near the cathode surface that could cause curvature of the electric field and lead to aberration or beam fringe. In addition, the button fitted the tantalum holder closely in a bid to ensure that side emission from the button did not contribute into the beam. During this research a button with a diameter of 2.8 mm was investigated.

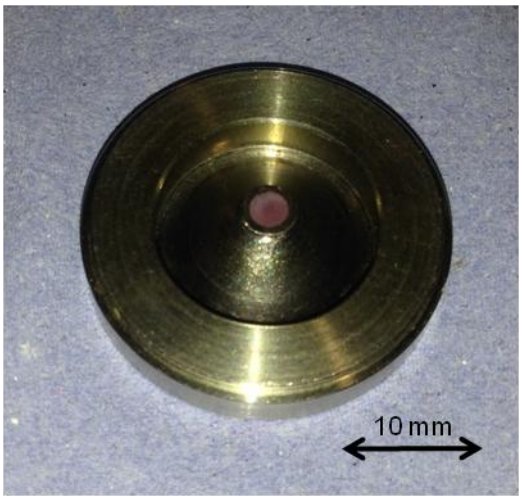

Figure 6-2 The laser heated 2.8 mm diameter cathode mounted in a tantalum holder.

The gun geometry was analysed in an identical way to the method described in Chapter 4. Following analysis the beam was sampled after the anode and the intersect file was then submitted into the beam characterisation software described in section 2.5, as used by the optimisation algorithm.

The electron beam trajectories are plotted in Figure 6-1. There are approximately 1000 trajectories that are generated from 20 equally spaced positions along the cathode surface. The model was initially solved with only 20 trajectories, one from each position, which was relatively quick taking a few minutes. Then the additional trajectories, with thermal velocity spread, were added at the cathode surface and the model resubmitted for further solution. This stage took longer to converge to a solution - approximately 10 minutes. This was due to the finer distribution of charge throughout the model requiring more computation to determine the vector field distribution. Each trajectory had a beam current assigned to it which was calculated at the cathode surface according to the Langmuir-Fry emission relationship, see section 2.2 .

The trajectory plane intersection with the beam was carried out at a position where the electrons were no longer being accelerated. It can be assumed after the anode that the electrons are in a near field free region.

Any path deviation due to space charge is insignificant as the electron density is low and the electron momentum is high, see section 2.2. Therefore, it was assumed that the trajectories would continue in straight lines after the anode and it was only necessary for the intersect file to collect, for each trajectory, their velocity vector, position and the assigned beam current. A number of these files were collected for analyses of the same geometry operating over a range of cathode temperatures.

These files were then submitted into the beam characterisation algorithm which generated a table of beam characteristics over the operating range of the cathode. The salient characterisation data is presented in Table 6-1. As previously in Table 2-3, the brightness characteristic changes an order of magnitude, due in this case, mainly to the change in beam angle.

Table 6-1 Beam characterisation data for the LHCD gun geometry operated over a cathode temperature range 1400 K to 1700 K.

Temperature (K)	total_current (A)	zsrc_imn (mm)	rsrc_imn (mm)	angdiv_imn (rad)	Brightness ($Amm^{-2}sr^{-1}$)	f_lens (mm)	foc_d_imn (mm)	foc_fwhm (mm)	foc_fwhp (mm)	Max_diameter_at_-275 (mm)
1400	-0.0008	-75.1	-0.106	0.013	-3	154.6	0.722	0.044	0.711	8.4
1425	-0.0013	-76.4	-0.106	0.013	-4	153.8	0.726	0.023	0.719	8.4
1450	-0.0019	-78.0	-0.105	0.013	-6	152.9	0.729	0.024	0.730	8.3
1475	-0.0028	-80.3	-0.104	0.013	-9	151.5	0.730	0.028	0.733	8.2
1500	-0.0041	-83.7	-0.101	0.013	-15	149.5	0.721	0.044	0.703	8.1
1525	-0.0060	-88.2	-0.099	0.013	-23	146.7	0.721	0.022	0.687	7.9
1550	-0.0087	-94.7	-0.097	0.012	-41	142.6	0.735	0.267	0.684	7.6
1575	-0.0123	-104.5	-0.094	0.007	-183	136.5	0.750	0.024	0.646	7.3
1600	-0.0172	-114.5	-0.094	0.007	-225	129.9	0.797	0.027	0.675	6.9
1625	-0.0240	-131.8	-0.095	0.012	-114	118.4	0.904	0.030	0.820	6.5
1650	-0.0329	-149.7	-0.118	0.013	-88	105.9	1.284	0.292	1.197	6.9
1675	-0.0393	-138.4	-0.114	0.017	-70	113.9	1.141	0.046	1.110	7.7
1700	-0.0375	-133.9	-0.077	0.018	-117	117.0	0.748	0.104	0.663	8.5

Measurement of the beam characteristics in an experimental set up was necessary to allow comparison of this data derived from the model. The LHCD was mounted onto a lower gun column containing an electromagnetic focusing lens and a set of deflection coils. A slit probe for measuring the beam width was set up in a vacuum chamber. The slit width was 0.1 mm. The beam was swept across the probe in a circular beam path, see Figure 6-3. The beam was deflected around a 30 mm diameter circle at a speed of 133 ms^{-1} to avoid melting of the probe by the beam.

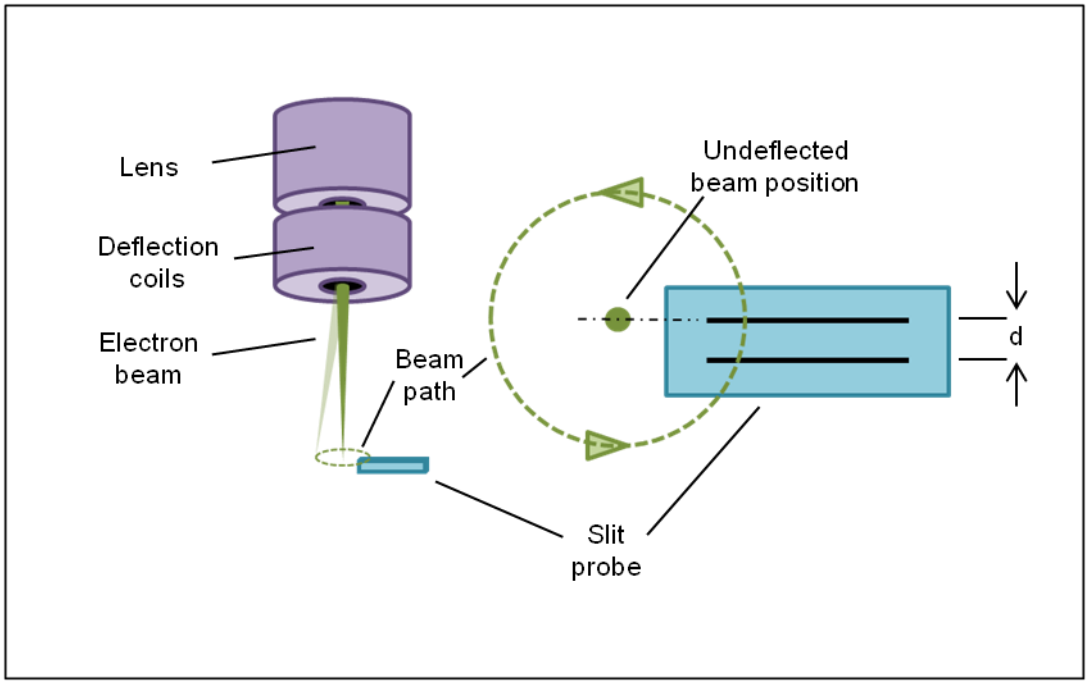

Figure 6-3 Experimental set up to determine beam characteristics.

The signal from the slit probe was collected on a digital storage oscilloscope and transferred into a spreadsheet. A template was built to analyse the traces to determine a beam width measurement. The beam speed was found from knowing the distance between the slits (d) and measuring the time between the two signal pulse peaks. Only one of the peaks was used to measure beam width, this being the one from the slit radial to the undeflected beam position so that the beam was not angled to the slit, which would reduce its apparent width. The template integrated the signal to find the interquartile range of the measurement pulse, which was equivalent to the FWHP. It also double-differentiated the signal to find the

peaks of the pulses, which were then used to determine the FWHM. An example of the analysis is shown in Figure 6-4 for a 1.5 mm diameter cathode at 5 mA beam current.

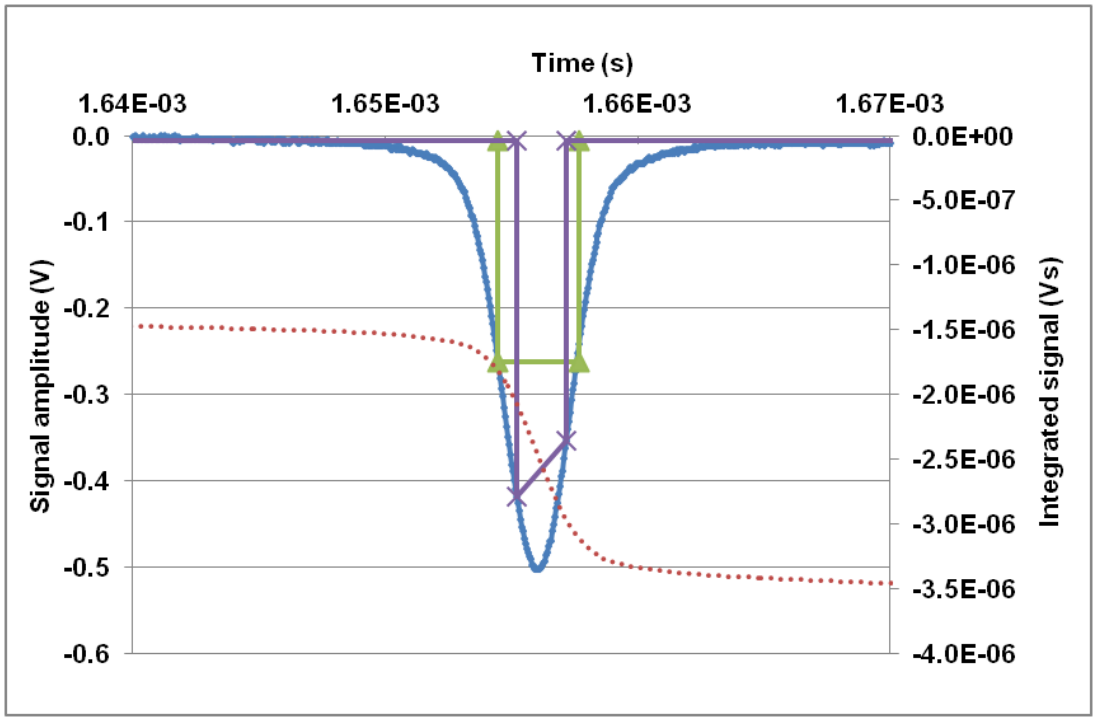

Figure 6-4 Analysis of probe trace (blue) to find FWHM (green) and FWHP (violet). FWHP is derived from the integrated signal (red dotted).

It can be seen from the FWHM analysis that the pulse generated by the slit probe was asymmetric as the signal amplitude at the 1st and 3rd quartile times were not the same. This was attributed to the capacitance of the cabling. On the negative slope of the pulse the beam was a current source with near zero impedance and was capable of charging up the cable capacitance with a negligible time constant. On the positive going slope of the pulse, the cable capacitance discharged current through the sensing resistor and this longer time constant caused the pulse to be skewed.

The results from beam measurements were collated for a range of beam currents to allow comparison with the beam characteristics data derived from the model analysis.

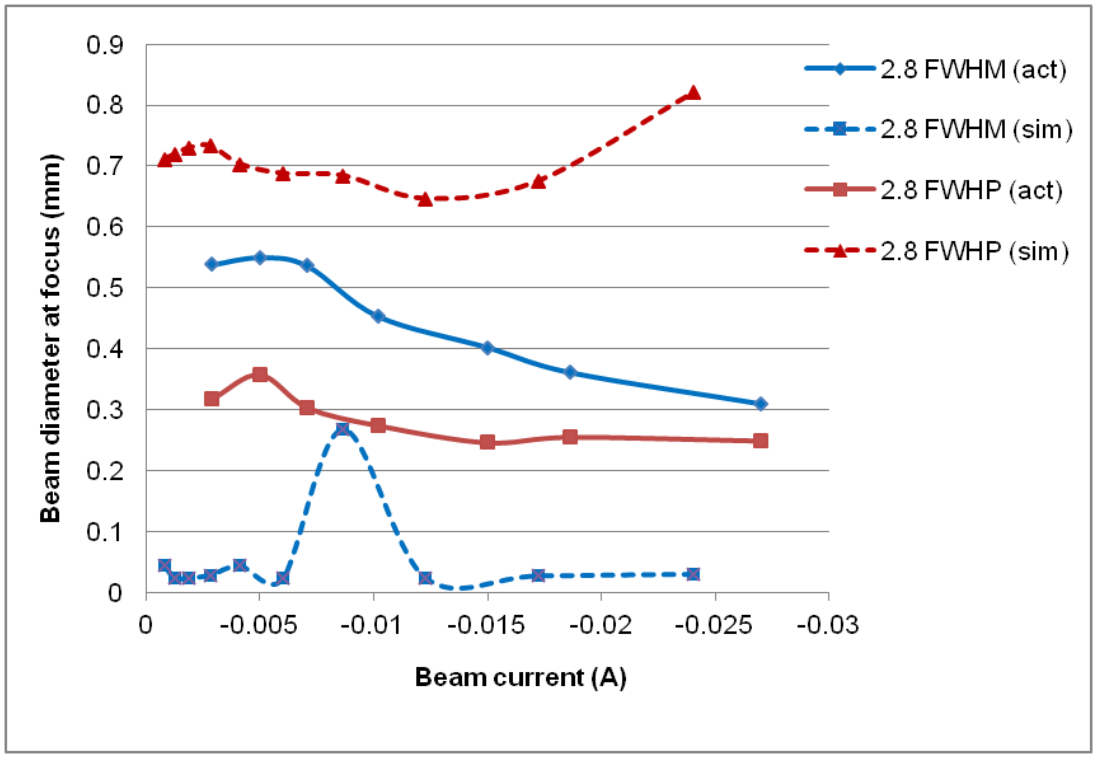

Figure 6-5 Comparison of measured beam widths, shown as solid lines for FWHM and FWHP and marked act, with the widths derived from the beam current intensity distribution, shown as dotted lines and marked sim, over the beam current range 0 A to 0.027 A for the 2.8 mm diameter cathode.

It can be seen that the beam characterisation data derived from the model gives much lower values for the beam width derived as FWHM than those measured in practice, by a factor of ten, and for FWHP the values derived from the model are greater than those measured by a factor of 2 to 3. However, the measurement of the beam, in this case with a slit probe, generated a pulse and the FWHM and FWHP values plotted in Figure 6-5 as dotted lines were characteristics of this pulse. The model data was processed to give the FWHM and FWHP of the radial beam intensity distribution, which is a different characteristic.

A better comparison between modelled and measured values was made by following the methodology described in section 2.6. This essentially simulated the probing of the beam by taking a line integral across a 2-D map of the beam intensity distribution, derived from the radial intensity plot. The results from this are shown in Figure 6-6:

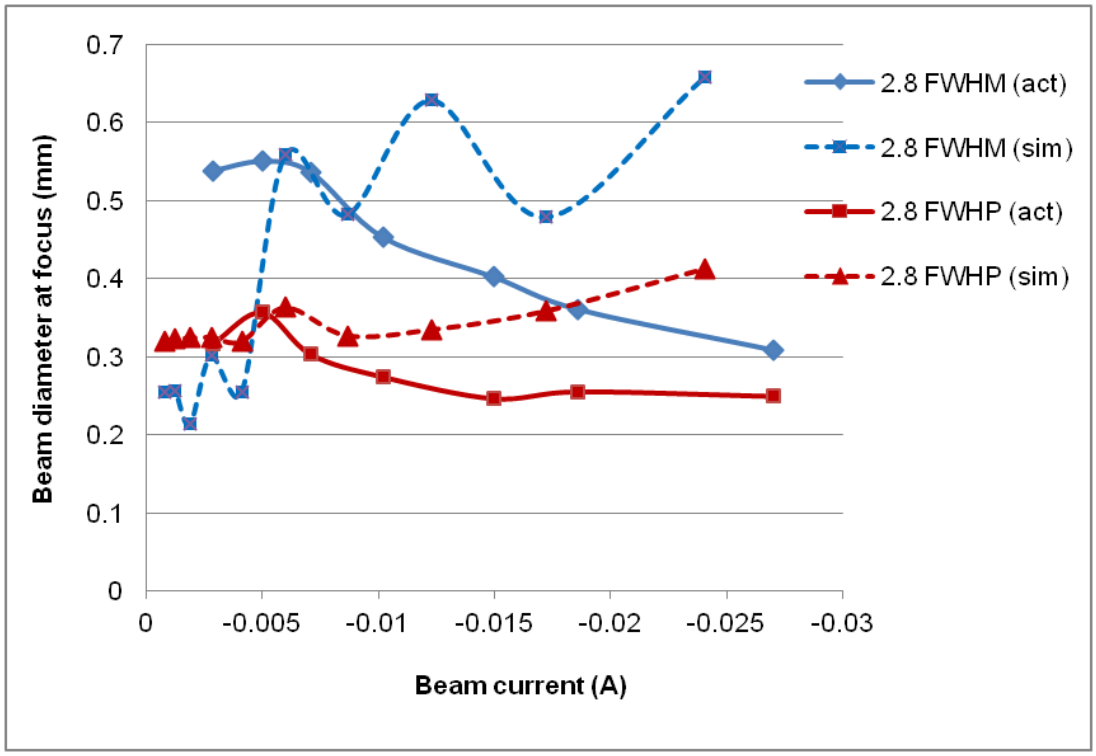

Figure 6-6 Comparison of measured beam widths, shown as solid lines for FWHM and FWHP and marked 'act' with the widths derived from simulated probing of the model data, shown as dotted lines and marked 'sim', over the beam current range 0 A to 0.027 A for the 2.8 mm diameter cathode.

The FWHM measurement tended to fluctuate more over the beam current range examined. This can be explained by considering the sensitivity of this measurement to the shape of the probed pulse - if this had a large peak in its core it may be a measure of this peak width, or if the amplitude of the peak is reduced the shoulders of the pulse would be measured giving a large change in this value. The FWHP is less sensitive to spikes on the pulse as it is a measure of the interquartile range of the integral of the probe signal or simulated signal. This integral will tend to be a smooth continuous signal - see Figure 6-4 for example.

Sometimes the beam diameters predicted by the model data were very large, and disagree with the measured data. In some cases, this could have been due to the way that the lens focal length was set to give optimum focus at the surface. This was carried out as described in section 2.5.1, and relied upon deriving the beam apparent source distance to the lens centre plane from the current weighted average source position of the trajectories.

Although this was found to be effective in the majority of cases, it could not be guaranteed to give the minimum circle of confusion for the focus of the beam in every case. An alternative strategy was implemented in the beam characteristic software where the focal length of the lens was swept to find its optimum value for minimising the spot diameter, which would be the action carried out practically.

There was not perfect agreement between the modelled characteristics and those measured practically. This needed to be taken into account when the scoring function was being designed to ensure that this was not an impediment to the optimisation process. It was possible to design scoring functions that minimised beam focal spot diameters whilst operating the gun within specific constraints. However, it was not possible to eliminate practical measurement of the beam to provide assurance that the target specification had been reached. Generally, as can be seen in Figure 6-6, the simulation over-estimated the beam width at focus when it was compared with practical measurements.

Chapter 7: Conclusions and recommendations for future work

This chapter gives conclusions from the research carried out, and provides recommendations that arise from the results of this work, with a brief description of the objective and motivation for potential further research.

7.1 Conclusions

Electron beam gun design is at best a trial and error process. An evolutionary design algorithm has been implemented, which enables the automatic design of an electron beam gun to produce an electron beam with characteristics to meet specified requirements. This algorithm has been trialled on a novel RF excited plasma cathode gun design and a low voltage high power diode gun, and shows promising results.

Analysing electron guns and deriving electron beam characteristics is necessary within any automatic design process in order to assess the suitability of the design to meet requirements. However, this is a process that uses substantial computing resource. Until recently, the solution times required meant that solving the large number of designs that necessarily make up a population was impractical on normal desktop computers and was expensive if implemented on multicore supercomputers. Current analysis software for analysing electron beam guns in 2-D is relatively fast. For example, a 10,000 element model of an electron gun will converge to a solution, taking into account the space charge of the electron beam, in a time of less than 1 minute running on a desktop PC. These recent advances in software implementation and computing hardware have made the implementation of automatic design algorithms possible.

There are two key steps in implementing an evolutionary algorithm for design: the design features to be evolved must be encoded in a genome, and the suitability of the design must be able to be quantified in a fitness score. As such the implementation of evolutionary algorithms for design could be applied to a very wide range of design challenges.

Within this work an evolutionary design algorithm for electron guns was developed and tested. Monitoring of the score function for the best of each generation shows incremental improvements and on one occasion a significant jump going from one generation to the next. The optimisation process has been run several times with the same parameters and this usually occurs, corresponding to a mutation or gene spliced combination of features that gives a near optimum diameter of beam in the lens and a high brightness.

All optimisation processes require the design to be scored against the requirements. For electron beam gun design, this has required methods to be developed to extract the beam characteristics and to quantitatively assess them.

There are a wide range of meta-heuristic methods for design optimisation which could have been applied. The evolutionary method has been investigated in this work - it is particularly suitable for geometric design and has been used widely in engineering and other disciplines. The parameters for evolution - which include the parent group size, number of offspring in a generation, the mutation rate and the mutation scale have been shown to have a large effect on the efficiency of the optimisation. This was investigated using an experimental problem where the optimisation method searched for a matching shape. Although some general trends could be extracted from this study, picking the best evolutionary parameters is in itself a trial and error process. This offers the tantalising possibility of being able to optimise the optimisation method, for example, the evolutionary process could itself evolve to become ever more efficient.

From the work reported the following summary statements can be drawn

- Electron beam gun design, particularly that carried out for material processing applications, has been reviewed. The operation and choice of cathodes has been described.

- Optimisation methods currently available have been reviewed and evolutionary optimisation has been selected for this research.
- Assessment of a gun design against required electron beam characteristics has been quantified by developing methods to derive key beam qualities from field analysis and trajectory plotting.
- A customised evolutionary design optimisation method has been developed to allow electron gun designs to be automatically optimised.
- The design method has been tested through application to a novel plasma cathode electron gun and a low voltage high power EB welding gun.
- Experimental measurements of beam characteristics have been compared with characteristics predicted by the modelling software and these have been found to be in good agreement.

In conclusion, design optimisation of electron guns has been demonstrated using bespoke evolutionary algorithm code that interfaced with a gun simulator and specially written code to extract beam characteristics that were assessed against requirements.

7.2 Recommendations for future work

Following the results from this research work, further questions raised, the areas of future work and the reasons to investigate them are listed below.

- It would be interesting to extend the methodology to 3-D designs and other electro-magnetic designs that influence beam characteristics, such as magnetic beam deflection and electron optics.
- A very similar process could be used for the design of ion beam systems.
- There are many factors that influence the efficiency and stability of evolutionary design processes. It would be useful to understand

the influence of different error spread functions in the scoring function, the correlation between the complexity of the problem space and evolutionary parameters such as mutation and population size and whether progressive evolutionary improvement is more efficient than jumps made sporadically in the best score.

- It would be interesting to understand where and why evolutionary processes do not find the optimum solution and to derive methods to correct the process where necessary.
- It seems that the evolutionary parameters are found by a process of informed trial and error. Such processes are ideally suited to being solved by evolution. If computing power becomes available, then the optimum evolutionary parameters could be determined in this way for problems of a categorised complexity.
- The same beam characterisation processing could be used with alternative optimisation strategies, for example particle swarm optimisation.
- Methods for the assessment of the robustness of the design could be built into the scoring function. To achieve this, response surface modelling methods, such as Kriging could be usefully employed.

Reference List

Andersson, J. (2001) “Multiobjective optimization in engineering design applications to fluid power systems,” *Linkoping studies in science and technology - dissertations*. Linköping University.

Bacquet, C., Zincir-Heywood, A. N. and Heywood, M. I. (2011) “Genetic optimization and hierarchical clustering applied to encrypted traffic identification,” in *Computational Intelligence in Cyber Security (CICS), 2011 IEEE Symposium on*, pp. 194–201.

Bakish, R. and White, S. (1964) “Handbook of electron beam welding”, John Wiley and Sons, Inc.

Bedau, M. A., McCaskill, J. S., Packard, N. H., Rasmussen, S., Adami, C., Green, D. G., Ikegami, T., Kaneko, K. and Ray, T. S. (2000) “Open problems in artificial life,” *Artificial life*. MIT Press, 6(4), pp. 363–376.

Bianchi, L., Dorigo, M., Gambardella, L. M. and Gutjahr, W. J. (2009) “A survey on metaheuristics for stochastic combinatorial optimization,” *Natural Computing*. Springer, 8(2), pp. 239–287.

Biddlecombe, C. and Simkin, J. (1983) “Enhancements to the PE2D package,” *Magnetics, IEEE Transactions on*. IEEE, 19(6), pp. 2635–2638.

Borel, É. (1913) “La mécanique statique et l’irréversibilité,” *Journal de Physique Théorique et Appliquée*. Société Française de Physique, 3(1), pp. 189–196.

Box, M. (1965) “A new method of constrained optimization and a comparison with other methods,” *The Computer Journal*. Br Computer Soc, 8(1), pp. 42–52.

Bratton, D. and Kennedy, J. (2007) “Defining a standard for particle swarm optimization,” in *Swarm Intelligence Symposium, 2007. SIS 2007.* IEEE, pp. 120–127.

Child, C. D. (1911) “Discharge From Hot CaO,” *Phys. Rev. (Series I)*. American Physical Society, 32(5), pp. 492–511. doi: 10.1103/PhysRevSeriesI.32.492.

Clerc, M. (1999) “The swarm and the queen: towards a deterministic and adaptive particle swarm optimization,” in *Evolutionary Computation, 1999. CEC 99. Proceedings of the 1999 Congress on*.

Cobham (2012a) “Opera v15R3 Build 28675 (x64).”

Cobham (2012b) *Opera-2d Reference Manual*. 15R3 ed. Cobham CTS Limited.

Dantzig, G. B. (1990) "Origins of the simplex method", *A History of Scientific Computing,* (S. G. Nash, ed) ACM Press.

Davis, P. R., Swanson, L. W., Hutta, J. J. and Jones, D. L. (1986) “Fabrication and characterization of rare earth hexaboride single-crystal materials,” *Journal of materials science*. Springer, 21(3), pp. 825–836.

Dawkins, R. (1986) “The blind watchmaker: why the evidence of evolution reveals a universe without design, 1986.” WW Norton.

Dorigo, M., Caro, G. D. and Gambardella, L. M. (1999) “Ant algorithms for discrete optimization,” *Artificial life*. MIT Press, 5(2), pp. 137–172.

Dushman, S. (1923) “Electron emission from metals as a function of temperature,” *Physical Review*. APS, 21(6), p. 623.

Elmer, J. and Teruya, A. (2001) “An enhanced Faraday cup for rapid determination of power density distribution in electron beams,” *Welding Journal*, AWS, 80(12), p. 288–s.

Fonseca, C. M. and Fleming, P. J. (1995) “An overview of evolutionary algorithms in multiobjective optimization,” *Evolutionary computation*. MIT Press, 3(1), pp. 1–16.

Fourie, P. and Groenwold, A. (2002) “The particle swarm optimization algorithm in size and shape optimization,” *Structural and Multidisciplinary Optimization*. Springer, 23(4), pp. 259–267.

Franz, R. (2006) “Representations for genetic and evolutionary algorithms.” Springer-Verlag.

Frost, R., Purl, O. and Johnson, H. (1962) “Electron guns for forming solid beams of high perveance and high convergence,” *Proceedings of the IRE*. IEEE, 50(8), pp. 1800–1807.

Fry, T. C. (1923) “Potential distribution between parallel plane electrodes,” *Physical Review*. APS, 22(5), p. 445.

Hawe, G. I. and Sykulski, J. K. (2007a) “An enhanced probability of improvement utility function for locating pareto optimal solutions.” *Proc. COMPUMAG,* pp. 965-966.

Hawe, G. I. and Sykulski, J. K. (2007b) “Considerations of accuracy and uncertainty with kriging surrogate models in single-objective electromagnetic design optimisation,” *Science, Measurement & Technology, IET*. IET, 1(1),

pp. 37–47.

Haynes, W. (2016) “CRC handbook of chemistry and physics" Taylor & Francis.

Herrmannsfeldt, W. (1988) *EGUN, an electron optics and gun design program*. Stanford Linear Accelerator Center, Stanford University.

Higashi, N. and Iba, H. (2003) “Particle swarm optimization with Gaussian mutation,” in *Swarm Intelligence Symposium, 2003. SIS’03. Proceedings of the* IEEE, pp. 72–79.

Iiyoshi, R., Shimoyama, H. and Maruse, S. (1996) “A comparison of thermionic emission current density and brightness against evaporation loss for LaB6 and tungsten,” *Journal of electron microscopy*. Jpn Soc Microscopy, 45(6), pp. 514–517.

ISO (2005) “Lasers and laser-related equipment-Test methods for laser beam widths, divergence angles and beam propagation ratios,” *ISO 11146-1:2005* . doi: BS EN ISO 11146-1:2005 .

ISO (2008) “Welding - Acceptance inspection of electron beam welding machines - Part 1: Principles and acceptance conditions,” *ISO 14744-1:2008*. doi: ISO 14744-1:2008.

Jin, Y. (2011) “Surrogate-assisted evolutionary computation: Recent advances and future challenges,” *Swarm and Evolutionary Computation*. Elsevier, 1(2), pp. 61–70.

Jones, H. A., Mackay, G. and others (1927) “The rates of evaporation and the vapor pressures of tungsten, molybdenum, platinum, nickel, iron, copper and silver,” *Physical Review*. APS, 30(2), p. 201.

Karafotias, G., Hoogendoorn, M. and Eiben, A. (2014) “Parameter control in evolutionary algorithms: Trends and challenges,” *IEEE Transactions on Evolutionary Computation,* 19(2), pp.167-187.

Kirkpatrick, S., Jr., D. G. and Vecchi, M. P. (1983) “Optimization by simmulated annealing,” *Science*. 220(4598), pp. 671–680.

Klemperer, O. (1959) “Electron Physics - The physics of the free electron.” Butterworths Scientific Publications.

Koleva, E., Vutova, K., Wojcicki, S. and Mladenov, G. (2001) “Use of radial distributions of the beam current density for evaluation of beam emittance and brightness,” *Vacuum*. Elsevier, 62(2), pp. 105–111.

Lafferty, J. (1951) “Boride cathodes,” *Journal of Applied Physics*. AIP Publishing, 22(3), pp. 299–309.

Langmuir, I. (1923) “The Effect of Space Charge and Initial Velocities on the Potential Distribution and Thermionic Current between Parallel Plane Electrodes,” *Phys. Rev.* American Physical Society, 21(4), pp. 419–435. doi: 10.1103/PhysRev.21.419.

Lawson, J. D. (1977) *The physics of charged-particle beams*. Clarendon Press .

Lebensztajn, L., Marretto, C. A. R., Costa, M. C. and Coulomb, J.-L. (2004) “Kriging: a useful tool for electromagnetic device optimization,” *Magnetics, IEEE Transactions on*. IEEE, 40(2), pp. 1196–1199.

Lewis, B. M., Tran, H. T., Read, M. E. and Ives, R. L. (2004) “Design of an electron gun using computer optimization,” *Plasma Science, IEEE Transactions on*. IEEE, 32(3), pp. 1242–1250.

Liebmann, G. (1955) “A unified representation of magnetic electron lens properties,” *Proceedings of the Physical Society. Section B*. IOP Publishing, 68(10), p. 737.

Nguyen, A.-T., Reiter, S. and Rigo, P. (2014) “A review on simulation-based optimization methods applied to building performance analysis,” *Applied Energy*. Elsevier, 113, pp. 1043–1058.

Pierce, J. R. (1954) “Theory and design of electron beams.” van Nostrand.

Ponsich, A., Jaimes, A. L. and Coello, C. A. C. (2013) “A survey on multiobjective evolutionary algorithms for the solution of the portfolio optimization problem and other finance and economics applications,” *IEEE Transactions on Evolutionary Computation*. IEEE, 17(3), pp. 321–344.

Del Pozo, S., Ribton, C. N. and Smith, D. R. (2014) “A novel RF excited plasma cathode electron beam gun design,” *IEEE Transactions on Electron Devices*. IEEE, 61(6), pp. 1890–1894.

Ribton, C. and Sanderson, A. (2015) “Plasma source apparatus and methods for generating charged particle beams.” U.S. Patent 9,076,626.

Richardson, O. W. (1913) “The Emission Of Electrons From Tungsten At High Temperatures: An Experimental Proof That The Electric Current In Metals Is Carried By Electrons,” *Science*. JSTOR, pp. 57–61.

Sen, M. K. and Stoffa, P. L. (2013) *Global optimization methods in geophysical inversion*. Cambridge University Press.

Septier, A. (1967) “Focusing of charged particles.” Academic Press Inc.

Sims, K. (1994) “Evolving 3D morphology and behavior by competition,” *Artificial life*. MIT Press, 1(4), pp. 353–372.

Song, Y.-H. (2013) *Modern optimisation techniques in power systems*. Springer Science & Business Media.

Thomson, J. J. (1897) “XL. Cathode rays,” *The London, Edinburgh, and Dublin Philosophical Magazine and Journal of Science*. Taylor & Francis, 44(269), pp. 293–316.

Tsong, T. T. and Mueller, E. W. (1970) “Field evaporation rates of tungsten,” *physica status solidi (a)*. Wiley Online Library, 1(3), pp. 513–533.

v. Borries, B. and Ruska, E. (1939) “Ein Übermikroskop für Forschungsinstitute,” *Naturwissenschaften*. Springer, 27(34), pp. 577–582.

v. Dobeneck, D. (2007) *An International history of electron beam welding*, pro-beam.

Varian, R. H. and Varian, S. F. (1939) “A high frequency oscillator and amplifier,” *Journal of Applied Physics*. AIP Publishing, 10(5), pp. 321–327.

Wilson, C. T. R. (1895) “The effect of Rontgen’s rays on cloudy condensation,” *Proceedings of the Royal Society of London*. The Royal Society, 59(353-358), pp. 338–339.

Wolpert, D. H. and Macready, W. G. (1997) “No free lunch theorems for optimization,” *IEEE transactions on evolutionary computation*. IEEE, 1(1), pp. 67–82.

Xiao, S., Rotaru, M. and Sykulski, J.K., 2014. Robust design optimisation of electromagnetic devices exploiting gradient indices and Kriging. *IET Science, Measurement & Technology*, *9*(4), pp.400-409.

Zhu, J.-H., Zhang, W.-H. and Xia, L. (2016) “Topology optimization in aircraft and aerospace structures design,” *Archives of Computational Methods in Engineering*. Springer, 23(4), pp. 595–622.

Appendix A: Random sentence generator

Random generation of sentence and match to target

The following script is in Python 2.7

```
from random import choice, random
alphabet = " ABCDEFGHIJLKLMNOPQRSTUVWXYZ"

#target sentence
shakespeare  = list("METHINKS IT IS LIKE A WEASEL")
# mutation probability
p = 0.05

#function to randomly mutate a sentance
def mutate(sentence):
    return [(choice(alphabet) if random() < p else
letter) for letter in sentence]

# initialise with a random sentance the same length as
the target
new_sentence = [choice(alphabet) for _ in
range(len(shakespeare))]
raw_input("Press Enter to continue...")
i = 0
print "%3d" % i, "".join(new_sentence)

while new_sentence != shakespeare:
    new_sentence = mutate(new_sentence)
    print "%3d" % i, "".join(new_sentence)
    i += 1
```

Appendix B: Dawkin's weasel program

Dawkin's weasel program for evolving optimisation, rescripted into Python.

The following script is in Python 2.7

```
from random import choice, random

def weasel (p,c):
    alphabet = " ABCDEFGHIJLKLMNOPQRSTUVWXYZ"

    shakespeare  = list("METHINKS IT IS LIKE A WEASEL")

    #function to score the how close the sentence is to
the target
    def score(trial):
        return  sum(t  !=  h  for  t,h  in  zip(trial,
shakespeare))

    def mutate(sentence,mutation):
        return [(choice(alphabet) if random() < mutation
else ch) for ch in sentence]
    #initial random parent sentence
    parent    =    [choice(alphabet)    for    _    in
xrange(len(shakespeare))]
    i = 0
    while (parent != shakespeare) and (i*c < 100000):
        child = (mutate(parent,p) for _ in xrange(c))
        parent = min(child, key=score)
        i += 1
    return p,c, i*c

with open ("weasel_results.csv", "w") as text_file:
    text_file.write( "probability" + "," + "population"
+ "," + "total_calls" + "\n" )

    for prob in range(5,210,5):
        p_frac=float(prob)/1000
        for children in range(5,220,5):
            a,b,c = weasel(p_frac,children)
            text_file.write( str(a) + "," + str(b) + ","
+ str(c) + "\n" )
text_file.close()
```